UNIVERSITÀ DEGLI STUDI DI PADOVA

Dipartimento di Fisica e Astronomia “Galileo Galilei”

Master Degree in Physics

Final Dissertation

A FL* approach to high T_c cuprates

Thesis supervisor

Prof. Pieralberto Marchetti

Thesis co-supervisor

Prof. Luca Salasnich

Candidate

Marco Malfatti

Academic Year 2022/2023

Contents

Introduction

The discovery in the cuprate compounds in 1986 of high-temperature superconductivity, quite different from BCS superconductivity, posed numerous challenges to quantum theories of electronic matter, being among the major scientific events of the twentieth century. As a strongly correlated material, that can be tuned from an insulator to high-temperature superconductor, and then to a metal via hole or electron doping, cuprates are perhaps the most importante example to refine the description of correlated electronic system. As the properties of hole-doped cuprates (the ones discussed in this thesis) were studied with ever increasing precision and sensitivity, it indeed became clear that much of the well understood quantum theory of the electronic properties of solids, which has been spectacularly successful in explaining the properties of conventional metals and superconductors, fails entirely to address many features of the cuprates, and, more generally, of a broad array of highly correlated electronic systems, of which the cuprates are perhaps the most studied.

Very many experimental results and theoretical approaches have been presented in the last four decades in order to study the exotic phases that emerge alongside superconductivity in cuprates, but without obtaining a successfully shared agreement, and until now a complete microscopical model is still lacking. Among these phases, the pseudogap, standing out for its enigmatic nature, has emerged as the "mystery phase" in condensed matter physics, as there in no consensus on its nature and on its connection to superconductivity. The pseudogap is characterized by several experimental signatures, in particular the opening of a momentum-dependent spectral gap (reminescent of the superconducting gap that opens at transition temperature T_c, hence the name pseudogap) detected by angle-resolved photoemission spectroscopy, and a loss of density of states, detected by specific heat and nuclear magnetic resonance, thus giving a loss of coherent quasiaparticles below an onset temperature T^* and below a critical doping p^*. Moreover, this substantial suppression ot the electronic density of states at low energies cannot be simply related to the occurrence of any form of broken symmetry, thus making necessary to go beyond the well known Landau-Ginzburg-Wilson paradigm to classify the different phases. Transport measurements in magnetic fields high enough to suppress superconductivity down to $T \cong 0$ have also unveiled the otherwise hidden properties of the pseudogap phase in its ground state. Characterizing what remains of the coeherent Fermi surface inside the pseudogap phase is therefore a critical step towards understanding how this peculiar metallic state gives rise to, or it is compatible to, high-temperature superconductivity: from this point of view the Luttinger's theorem is clearly a basic and powerful tool, and new nonperturbative arguments can be used to discuss its modified version .

The FL* liquid is a concept introduced some years ago and proposed for the cuprates, going clearly beyond the usual Fermi liquid theory; it describes an electronic Fermi liquid where the particle excitations are not only the standard spin $1/2$ charged electrons, but also particle excitations carrying charge but spinless, named holons, and carrying only spin $1/2$ but neutral, named spinons: thus with this proposal it is clear how, in order to obtain a good model for the hole-doped cuprates, we really need to go beyond the well understood paradigms of condensed matter theory.

In the first chapter we present the basic features of the hole-doped cuprates, with their more general phase diagram, specially presenting the characteristics of the pseudogap phase. In the second chapter we report how it was realized that the Luttinger's theorem has a topological character, and how it is possible for topological order associated with emergent gauge fields to change the volume enclosed by the Fermi surface. Recent developments have shown that the topological order associated with emergent gauge fields can also require a phase transition between states which cannot be distinguished by symmetry, thus going outside the traditional theory of phase transitions which relies crucially on symmetry. So we can have a phase transition associated with the onset of topological order, across which the Fermi surface reconstructs, even though there is no symmetry breaking on either side of the transition. The third chapter contains a theoretical approach analyzing a possible FL* nature of the low-energy physics of the pseudogap phase of hole-doped cuprates, with an approach proposed by Sachdev and collaborators, based on the angular fluctuations of antiferromagnetic spin waves with a sort of Higgs' transition to a phase with a topological order. In the fourth chapter we present a theoretical model proposed by P. A. Marchetti and collaborators, based on a spin-charge gauge approach with semionic statistics of holons and spinons and antiferromagnetic spin vortices as pairing glue excitations emerging from the antiferromagnetic phase. In the fifth chapter we repott the more recent experimental results, specially regarding the Fermi surface for the hole-doped cuprates, and in the sixth chapter we make some considerations about the models presented in the thesis, giving some indication for current and future developments.

Chapter 1

Cuprates – History, basic features, phase diagram, and the pseudogap

1.1 History

The first cuprate high-T_c superconductor was discovered by Bednorz and Muller in early 1986 [1], and in December 1986 the structure and chemical composition were identified as $La_{2-x}Ba_xCuO_4$ (LBCO) with $T_c \sim 30\ K$, and a perovskite structure, as shown in Fig. 1.1a. By simply replacing Ba with Sr, it was obtained $La_{2-x}Sr_xCuO_4$ (LSCO) with $T_c \sim 40\ K$. The most remarkable features of these cuprates were [2]:

- The undoped parent compound La_2CuO_4 is a Mott insulator due to strong repulsive interactions between electrons, while the LDA (Local Density Approximation) band structure calculation predicted a metal with a half-filled band [3].
- Superconductivity emerges by doping holes, whose density is parametrized by x into this parent compound.

Many researchers tried to replace La by other rare earth elements, and in January 1987 it was obtained a $T_c \sim 90\ K$ for the cuprate $YBa_2Cu_3O_{7-y}$ (YBCO): this was really a great discovery of a superconductor with T_c exceeding the liquid nitrogen temperature ($77\ K$). The crystal structure of YBCO was found to be really new, with double CuO_2 planes, Ba_2O_2 blocks, and incomplete CuO_{1-y}, see Fig. 1.1b. The parent compound for YBCO is the Mott insulator $YBa_2Cu_3O_6$, with hole doping made by adding oxygen atoms to the CuO chains.

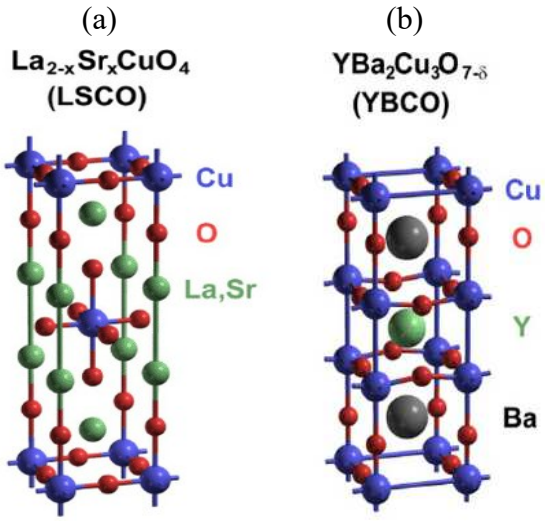

Figure 1.1. Crystal strucures of (a) LSCO cuprate (b) YBCO cuprate [4].

In 1988 T_c reached 100 K in another new cuprate structure $Bi_2Sr_2Ca_2Cu_3O_{10+\delta}$ (Bi2223), with trilayer CuO_2-Ca-CuO_2-Ca-CuO_2 unit: in this cuprate $Bi_2O_{2+\delta}$ blocks are charge reservoirs layers, and excess oxygen atoms O_δ provide holes to the CuO_2 planes. The Bi-based cuprates are the first multilayer homologous series with the generic chemical formula given by $Bi_2Sr_2Ca_{n-1}Cu_2O_{2n+4+\delta}$ [$Bi22(n\text{-}1)n$], including:

- Single-layer (n=1) $Bi_2Sr_2CuO_{6+\delta}$ (Bi2201)
- Bilayer (n=2) $Bi_2Sr_2CaCu_2O_{8+\delta}$ (Bi2212)

Soon after, another homologous series $Tl_2Ba_2Ca_{n-1}Cu_nO_{2n+4+\delta}$ [$Tl22(n\text{-}1)n$] was discovered by replacing Bi and Sr by Tl and Ba respectively, and T_c~125 K was achieved for Tl2223. By replacing Bi or Tl by other heavy elements, such as Pb or Bi, it was straightforward to find other homologous series, so in 1993 $HgBa_2Ca_{n-1}Cu_nO_{2n+2+\delta}$ [$Hg12(n\text{-}1)n$] was successfully synthesized. The HgO_δ blocks are charge reservoirs, and excess oxygen atoms O_δ supply holes to the CuO_2 planes. $HgBa_2Ca_2Cu_3O_{8+\delta}$ (Hg1223) recorded the highest T_c value, 135 K, at ambient pressure; the same compound at pressure higher than 20 GPa, obtained T_c~164 K in 1994. Striking feature of the Hg-based cuprates is that the multilayers up to n=8 or larger were synthesized: T_c also increases with n up to n=3, and then decreases for n larger than 4, and this feature turned out to be generic for multilayer cuprates. As simple examples, see in Fig 1.2 the crystal structures for Tl2201 and Hg1201

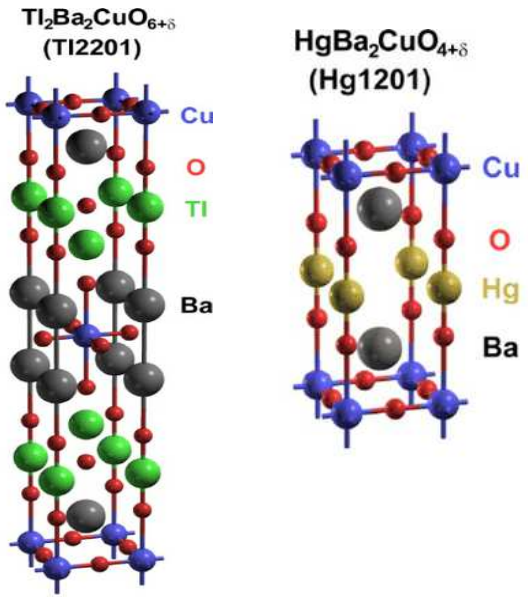

Figure 1.2. Crystal strucures of (a) Tl2201 cuprate (b) Hg1201 cuprate [4].

1.2 Basic features

High-temperature superconductivity with T_c well exceeding the liquid nitrogen temperature is found only in materials whose basic structural unit is the surprisingly simple CuO_2 plane depicted in Fig. 1.3, layers of Cu and O atoms arranged in a square lattice, as also illustrated at the top and the bottom of the unit cells of LSCO in Fig. 1.1a, of Tl2201 and Hg1201 in Fig 1.2, and in the middle of the unit cell of YBCO in Fig. 1.1b.

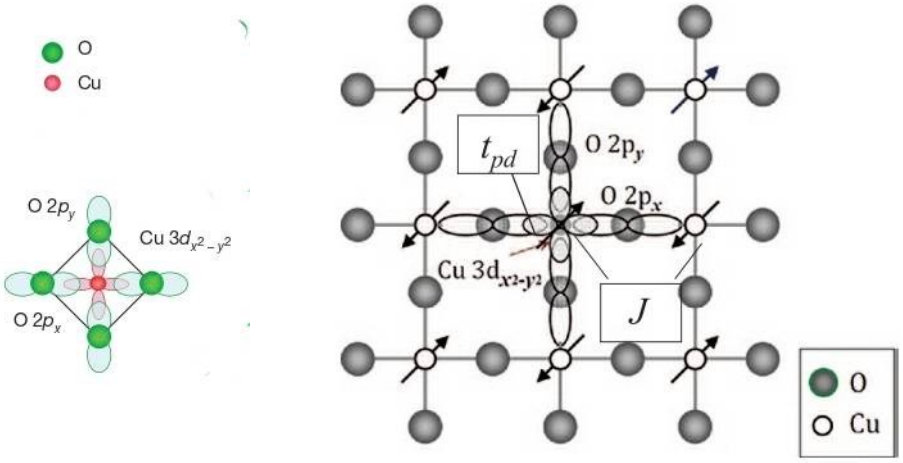

Figure 1.3. Structure of CuO_2 plane showing relevant $Cu\ 3d_{x^2-y^2}$ and $O\ 2p_{x,y}$ orbitals, both being strongly hybridized [2, 5].

The neighboring CuO_2 planes are separated by "charge reservoirs" layers or blocks, whose functions are [2]:

- To supply carriers to the CuO_2 planes by chemical substition and/or by adding or reducing oxygen atoms.
- To neutralize the negative charged CuO_2 plane $[Cu^{2+}O_2^{2-}]^{2-}$ by forming an alternating stack with positively charged layers.
- To stabilize the cuprate crystal structure by inserting layers consisting of cations with large ionic radii.

Given that the electronic structure in the CuO_2 square lattice is $Cu^{2+} = 1s^2 2s^2 2p^6 3s^2 3p^6 3d^9$ and $O^{2-} = 1s^2 2s^2 2p^6$, with the key copper orbital $3d_{x^2-y^2}$ containing a single electron, thus being half-filled, traditional band theory dictates that this material should be a conductor, but this is not what happens: in fact the undoped CuO_2 plane is a Mott, or more precisely a "charge transfer" insulator, due to the strong Coulomb repulsion ($U \sim 6-8\ eV$) between electrons on the $3d$ orbitals of the Cu atoms. As schematically depicted in Fig. 1.4, the energy gap is actually created between occupied $O2p$ orbitals and empty $Cu3d$ bands (the upper Hubbard band UHB), and not between the two Hubbard Cu bands, so this is called a charge transfer gap E_{CT}. In fact we know that a Cu^{2+} has 9

electrons in its $3d$ orbitals, and also it is fourfold coordinate in a CuO_2 square lattice, so the uppermost $3d$ orbital, $3d_{x^2-y^2}$, is occupied by a single electron and a single hole, as shown in Fig. 1.5.

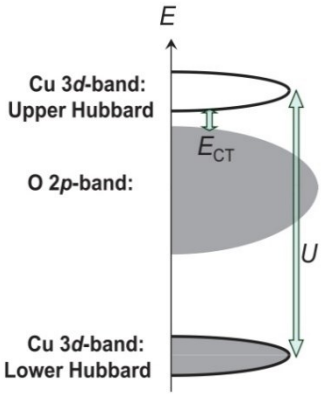

Figure 1.4. Schematic energy scheme of the insulating undoped cuprate, showing a strong electronic correlation U on a Cu atom, and a charge-transfer (CT) energy gap between $O2p$ and $Cu3d$ upper Hubbard band [2].

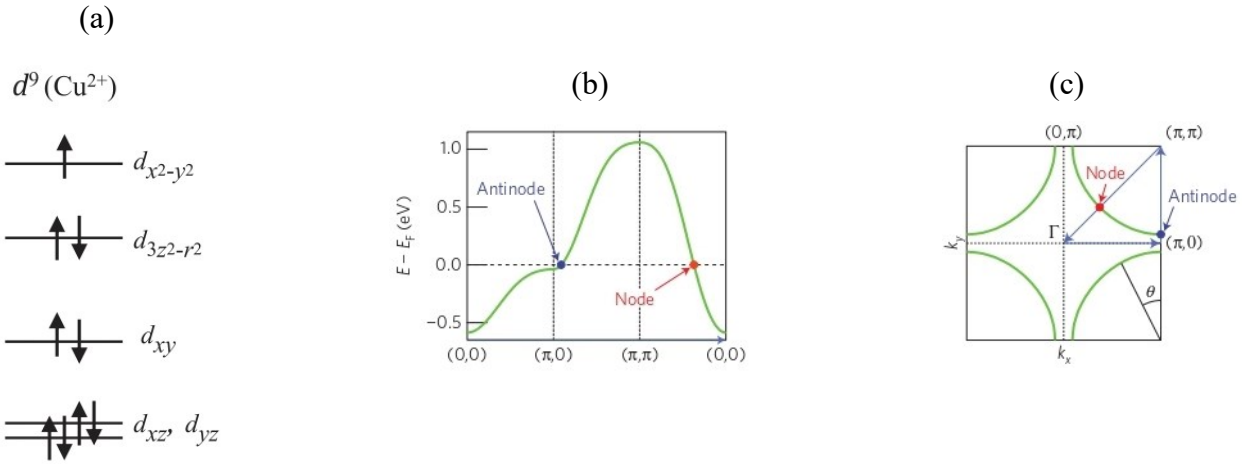

Figure 1.5. (a) Electron filling of the $3d$ orbitals of the $Cu^{2+}(d^9)$ state [2]. (b) Schematic band dispersion in reciprocal space for cuprates along the high-symmetry cuts, as shown in blue in (c) [6]. (c) Fermi surface, where the nodal and the antinodal momenta and Fermi angle θ are defined [6].

This electron (hole) is localized on the Cu sites, due to the strong Coulomb repulsion between other electrons, leaving a magnetic moment associated with the $S = 1/2$ spin quantum number: in the undoped cuprate the Cu spins align antiferromagnetically on the CuO_2 plane, due to the superexchange term J between neighboring ones, via an intervening O atom, as discussed later on. In this way the single occupied $Cu3d_{x^2-y^2}$ level forms a single-band by the hybridization with the $O2p_x$ and $O2p_y$ states. If we introduce a doping hole, it preferentially goes in the combinations of the four $O2p_x, p_y$ orbitals centered around the Cu site, forming a spin-singlet with the spin of this corresponding Cu site: these are the so-called Zhang-Rice singlets [7], and this site has clearly zero charge and no spin. An explanation of this is that, since Cu is at the end of the $3d$ transition metal series in the periodic table, the energies of $Cu3d$ states are incidentally close to those of the $O2p$ states (see Fig. 1.4), and this makes the charge-transfer energy gap small, $E_{CT} \sim 1.5 - 2.0\, eV$, compared with that in other transition-metal oxyde. In particular, the wavefunction of $Cu3d_{x^2-y^2}$ has large overlap with that of $O2p_x$ and $O2p_y$ states, so the overlap/hopping matrix element t (t_{pd} in Fig.

1.3) is large, $\sim 0.3 - 0.4\ eV$, leading to strong hybridization between the two orbitals. This hybridized single band crosses the Fermi level E_F as shown in Fig 1.5b, typically forming a large holelike Fermi surface as depicted in Fig. 1.5c.

In the parent compound every site of the square lattice has exactly one electron because the Coulomb repulsion between the electrons keeps their charges on the Cu lattice sites, but it is insensitive to the spins of the electron, so it would appear that each electron spin is free to rotate independently on each site. As seen above, the localized electrons have a spin whose orientation remains a dynamicall degree of freedom, and virtual hopping of these electrons produces, via the Pauli exclusion principle, an antiferromagnetic interaction J between neighboring spins. This, in turns, leads to a simple Néel ordered phase below room temperature , in which there are static magnetic moment on the Cu sites with a direction that reverses from one Cu to the next. The optimal state turns out to be the antiferromagnetic one sketched in Fig. 1.6, where the spins are arranged in a checkerboard pattern, so that all the spins in one sublattice are parallel to each other, and antiparallel to spins on the other sublattice.

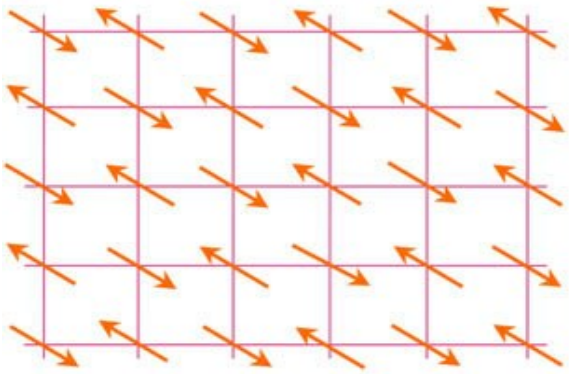

Figure 1.6. The undoped insulating antiferromagnetic state [8].

In Fig. 1.6 we can observe the quasi-two-dimensional structure of the undoped parent compound; we also can regard the $O2p$ orbitals as filled with pairs of electron and inert, while only one of the $Cu3d$ orbitals is active, having a density of exactly one electron per site of the square lattice.

We can thus summarize the unique features of the cuprates, and also necessary conditions for high T_c [2]:

- Layer structure.
- Strong electronic correlation.
- A single band.
- $S = 1/2$ spin state.
- Accidental degeneracy between $Cu3d$ and $O2p$ energies.

No other materials so far known have all these features simultaneously, and these features also have fundamental physical consequences:

1. The large overlap/hopping integral t_{pd} and the closeness of $Cu3d$ and $O2p$ levels, with small value of E_{CT}, give rise to strong covalent nature of the Cu-O bonds, as well to the inusually large spin superexchange interaction, given by $J{\sim}0.15\ eV$[1]. The strong covalent bond makes the phonon frequency corresponding to the modulations of the Cu-O bond length (or bond angle) fairly high ($\Omega_0{\sim}0.07\ eV$); the large energy scales of the charge (t_{pd}), spin (J), and phonon (Ω_0) related excitations are probably sources of strong pairing interactions and hence high T_c.
2. The layer structure leads to highly two-dimensional (2D) character of the electronic state of the cuprates, and $S = 1/2$, the minimal spin quantum number, makes the spin fluctuation maximal. Thus, the otherwise very stable antiferromagnetic order becomes fragile against doping and raising temperature.
3. Strong correlations favour unconventional pairing with nodes in the superconducting gap.

Summarizing, representing the system in terms of a Hubbard model, the system gains kinetic energy $t \equiv t_{pd}$ when the hole hops between sites, and pays an energy cost U when double occupancy occurs on the same site: long-range antiferromagnetic order forms on the Cu sites, since the electrons gain kinetic energy by virtual intersite hopping, which is maximized when nearest-neighboring spins are antiparallel to each other. This effective low-energy single band approximation has enabled wide applications of the two-dimensional single-band Hubbard model to describe the behavior of doped charge carriers in cuprates [3], as we will discuss in Chapter n. 3. In Chapter n. 4 we will discuss the widely used t-J model [9], that in general for the cuprates is advocated directly from the Zhang-Rice singlets [7] without passing through the Hubbard model, with a ratio $J/t \approx 1/3$ (in the large U limit, to effectively describe the hopping of the singlet, the Hubbard model may be expanded in powers of t, leading to $J = 4t^2/U$).

1.3 Phase diagram and the pseudogap phase

The undoped parent compound depicted in Fig. 1.6 can be doped by changing the chemical makeup of interleaved charge-reservoirs layers, so that electrons are removed (hole-doped) or added (electron-doped) to the CuO_2 planes: in this paper we will confine our discussion to hole-doped systems. In Fig. 1.7 we show some proposed phase diagrams by different authors, as there are so far various disagreements about both theoretical models and interpretations of the many experimental results. Part of the difficulty stems form the fact that the many hole-doped cuprate superconductors exhibit non-universal T-p phase diagrams, with p denoting the in-plane hole doping, due to significant differences in T_c, crystal structures, disorder effects, competing phases, etc., and so it is not easy to

[1] $J \approx t_{pd}^4/E_{CT}^3$ [2].

obtain the determination of their essential universal properties, especially in the pseudogap regime. However, some fixed points seem so far assured: hole doping rapidly suppresses the antiferromagnetic (AF) order, and at a critical doping p_{min}, superconductivity (SC) sets in, with a transition temperature that grows to a maximum at p_{opt}, then declines for higher dopings and vanishes for p_{max}. Materials with $p < p_{opt}$ are referred to as underdoped, and those with $p > p_{opt}$ are referred as overdoped.

The superconducting transition temperature has a dome-like shape in the temperature-doping plane, with a maximum near a doping p_{opt}~0.167.

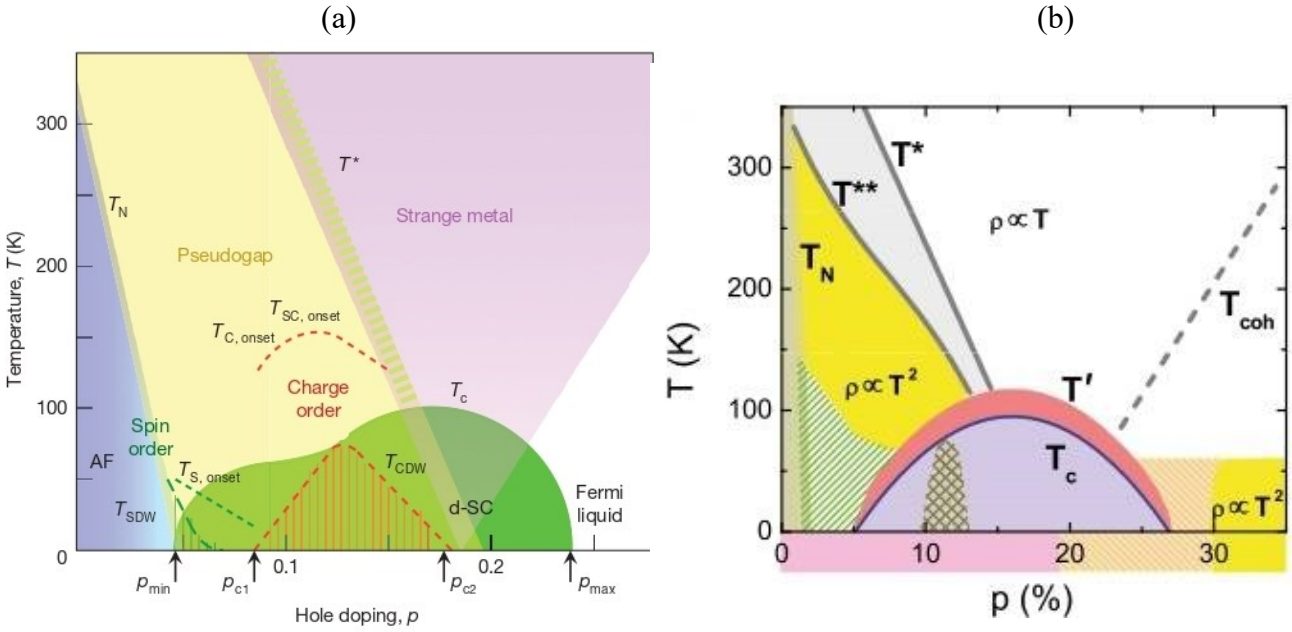

Figure 1.7. Phase diagram with variuos orders and their fluctuations in the underdoped regime [2]. (b) Phase diagram with superconductivity, disorder, competiting orders, T^* and T^{**} transition temperatures [4].

It is important to recognize [5] that the strong electronic repulsions that cause the undoped system to be an insulator, are still the dominant microscopic interactions, even in optimally doped cuprates. Thus the resulting electron fluid is highly correlated, in the sense that for an electron to move through the crystal, other electrons must shift to get out of its way. In contrast, in the Fermi liquid description of simple metals, the quasiparticles ("dressed" electrons) propagate freely through an effective medium defined by the rest of the electrons. The failure of the quasiparticle paradigma is most acute in the "strange metal" regime, that is the normal state out of which the pseudogap and the superconducting phases emerge when the temperature is lowered. Nonetheless we will see in Chapter n. 5 that recent experimental results have showed that, even in underdoped materials, at temperatures low enough to quench superconductivity by the application of a high magnetic field, emergent Fermi liquid behavior arises, even if with characteristics (for example, a reconstructed Fermi surface) that are quite different from those predicted by band theory. Nevertheless, over most of the phase diagram, the frustration of the coherent electrons motion produces physics that is qualitatively distinct from

that of simple metals. Briefly summarizing as depicted in Fig. 1.7, hole doping induces a series of low temperature phases (apart from the AF and SC phases, the others might be separated not exactly by a phase transition, but by a crossover) [2, 5]:

- A spin glass region characterized by slow spin dynamics.
- A dome-shape superconducting described mostly by d-wave[2] symmetry.
- A valence electron charge density wave (CDW) and spin stripes.
- Non-Fermi liquid charge transport, often referred to as a "strange metal".
- Eventually a more coherent region.
- A pseudogap phase, detailed below.

In this paper we will discuss only the pseudogap regime of the phase diagrams depicted in Fig. 1.7. The pseudogap phase, a novel state of electronic matter found in the hole-doped cuprates, is perhaps the most mysterious regime in the phase diagram, and understanding its origin and nature is considered a key to resolve the high-T_c mechanism: it is essential to develop a microscopic understanding of the pseudogap (and the strange metal) phases, in order to resolve the mystery of cuprate superconductivity, as they are the "normal" states out of which superconductivity and various other ordering tendencies arise at low temperatures. The pseudogap regime covers a wide T-p area of the phase diagram, in which various spectroscopies indicate a suppression of low energy excitations below the pseudogap temperature T^*. It has been proposed some evidence of electrical transport with the temperature and frequency dependence of a conventional metal obeying the Fermi liquid theory [10, 11]. Furthermore, a long-standing mystery in the study of the cuprates is that photoemission experiments do not show the large Fermi surface that is expected from the Luttinger's theorem of Fermi liquid theory [12]. One way to obtain such a Fermi reconstruction, from the large Fermi surface to Fermi arcs, is by a broken translational symmetry: however there is no sign of broken translational symmetry over a wide temperature range [5], and also at low temperature and intermediate doping [13], over which the pseudogap is present. As we will discuss in Chapter n. 2, there are nonperturbative arguments [14-18] that deviations from the Luttinger volume are only possible in quantum states with topological order. We will discuss in Chapter n. 3 and Appendix C a possible presence of topological order in the pseudogap phase, that until now has so far been lacking.

Various properties show a rather dramatic change at T^* [2]:

1. Temperature dependence of the spin-lattice relaxation and Knight-shift[3] in nuclear magnetic resonance (NMR) and magnetic susceptibilities showed a reduction in the low-frequency spin excitations. In underdoped compounds, as we lower the temperature, the Knight shift remains

[2] d-wave implies a gap as $\Delta = \Delta_0(cosk_x a - cosk_y a)$, where a is the in-plane lattice constant: this SC gap (order paramater) changes sign on the Fermi surface, vanishing at some **k**'s (gap nodes). The gap nodes are along the Brillouin-zone diagonal, and the gap magnitude is maximum at the "antinodes" at $(\pm\pi, 0)$ and $(0, \pm\pi)$ (See Fig. 1.5c).
[3] The Knight shift, due to the conduction electrons, is proportional to the electronic spin susceptibility, and from the shift in the nuclear energy levels seen in a NMR experiment, we can obtain the static response of the electrons (in metals Knight shifts are temperature independent).

constant until a upper crossover temperature is reached, then starts to decrease linearly with T, and finally for $T < T^*$ the decrease is faster than linear; strongly overdoped compounds do not show a pseudogap, and their susceptibility drops only in the superconducting phase (we remember that in an ordinary Fermi liquid one would have a temperature-independent susceptibility that is proportional to the density of states at the Fermi surface, as the temperature is lowered).

2. Spectroscopic measurements show evidence for a suppression in the density of states at the Fermi level along specific regions of the Brillouin zone, without clear evidence for any broken symmetry in this regime: ARPES revealed an anisotropic nature of the pseudogap in momentum space, having maximal magnitude in the antinodal region, that is in the vicinity of the Brillouin zone edges $\mathbf{k} = (\pi, 0)$ and $\mathbf{k} = (0, \pi)$. On the other hand, gapless excitations are observed on a Fermi arc centered around the nodes (see Fig. 1.8): in this regard the pseudogap has a d-wave-like anisotropy in the momentum space as the superconductivity gap does (that is a $d_{x^2-y^2}$ form). We can note that the existence of this spectral gap above T_c refutes the conventional wisdom of a coherent metallic normal state, that is required to precede a mean-field BCS superconducting transition. The nodal region involves a narrow region around the zone diagonals, which gradually grows with increasing doping until it encompasses the entire Fermi surface in sufficiently overdoped materials, while the antinodal pseudogapped region gradually shrinks to zero as T^* is approached. This striking difference in the nature of the electronic excitations measured in ARPES when crossing from the coherent nodal region to the anticoherent antinodal region in momentum space is called the "nodal-antinodal dichotomy" [6, 19]. This anisotropy is reflected in the resistivity anisotropy: the in-plane resistivity appears to be dominated by the nodal region of the Fermi surface, while the c-axis resistivity by the antinodal region. Moreover, the detailed momentum dependence of the excitation gap along along the Fermi surface contour, and the different temperature trends observed in the nodal and antinodal regions, suggest the coexistence of two distinct spectral gap components over the whole superconducting dome: superconducting gap and pseudogap, dominating the response in the nodal and antinodal regions, respectively, which would eventually collapse to one single energy scale in the very overdoped regime.

3. The antinodal region lacks any quasiparticle-like spectral peaks, throughout the pseudogap regime it exhibits a suppression of low-energy electronic spectral weight on an energy scale that corresponds to the pseudogap. Nevertheless, the antinodal region is not only probably important for pairing, but it also is the place where the charge order (and possibly other orders) is supposed to get born.

The astonishing character of these observations is best illustrated by showing a map of the spectral weight at low energies as a function of **k** in the first Brillouin zone in Fig. 1.8. We know that in a Fermi liquid, the Fermi surface delineates the boundary between occupied and unoccupied quasiparticles states, so no matter how complicated it may be, the one thing it cannot do is to end abruptly. But in the pseudogap regime there appears to be "Fermi arcs" in the nodal regime, as we will see in Chapter n. 5, briefly summarizing many experimental results form ARPES, and it could be plausible that these arcs are actually the front half of Fermi hole pockets, giving rise to an intense search to find the "backsides of the pocket", as we will discuss in Chapter n. 3.

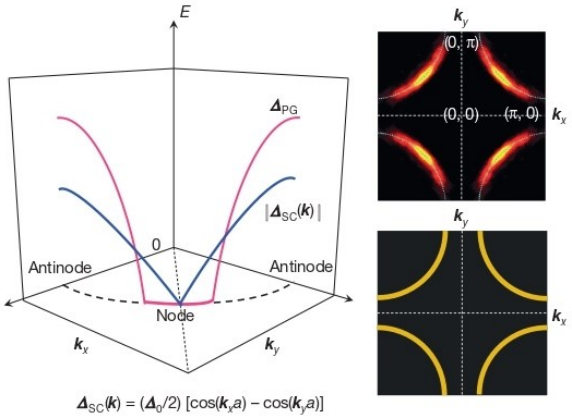

Figure 1.8. Fermi surface, Fermi arc and gap functions. The large Fermi surface predicted by band theory is observed by ARPES and scanning tunnelling spectroscopy (STS) for overdoped compounds (bottom right). But once the pseudogap sets in, the antinodal regions of the Fermi surface near the Brillouin zone edge are gapped out, giving rise to Fermi arcs (top right). This is reflected in the angle dependence of the energy E of the superconducting gap Δ_{sc} (blue line) and pseudogap Δ_{PG} (red line), as functions of the momenta $\boldsymbol{k_x}$ and $\boldsymbol{k_y}$ in one quadrant of the Brillouin zone around the underlying large Fermi surface (dashed line) as revealed by ARPES and STS [5].

Looking at the most important difference among the two phase diagrams in Fig. 1.7, there are many unsolved questions [2, 5, 20] concerning the pseudogap in hole-doped cuprates: what is its cause, how does it relate to and interact with the superconducting gap, where does T^* goes to zero (a potential quantum critical point) as a function of doping? Despite an enormous amount of data and theoretical models, there exist no consensus. Furthermore, there is the matter of debate whether the T^* line indicates a phase transition or a crossover, with the existence of the low-temperature pseudogap regime T^{**} ($T_c < T^{**} < T^*$), presenting other competing orders (that is, patterns of some broken symmetry). We here briefly also observe that, recently, many remarkable experiments have revealed the nature of this possible low-temperature pseudogap regime $T^{**}(T^{**} < T^*)$, where a number of broken symmetries have, in fact, been observed [2, 5, 20]:

1. Spin-flip neutron scattering experiments on underdoped YBCO, Hg1201, and Bi2212 indicate intra-unit cell time-reversal symmetry breaking ($q = 0$ antiferromagnetic order), supposedly arising from counter-circulating orbital current inside the unit cell.

2. Scanning tunnelling spectroscopy (STS) also suggests a rotational symmetry breaking inside the unit cell ($q = 0$ "nematic" order), and this nematicity is ascribed to electronic inequivalence of the two oxygen atoms, $O2p_x$ and $O2p_y$, in the unit cell. However, these STS result, indicating a complete loss of coherence in the antinodal region, appears to be inconsistent with the ARPES, which sees antinodal quasiparticles below T_c, even for underdoped materials.

3. As depicted in Fig. 1.7a, the Mott physics and the short-range antiferromagnetic correlations inherited from their undoped parent compound combine to produce a local tendency to phase separations and various forms of order, which spontaneously break the translational symmetry of the underlying crystal. This is especially true in the pseudogap phase of the phase diagram, where it is unsurprising that various forms of order occur on intermediate length scales. The incommensurate spin and charge fluctuations/short-range order develop within the pseudogap regime, as $T_{C,onset}$ and $T_{S,onset}$[4] are significantly lower than T^*. There appears also a crossover between antiferromagnetic and superconducting phases, with a sort of "spin glass" region, and it has been firmly established [13], that it is a dome-shaped crossover, quite distinct from the superconducting dome, around doping $p\sim 1/8$. Pseudogap and d-superconductivity gap coexist in a non-trivial manner: given that there is no evidence that the superconductivity gap energy scale is diminished by the presence of pseudogap, it is likely that pseudogap is also home to superconductivity pairing correlation. In fact, for a range of temperature $T_c < T < T_{SC,onset}$[5] $< T^*$ a fairly large diamagnetism and sizeable fluctuations conductivity are observed in the pseudogap regime. Another evidence for local phase coherence is that the interlayer Josephson plasma resonance within a bilayer in YBCO persists up to $T\sim T_{SC,onset}$: $T_{SC,onset}$ is comparable with the onset of the charge fluctuations $T_{C,onset}$, and both show similar doping dependence: hence, pseudogap could not be necessarily a competing order of d-superconductivity, but appears to be home to various orders, including superconductivity. Note that the maximum T_c value of 164 K achieved at high pressure is also comparable to these two temperature scales. In the theoretical approach discussed in Chapter n. 4 we will recall the crossover line $T_{SC,onset}$, dome-shaped above the dome of the superconducting transition, signaling the onset of a Nernst signal[6], due to magnetic vortices and diamagnetism. This Nernst crossover line seems also to be universal in the cuprates, and a large Nernst signal has been indeed taken to provide evidence of well-defined vortices above T_c [81, 82]: these vortices drift along the thermal gradient and produce the phase winding, which indeed supports a transverse voltage by the Josephson effect.

[4] $T_{C,onset}$ and $T_{S,onset}$ indicate when precursor charge density wave and spin density wave orders, respectively, become apparent [4].
[5] $T_{SC,onset}$ indicates when precursor superconductivity order becomes apparent [4].
[6] The Nernst signal is the voltage transverse to a thermal gradient in the presence of a magnetic field perpendicular to the plane.

Thus the pseudogap regime exhibits discrete broken symmetries (lattice rotations, time-reversal, ecc.) over roughly the same region of the phase diagram over which there is the antinodal gap in the spectrum: Luttinger's theorem implies that none of these broken symmetries can explain the needed fermionic gap by themselves. The coexistence of the antinodal gap and the broken symmetries can perhaps be explained by intertwining them, i.e. by exploiting "flavours" of topological order which are tied to specific broken symmetries [21].

The experimental results summarized above, and their interpretations have been a matter of debate; furthermore, it appears difficult for the $q = 0$ order to create such a large gap, which may be rather linked to some local/fluctuating pairs, as we will discuss in Chapter n. 3. In fact, a more systematic study [22] has now made it quite clear that the somewhat fragile charge order density wave itself cannot be responsible for causing the pseudogap; it possibily arises at low temperatures out of the normal pseudogap phase with no broken symmetry. However, in this paper we will not discuss about competing orders (charge density wave order – CDW, spin density wave order – SDW, stripe order, ecc.), given by broken symmetries presented above. Broadly speaking, theoretical approaches for characterizing the pseudogap can be classified into two major hypotesis [22-25]:

I. The pseudogap is derivated from the superconducting pre-pairing: first the Cooper pairs are formed at higher temperature than T_c (that is $T_c < T < T^*$), but, because of the large phase fluctuations, cannot be coherent and only start being coherent at a lower temperature T_c: in this setting, the pseudogap is actually the same as the superconducting gap: see Fig. 1.9a for the relative possible phase diagram [25].The antiferromagnetic correlations are precursors to the appearance of antiferromagnetic, superconductivity and charge density wave phase, and also of other conventional order at low temperatures. Then in the pseudogap regime we have primarily thermal and classical, rather than quantum, fluctuations of these orders. This raises an immediate question: why do not other unconventional superconductors, many of which have a robust antiferromagnetic phase, also display a pseudogap behavior due to the precursor thermal fluctuations? And what is so different about the hole-doped cuprates?

II. Another approach is the one we will discuss in Chapter n. 3: the build-up of antiferromagnetic correlations/fluctuations and the opening of a spin-gap at T^* signal the onset of quantum spin liquid. As a function of decreasing temperature, there could be multiple crossovers within the metallic spin liquid, and there could also be instabilities to other symmetry-broken phases at lower temperatures. In order for this to be a useful characterization, there should be remnants of the topological order of this spin liquid at higher temperatures: here by topological order we mean states with emergent gauge excitations (for states with an energy gap, there are non trivial ground states degeneracies

on a torus, as we will see in Chapter n. 2). In this approach one possibility is the presence of closed Fermi pockets, which violate the Luttinger's theorem, constraining the total area enclosed by the Fermi surface, and this may be related to photoemission spectra which have intensity only on open arcs in the Brillouin zone. Thus the pseudogap regime at high temperature is a novel quantum state which, with moderate changes, could be stable at low temperatures for suitable model Hamiltonian, as we will discuss in Chapter n. 3, where we will consider the fractionalized Fermi liquid FL*, as a candidate which could fullfill the requirements for the pseudogap regime, as a quantum state with long-lived electron-like quasiparticles around a Fermi surface of size given by the hole doping p, even though such a Fermi surface would violate the Luttinger relation of a Fermi liquid. Clearly in this approach the pseudogap is not related to superconducting pairing, i.e. it has another origin, and, because it is competing with superconductivity, the pseudogap phase can extend into the superconducting phase (see Fig. 1.9b for the relative possible phase diagram), presenting, as anticipated above, a possible quantum critical point (QCP) at $T = 0$.

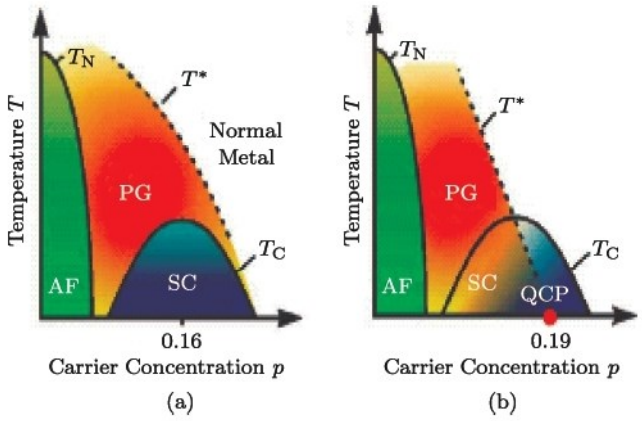

Figure 1.9. Pictures for the pseudogap in the normal state as a function of temperature T and hole doping p. (a) Pseudogap and superconducting phases with the same gap. (b) Pseudogap phase in competition with, and extending into, the superconducting phase, with a quantum critical point at $T = 0$ [25].

Though both scenarios seem radically different, they do have a point in common, in that the nature of the pseudogap phase below T^* determines the origin of the superconducting state. The different gap momentum dependence at different temperatures seen above, suggests that the pseudogap is more than a simple extension of the superconducting gap; additionally, low-energy spectral weight analysys near the antinode shows a competing relation between the pseudogap and superconductivity [27]: such a distinction is also confirmed by the distinct doping dependence of the low-energy spectral weight near the node and the antinode, as depicted in Fig. 1.8, which shows the potentially different nature of the high-energy pseudogap from fluctuating superconductivity. These considerations may lead to the postulation of pseudogap being a crossover phenomenon, as we will discuss in the next chapters, also considering hypothesis II (Fig. 1.9b) as the actual one for the phase diagram of hole-doped cuprates.

Chapter 2
Luttinger's theorem: from Oshikawa's argument and topological order to fractionalized Fermi liquid FL*

2.1 Luttinger's theorem: a nonperturbative approach

We know that free electrons in a translationally invariant system form a Fermi sea, and interacting electrons may be described by Landau's Fermi liquid theory, which when applicable states that interactions between electrons do not qualitatively modify the free electron picture, at most dressing the electrons as quasiparticles, which are fermions with renormalized quantities, such as mass. One of the most fundamental results of the Fermi liquid theory is the Luttinger's theorem [12], which states that the volume inside the Fermi surface is left invariant by the interaction, if the number of particles gets fixed. Luttinger's original proof was based on the perturbation theory, so Luttinger's theorem could be violated by nonperturbative effects, while, on the other hand, such nonperturbative effects could violate the Fermi liquid theory itself. In Appendix A.1 we report a synthesis of the elegant nonperturbative argument demonstrating the Luttinger's theorem, started by Oshikawa [15], and revisited in more recent papers [16-18, 28-32]. Oshikawa's argument does apply to a very wide range of lattice models, including the Hubbard and the t-J models, for which the violation of the Luttinger's theorem has also been proposed. In these cases a possibility is that the violation of the Luttinger's theorem requires the system to be a non Fermi-liquid, but we know that this is not sufficient, as the Tomonaga-Luttinger liquid in one dimension does satisfy the Luttinger's theorem, even not being a Fermi liquid. Another possibility is that the experimentally measured Fermi surface could be different from the true Fermi surface defined in the low-energy limit, to which Oshikawa's argument applies, thus getting the claimed violation of Luttinger's theorem as incorrect. In Oshikawa's proof we obtain that the Fermi volume V_F of the emergent (spinful) quasiparticles is precisely determined by the filling fraction υ of the underlying electrons per unit cell [15, 17, 29]:

$$\upsilon = 2\frac{V_F}{(2\pi)^2}(mod\ 2) \qquad (2.1)$$

where the relation holds modulo an integer, physically representing the number of filled bands. This relation might be one of the first examples of "topological quantization" discovered in quantum many-body problems, although the topological understanding has been missing for a long time. In fact, despite the complexity of the interacting many-body states, some physical quantity takes a special value, which is stable against various perturbations, such as interaction strength, and

presumably the most natural understanding of such a quantization is given by a trivial topological order. Therefore, this Oshikawa's argument implies that violation of the Luttinger's theorem should be accompanied by the presence of a non trivial topological order.

2.2 Topological enrichment of Luttinger's theorem

2.2.1 The concept of topological order. The concept of topology has revolutionized condensed matter-physics: it reveals that the classification of different phases can extend beyond the Landau-Ginzburg-Wilson (LGW) paradigm of classification by symmetry, generating a variety of new phases with topological characters [74, 75, 76]. We know indeed that the traditional theory of phase transitions relies crucially on symmetry, and that a central concept is that of the "order parameter". The traditional guiding principle behind the LGW theory of critical phenomena is the association of the critical singularities with fluctuations of an order parameter that encapsulates the difference between the two phases on either side of the critical point, and these critical singularities are thus associated with long-wavelength low-energy fluctuations of the order parameter degrees of freedom. However in recent years the development of a number of new theoretical concepts and many experimental results have provided additional means for classifying phases of matter beyond the LGW paradigm: the natural field theoretical description of their phase transitions and critical singularities is not in terms of the order parameter, that describes the bulk phases, but in terms of new degrees of freedom specific to the critical point. These different degrees of freedom may be thought of fractional quantum number particles that interact with each other through an emergent gauge field. This includes the discovery of topological phases, which respect all symmetries of a underlying Hamiltonian of the system, yet are distinguished from their topologically trivial counterparts through intricate structures in their quantum mechanical ground-state wave function. In this thesis we will indeed discuss how in the pseudogap phase of hole-doped cuprates the topological order associated with emergent gauge fields could also require a phase transition between states which cannot be distinguished by symmetry. We have just seen in section 2.1 and Appendix A.1 how the Luttinger theorem has a trivial topological character, and we will see below how it is possible for non trivial topological order associated with emergent gauge fields to change the volume enclosed by the Fermi surface. So we can have a phase transition associated with the onset of topological order, across which a Fermi surface reconstructs, even though there is no symmetry breaking on either side of the transition. Furthermore, we can make another notable observation: fractionalization of quantum numbers has been a focus of condensed matter physics, as it it refers to the emergence of a collective excitations having fractional quantum numbers with respect to the elementary particles, such as electrons, in a strongly correlated systems. While the details naturally depend on each model under consideration, the structure of the excitations spectrum is efficiently described in terms of a gauge theory, that is the excitations consist of objects that have long ranged nonlocal statistical interactions with each other, as an Aharonov-Bohm gauge interaction. This emergent gauge structure implies the

existence of a kind of topological order associated with the global properties of the ground-state wave function: in other words the fractionalized excitations carry charges w.r.t. the deconfined emergent gauge fields, in any effective theory we could consider on the bulk[7] of the of the materials under study. A typical signature of the topological order is the ground-state degeneracy depending on the topology of the system, and this cannot be understood as a consequence of a conventional spontaneous symmetry breaking, which is the standard mechanism behind the ground-state degeneracy. We have discuss in the previous chapter that a key issue for solving the high-T_c problem in the cuprates is to understand the normal state above T_c: only after well understanding this state, we can start to address what causes its instability above T_c toward superconducting state. Particularly, as we will see in Chapter n. 5, looking at the ARPES experiments above T_c, the pseudogap does not have the large Fermi surface enclosing the total number of electrons, which we would expect from the Luttinger's theorem: instead, it has Fermi arcs and small Fermi surfaces observed in quantum oscillation measurements [10, 35, 56]. Many efforts have been made trying to rescue the Luttinger's theorem in the pseudogap phase: most among them introduce long-range orders breaking the translational symmetry, to cut the large Fermi surface into small pieces, but we have just anticipated in the previous chapter (pag. 14) that in experimental results in pseudogap regime, no translational symmetry breaking is found as to give a satisfying explanation for the violation of the Luttinger's theorem. First examples of fractionalized Fermi liquid, having fractionalized excitations that coexist with conventional Fermi-liquid-like quasiparticle excitations, has been considered studying heavy-fermion models [16, 18]: in such phases a gapless Fermi liquid coexists with nontrivial topological order, and it has been demonstrated that a generalized version of the Luttinger's theorem as Eq. 2.1 even holds. This generalization to Luttinger's theorem can exactly be determined from the interplay of the symmetry with the topological order [Appendix A in 16, 17, 29].

2.2.2 Symmetry-enriched topological (SET) phases. The higher dimensional generalizations of the Lieb-Schultz-Mattis (LSM) theorem by Oshikawa [14] and Hastings [30], show that 2D systems with translationally invariant spin and an odd number of $S = 1/2$ moments per unit cell cannot have a symmetric, gapped and non-degenerate ground-state: *these systems must either have a continuum of low energy excitations (thus having a gapless phase), or spontaneously break some simmetries, or exhibit topological order with anyonic[8] excitations* [31]. The LSM theorem is remarkable because a microscopic property (the spin within a unit cell), constraints the universal long-wavelength physics in a non trivial way. Similar constraints as those required by the LSM theorem have been discovered to arise at the surface of symmetry-protected topological phases (SPT phases) [31]. Such phases are short-range entangled states that cannot be adiabatically connected to a trivial product state while preserving the symmetries of the system: an SPT phase can thus be seen as a generalization of a

[7] In this thesis we are not focusing on topological insulators and superconductors, where the topological order is associated with protected electronic states on their boundary, while the bulk contains only trivial excitations.

[8] Anyons are quasiparticles that occurs only in 2D systems, characterized by having an exchange statistics with a phase factor $e^{i\theta}$, that can assume other values than just +1 for bosons and -1 for fermions have in 3D systems

topological insulator. In general, the surface phases at the boundary of a SPT phase must also be either symmetry broken, gapless, or gapped with nontrivial "surface topological order", thus mirroring the three options allowed by the LSM theorem. In the case where the 3D SPT phase possesses surface topological order and preserves the symmetries, the 2D surface states are anomalous symmetry-enriched topological phases (SET phases): such phases are anomalous in the sense that they cannot be consistently realized in purely 2D systems when the symmetry is realized in a local manner, but there is an understanding even in theories of purely 2D SET phases with translational and on-site unitary symmetries, as hole-doped cuprates. For our purposes it is sufficient to say that [31] a purely 2D gapped and symmetric phase must have nontrivial topological order when the microscopic degrees of freedom transform as a nontrivial projective representation of the on-site symmetry for each unit cell, thus providing restrictions on the type of 2D SET order allowed. Thus, when a system with fractional symmetry charge per unit cell is gapless, there must also be constraints on the resulting phase: the Luttinger's theorem is an example, as, at filling υ, the volume of the Fermi sea, i.e. the volume enclosed by the Fermi surface, is proportional to υ. We can thus say that a symmetric system with topological order can manifest distint SET phases, which cannot be adiabatically connected to each other while respecting the symmetry. We can distinguish these phases by symmetry fractionalization, that allows quasiparticles to carry fractionalized quantum numbers of the symmetry.

2.2.3 Symmetry fractionalization and modified Luttinger's theorem. Let us now see how Luttinger's theorem may require modification for a fractionalized Fermi liquid, i.e. a Fermi liquid that is accompanied by SET order, thus making possible to apply Oshikawa's argument (see Appendix A.1) to 2D systems with general SET order. Symmetry fractionalization refers to the manner in which topological nontrivial quasiparticles carry quantum numbers of the underlying local constituents of the system, such as electrons or spins. Studying the interplay between symmetries, topological order and the Fermi sea we can derive (see Appendix A.2 for the details) a topologically generalization of Luttinger's theorem for fractionalized Fermi liquid [29, 31, 32], where υ_{topo} is the filling fraction of the SET sector

$$\upsilon - \upsilon_{topo} = 2\frac{V_F}{(2\pi)^2}(mod\ 2) \qquad (2.2)$$

We consider a system with an on-site $U(1)$ symmetry (which may be a subgroup of the full symmetry group, i.e. it can be the $U(1)$ associated with particle number conservation or $U(1) \subset SO(3)$ associated with spin rotational symmetry), and $\mathbb{Z}^2$ translational symmetry (i.e. the translational symmetry group $\mathbb{Z} \times \mathbb{Z}$ generated by the translational operators T_x and T_y along the x, y directions), surely comparable to hole-doped cuprates. We can show that (referring to Appendix A.2 for details):

- $U(1)$ symmetry fractionalization leads to quasiparticles with fractional charge, that is fractionalization classes by an anyon v, which is just the quasiparticle created by threading a 2π $U(1)$ flux in the system, as seen in the Oshikawa's argument in section 2.1. Thus we can consider the 2π-flux threading as gauge equivalent to create an anyon v-loop that wraps around the handle: in other words it looks as the 2π-flux is "divided" into fractional charges Q_{a_j} carried by the a_j anyons: the anyon a_j has a possibly fractional charge Q_{a_j}, which is given by the relation

$$e^{i2\pi Q_{a_j}} = \mathcal{M}_{a_j,v} \qquad (2.3)$$

- The mutual braiding anyonic statistics $\mathcal{M}_{a_j,v}$ between v and an excitation carrying topological charge a_j, through Eq. (2.3) determines the fractional $U(1)$ charge Q_{a_j} of a_j.
- In other words, adiabatically threading the 2π flux results in the anyonic excitation called the "vison" v, and the mutual braiding anyonic statistics between v and an excitation carrying topological charge a_j determines the fractional $U(1)$ charge of a_j through Eq. (2.3).
- $\mathbb{Z}^2$ symmetry fractionalization leads to fractionalization classes by an abelian anyon $\mathfrak{b}$, that physically can be thought as the background anyonic v-flux per unit cell of the torus (and it is visualized for simplicity in the center of the unit cell as depicted in Fig. A.2 in Appendix A.2). Moreover, the symmetry operation $T_y^{-1}T_x^{-1}T_yT_x$ is a sequence of translations corresponding to path that encloses one unit cell in a counterclockwise way, and this corresponds to the anyon v encircling the anyon $\mathfrak{b}$ in a counterclockwise fashion (in other words, transporting an anyon v around a unit cell gives to the wavefunction a phase corresponding to braiding the anyon v around the anyon $\mathfrak{b}$).
- We can thus conclude that there is an anyon $\mathfrak{b}$ per unit cell, whose fractional $U(1)$ charge is equal to the filling factor υ, that is $\upsilon = Q_{\mathfrak{b}} \equiv \upsilon_{topo}$, see Eqs. (2.2) and (A.38). Quasiparticles that carry topological charges $Q_{\mathfrak{b}}$ are called "spinons".
- We assume it is possible to consider separately the effect of flux threading on the SET sector, corresponding to wrapping a v-loop around the handle of the torus, and on the Fermi liquid sector, corresponding to "boosting" the Fermi sea as seen in the Oshikawa's argument. This crucial assumption means that topological and gapless excitations coexist, but are effectively decoupled from one another.

Thus we can obtain Eq. (2.2), which relates microscopic and emergent properties of the system, and can be viewed as a constraint on the allowed SET order that may exist at a given filling. Furthermore, we underscore that one of the characteristic features of topologically ordered states of matter in two dimensions is the presence of anyons, quasiparticles excitations with nontrivial braiding statistics. Another important feature is quantum number fractionalization: if some degree of symmetry is present, the anyons can carry fractional quantum numbers. *Thus for 2D systems there is a precise general definition of* υ_{topo}*: it is just the* $U(1)$ *charge of the background anyonic flux per unit cell that is specified by SET order*. Indeed, Eq. (2.2) states that the underlying degrees of freedom,

"transporting" topological order, should not contribute to the Fermi volume. Moreover, a consequence is that experimental observations of a Fermi volume that deviates from that of an ordinary Fermi liquid may point to the existence of a fractionalized Fermi liquid phase, as we are seeking in order to give an explanation to the experimental results, showed in Chapter n. 5, on the Fermi surface in the pseudogap of hole-doped cuprates. The SET order that is allowed for a given deviation results also constrained by the corresponding value of v_{topo}.

2.3 Introduction to FL* in hole-doped cuprates

From here to now, we return to discuss the specific case of hole-doped cuprates, appointing the fractionalized Fermi liquid seen until now as FL*, that we recap is a state with fractionalized excitations that coexist with conventional Fermi liquid-like quasiparticle excitations, and that satisfies the topological modification of the Luttinger's theorem seen above. We anticipate how the FL* metal can be simply viewed in terms of the two nearly decoupled elements, a small Fermi surface of conduction electrons and a spin liquid of the half-filled-band, thus being contrasted from the conventional Fermi liquid, in which there is a large Fermi surface, whose value counts both the conduction and d-electrons. Thus, as we will discuss in chapter n. 3 looking at a model by Sachdev, it could be possible to explain the pseudogap phase of the underdoped hole-doped cuprates as a FL* metal, considering the experimental results seen in Chapter n. 5, the results obtained in sections 2.1-2.2, Appendix A.1 and A.2, and the following considerations:

- The FL* phase is a metal [33] which breaks no symmetries, but differs from the conventional Fermi liquid in two crucial ways:
  - The FL* phase has gapless $S = 1/2$, charge $+e$ quasiparticle excitations, just like a Fermi liquid, but the number of these excitations is different: in a Fermi liquid the gapless quasiparticles lie on a Fermi surface which encloses a large volume equal to the total density of electrons (this is the familiar Luttinger's theorem). In contrast, in a FL* phase, the Fermi surface of electron-like excitations has a volume which differs from the total density by one electron per unit cell, and this leads to the small Fermi surface pocket, which now violates the conventional Luttinger relation.
  - In a Fermi liquid the quasiparticles around the Fermi surfaces are the only low energy excitations, while the FL* phase has also neutral $S = 1/2$ spinons, and associated gauge excitations.

- The FL* might resemble a usual Fermi liquid in terms of its transport and thermodynamical properties, but it violates Luttinger's theorem on the area enclosed by the Fermi surface, and this is closely linked to the presence of emergent excitations belonging to a gauge sector, and also to the presence of topological order as seen in section 2.2.

- The FL* has pocket Fermi surfaces with low intensity in the back-sides, because a small, but non zero, quasiparticle residue [34]: this is presumably the reason only Fermi arcs have been detected by photoemission so far. Fermi surface probes which do not involve adding or removing an electron could provide detection of the full pockets.

Because all of the considerations made until now, in the next chapter we will discuss how the FL* phase described here could be a candidate for the pseudogap regime of the hole-doped cuprates, in terms of an $SU(2)$ gauge theory and a Higgs' transition to a $U(1)$ or other subgroups. This could make us review Eqs. (2.1) and (2.2) for the specific cases of normal and pseudogap regimes in the phase diagram of hole-doped cuprates, with hole doping given by p, so that $n_e = (1-p)$ is the electronic density [28, 29]:

a) For the Fermi liquid and strange metal phases, we have the quantized volume V_F (volume occupied by the electrons in the **k**-space) defined by the usual Luttinger's theorem, so Eq. 2.2 becomes, as there is no topological order, thus with $v_{topo} = 0$

$$2\frac{V_F}{(2\pi)^2}(mod\ 2) = v = n_e \qquad (2.4)$$

Eq. (2.4) ideally corresponds to the large hole-like Fermi surface, enclosing an area proportional to $(1+p)$ seen by ARPES in Fermi liquid and strange metal phases.

b) As anticipated above, we will see in the next chapter that the underdoped cuprate may be described as a doped Mott insulator: in this model the doped Mott insulator is seen just as a Fermi liquid of p holes moving in a background with local antiferromagnetic order, just a topological order, so Eq. 2.3 becomes, with a nonzero value of v_{topo}:

$$-2\frac{V_F}{(2\pi)^2} mod\ 2\ = (n_e - 1) = -p \Rightarrow 2\frac{V_F}{(2\pi)^2} mod\ 2\ = p \qquad (2.5)$$

With the minus sign in the l.h.s. is for hole pockets, Eq. (2.4) thus seems to correspond to the small Fermi pockets, enclosing an area of order p, seen by ARPES in the pseudogap phase, also resembling how in this phase the Fermi surface of electron-like excitations has a volume differing from the Fermi liquid and strange metal phases by one electron per unit cell.

In Chapter n. 5 we will discuss on some recent experimental results that seem to confirm these conclusions.

2.4 General topological considerations on Luttinger's theorem

As seen above, with Eq. (2.2) we have obtained a topologically enriched version of Luttinger's theorem, exactly as with Eq. (2.1) we have obtained a nonperturbative demonstration of the Luttinger's theorem, that we can also rewrite, in its "hard" variant, as

$$v = 2 \int_{G(\omega=0,\boldsymbol{k})>0} \frac{d^D \boldsymbol{k}}{(2\pi)^D} \qquad (2.6)$$

being invariant with respect to the particles interaction, where $G(\omega, \boldsymbol{k})$ is just the single-particle Green's function (its "soft" variant corresponds to systems where the right-hand site of Eq. (2.6) corresponds to some fraction of the total non-interacting density). We have just discussed in Chapter n. 1 how in the pseudogap phase of hole-doped cuprates we lack a conventional Fermi surface, and we will see in Chapter n. 5 some relative ARPES experimental results: this includes the possible presence of a Luttinger surface, which corresponds to zeroes of the interacting Green's function $G(\omega, \boldsymbol{k})$. It has been demonstrated [71] that a hard Luttinger's theorem in a D-dimensional system is directly dependent on the existence of a $(D-1)$-dimensional manifold of gapless chiral excitations at the Fermi level, regardless of whether the system exhibits Luttinger (manifolds of zeroes of the Green's function) or Fermi surfaces (manifolds of zeroes of the inverse Green's function). This result is obtained by defining a generalized Fermi surface in terms of a non-zero topological index, so reprising the topological nature of the Luttinger's theorem presented in this Chapter [15, 17, 29], and showing what properties the propagator $G(\omega, \boldsymbol{k})$ must have to ensure the Fermi volume remains invariant as interactions become arbitrary large. Such an analysis allows us to write down the exact form of the self-energy $\Sigma(\omega, \boldsymbol{k})$ that simultaneously satisfies Luttinger's theorem, while also entailing the existence of a Luttinger surface: if $Im\ \Sigma(\boldsymbol{k}, \omega \to 0) \sim \omega^{\alpha}$, with $\alpha < 1$, then either a gap opens (for $\alpha < 0$), or the density of states become discontinuos (for $0 < \alpha < 1$). The power α is a function of doping , with $\alpha > 1$ corresponding to the overdoped metallic phase, $\alpha \approx 1$ to the optimally-doped strange metal/marginal Fermi liquid phase, and $0 < \alpha < 1$ to the underdoped pseudogap phase. This behavior is even supported experimentally in ARPES data, confirming that the overdoped phase respects Luttinger's theorem, while the underdoped pseudogapped phase violates it [71]. Not going into detail in this analysis, we will remind this condition in the next Chapter, in section n. 3.3 when we will discuss the electronic spectral weight and the retarded electronic self-energy at the antinodal point obtained from the $SU(2)$ gauge theory that will be presented.

Chapter 3

FL* in cuprates by Sachdev and collaborators

In this chapter we discuss a theory trying to explain the pseudogap phase of hole-doped cuprates as a FL*: this FL* phase inherits the global topological excitations from a spin liquid, where these excitations are associated with the emergent gauge fields present in a theory of deconfined spinons. Let us note that this FL* phase has, as seen above, small pocket Fermi surfaces, enclosing the same total volume as those in the antiferromagnetic phase of hole-doped cuprates, but the antiferromagnetic phase does not possesses topological excitations, because of the doubling of the unit cell by the antiferromagnetic order, so this phase obeys in usual way the Luttinger's theorem. In fact, in the antiferromagnetic phase, the Fermi pockets are created by Bragg reflection of the Fermi surface across the magnetic Brillouin zone boundary, where these pockets are centered on, as depicted in the left image in Fig. 3.1. The phenomenological field theory that we are going to discuss in this chapter will lead to the Fermi pockets of the FL*-pseudogap as depicted in the middle image in Fig. 3.1. We can note that in this phase there is full symmetry of the square lattice and the magnetic Brillouin zone boundary plays no special role: consequently, the Fermi (hole) pockets are centered at a generic point in momentum space, which generally does not lie on the magnetic Brillouin zone. This theory yields a metallic state with the same basic characteristics of the FL* phase: we will show how arguments based upon symmetry and gauge invariance allow the construction of an effective theory for the electron spectrum, containing a number of coupling constants, whose values should be determined by comparing to numerical studies or experiments. Such analysis will allows us to compute the Fermi surface structure, understand potential low temperature instabilities, and also possibly connect to other phases in the globale phase diagram of the hole-doped cuprates.

3.1 Field Theoretical Model – spin fluctuations density waves

The basic idea [8, 21, 22, 33, 34, 36-42, 73] of this model is that the large Fermi surface of the Fermi liquid phase is broken apart into pockets by local antiferromagnetic Néel order: we allow quantum fluctuations in the orientations of the Néel order, but without a global long-range order. Space-time "hedgehog" defects in the Néel order are suppressed, so that a spin liquid with bosonic spinons and a non compact $U(1)$ gauge boson excitation is realized (we will see details below). Alternatively, the Néel order could develop spiral spin correlations, and, suppressing $\mathbb{Z}_2$ vortices in the spiral order, could realize a $\mathbb{Z}_2$ spin liquid with bosonic spinons. In this process the Fermi pockets also fractionalize, and we are left with Fermi pockets of spinless fermions, with the resulting phase called the algebric charge liquid (ACL) [43, 44]. Depending upon the nature of the gauge excitations of the

spin liquid, the ACL can have different varieties: the $U(1)$-ACL and the $SU(2)$-ACL [36], and $\mathbb{Z}_2$-ACL descends from these by a Higgs transition involving a scalar with $U(1)$ charge 2. We will use a $SU(2)$ gauge theory of fluctuating antiferromagnetism in metals to describe the pseudogap phase of hole-doped cuprates, discussing how this theory yields a pseudogap metal only when the gauge group is "Higgsed" down to a smaller group, that is the $U(1)$-FL* state with bosonic spin liquid [39, 41, 42], having electron-like quasiparticles coupled to the fractionalized excitations of the fluctuating antiferromagnetism. We thus describe a phenomenological theory of the pairing of these quasiparticles, showing that a large class of mean-field theories generically displays the well known nodal-antinodal dichotomy: the interplay of local antiferromagnetism and pairing leads to a small gap near the nodes of the d-wave pairing along the Brillouin diagonals, and a large gap near the antinodal regions, as seen in experimental results in the superconducting phase.

We begin by first reviewing [22] the standard description for the evolution of antiferromagnetism in metallic phases of the one-band Hubbard model, which is believed, together with its strong-coupling variant, that is the t-J model, to contain the essentially physics of the cuprates [3]. For electron hoppings on the sites of a square lattice we have:

$$H_{HUB} = H_t + H_U \qquad (3.1a)$$

$$H_t = -\sum_{i<j} t_{ij}\left(c_{i\alpha}^{\dagger} c_{j\alpha} + h.c.\right) - \mu \sum_i c_{i\alpha}^{\dagger} c_{i\alpha} \qquad (3.1b)$$

$$H_U = U \sum_i \left(n_{i\uparrow} - \frac{1}{2}\right)\left(n_{i\downarrow} - \frac{1}{2}\right) \qquad (3.1c)$$

In Eqs. (3.1) t_{ij} represent the hopping parameters, U is the on-site Coulomb repulsion, μ is the chemical potential, $c_{i\alpha}$ and $c_{i\alpha}^{\dagger}$ are usual fermionic annihilation and creation operators for electrons (holes) with spin $\alpha = \uparrow, \downarrow$ (summation over repeated indices is implied). As the metallic state is near an antiferromagnetic instability, close to half-filling, we use the exact operator equation given for every site i, by:

$$U \sum_i \left(n_{i\uparrow} - \frac{1}{2}\right)\left(n_{i\downarrow} - \frac{1}{2}\right) = -\frac{2}{3} U \boldsymbol{S}_i^2 + \frac{U}{4} \qquad (3.2)$$

Where $\boldsymbol{S}_i = c_{i\alpha}^{\dagger}\left(\boldsymbol{\sigma}_{\alpha\beta}/2\right) c_{i\beta}$ ($\boldsymbol{\sigma}_{\alpha\beta}$ are the Pauli matrices). Upon decoupling the interaction via a Hubbard-Stratonovich transformation we obtain (with $\boldsymbol{J}_i$ as the bosonic field representing the local magnetization above the Néel order, that is, the collective modes associated with spin fluctuations over antiferromagnetic order)

$$exp\left(\frac{2}{3} U \sum_i \int d\tau \boldsymbol{S}_i^2\right) = \int D\boldsymbol{J}_i \; exp\left[-\sum_i \int d\tau \left(\frac{3}{8U}\boldsymbol{J}_i^2 - \boldsymbol{J}_i \cdot \boldsymbol{S}_i\right)\right] \qquad (3.3)$$

We can thus integrate out the fermions and look for the saddle point of the resulting action for $\boldsymbol{J}_i$: this leads to the Néel state with a wavevector $\mathbf{Q} = (\pi, \pi)$. In the long-wavelength limit, it is then useful to introduce a field $\boldsymbol{\varphi}_i$ so that

$$\boldsymbol{J}_i = \boldsymbol{\varphi}_i e^{i\mathbf{Q}\cdot\mathbf{r}_i} \qquad (3.4)$$

This is the familiar route towards arriving at the spin-fermion model (see Appendix B.1 for the detailed passages in order to obtain the insulating antiferromagnetic ordered phase as the ground state of the parent compound of hole-doped cuprates). However, to discuss the FL* we switch from the above description of spin density wave order by a "soft-spin" $\boldsymbol{\varphi}$-field with large amplitude fluctuations, to a "hard-spin" perspective in which we have primarily *angular fluctuations* of the antiferromagnetic order: so we replace $\boldsymbol{\varphi}$ by a unit vector field $\mathbf{n}$: it is an $O(3)$ field, which describes the local orientation of the antiferromagnetic Néel order at $\mathbf{Q} = (\pi, \pi)$, and obeying the local constraint $\sum_a (n^a)^2 = 1$.

In such a hard-spin theory, we argue that the evolution of the phases can be represented as in Fig. 3.1:

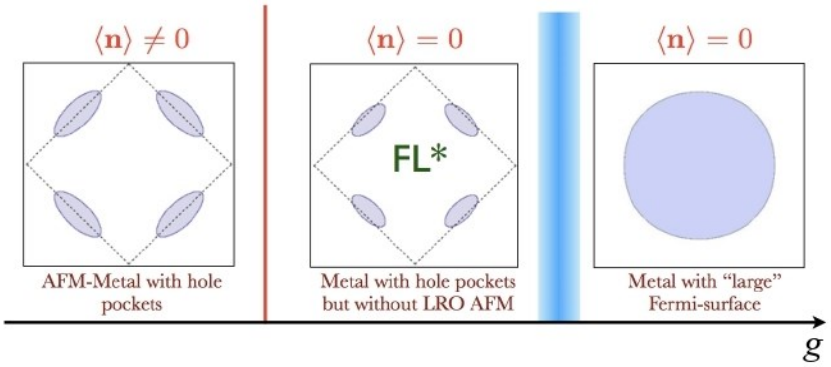

Figure 3.1 . Description for the loss of antiferromagnetic order in a metal in a theory with angular fluctuations of the fixed-length order $\mathbf{n}$. The middle phase is FL* [22].

We will see below the meaning of the parameter g, while in Fig. 3.1 the blue line represents a sort of quantum critical point (QCP) g_c, as for $g < g_c$ we have the metal with reconstructed hole pockets, and for $g > g_c$ we have the metallic Fermi liquid phase with a large Fermi surface. In Chapter n. 5 we will report recent experimental results, carried at the quantum critical point p^*, with the hole doping density p playing the role of g in the cuprates.

Let us write an explicit presentation of this theory of a metal with angular fluctuations of the antiferromagnetic order, where we are only interested in long-wavelength fluctuations of $\mathbf{n}_i$: indeed a key feature [34, 36] of our analysis is that we assume that it is only the spin density wave order n_i^a which varies slowly on the lattice scale: we do not make the same assumption for the fermionic field $c_{i\alpha}$, which is allowed to have a general dispersion over spatial coordinates $\mathbf{r} = (x_i, y_i)$ with arbitrary Fermi surface. Using τ to denote the imaginary time, β as the inverse temperature, we have the path integral of H_{HUB} from Eqs. (3.1) in the "spin-fermion" form as (see Appendix B.2 for detailed passages):

$$S = \int_0^\beta d\tau \mathcal{L}_{sf} \qquad \text{with} \quad \mathcal{L}_{sf} = \mathcal{L}_f + \mathcal{L}_n + \mathcal{L}_{fn} \tag{3.5}$$

$$\mathcal{L}_f = \sum_{i,j} c_{i\alpha}^\dagger \left[(\partial_\tau - \mu)\delta_{ij} - t_{ij} \right] c_{j\alpha} + h.c. \tag{3.6}$$

$$\mathcal{L}_n = \frac{1}{4g_0}\int d^2\mathbf{r}\left[\left((\partial_\tau \mathbf{n})\right)^2 + v^2(\nabla \mathbf{n})^2\right] \quad (3.7)$$

$$\mathcal{L}_{fn} = -\lambda \sum_i (-1)^{x_i+y_i}\, \mathbf{n}_i \cdot c^\dagger_{i\alpha}\boldsymbol{\sigma}_{\alpha\beta}c_{i\beta} \quad (3.8)$$

- Eq. (3.6) is the kinetic term for fermion fields $c_{i\alpha}, c^\dagger_{i\alpha}$ (annihilation and creation operators for electrons/holes as in Eqs. (3.1)), with spin $\alpha = \uparrow, \downarrow$, with t_{ij} as hopping matrix elements describing the large Fermi surface.
- Eq (3.7) represents the fluctuations of n_i^a, expressed by a continuum $O(3)$ nonlinear sigma model, where g_0 controls the strength of the antiferromagnetic fluctuations associated with the orientation of the n_i^a, and v is a spin-wave velocity.
- Eq. (3.8) describes how these fermions are coupled to fluctuations of the unit vector field n_i^a $(a = x, y, z)$, representing as seen above the local orientation of the collinear Néel order at wavevector $\mathbf{Q} = (\pi, \pi)$. λ is this spin-fermion coupling: here we will not expand in powers of λ, treating it as a coupling of order unity; instead our analysis will be in either the number of field component, or by small g_0 (remember, as seen above, that we will freely make a gradient expansion of n_i^a over spatial coordinates $\mathbf{r} = (x_i, y_i)$, focusing on the long wavelength fluctuations of the order parameter, while the fermion fields have important low-energy modes at many locations in the Brilllouin zone, and so we will not make any gradient expansion on the fermion operator). Generally in Eq. (3.8), instead of the term $(-1)^{x_i+y_i}$, there is a term as a fixed-form factor $f_i = \sum_m f_m e^{im\mathbf{Q}\cdot\mathbf{r}_i}$, determined by the particular nature of the spin density wave order: for the Néel order with wavevector $\mathbf{Q} = (\pi, \pi)$ we have $f_i \sim (-1)^{x_i+y_i}$, while for arbitrary commensurate $\mathbf{Q}$ we have $f_i \sim \sum_m f_m e^{im\boldsymbol{Q}\cdot\boldsymbol{r}_i}$, with m are integer numbers, and f_m are the coefficients determining the form factor

We have assumed g_0 as a generic coupling measuring the degree of frustration in the insulating antiferromagnet, which can drive the insulator into a non-magnetic state with valence bond solid (VBS) order across a deconfined quantum critical point: it is therefore useful to discuss [22, 33, 34, 38] in Fig. 3.2 the phase diagram of a generic class of frustrated doped antiferromagnets, as a function of the coupling g and the hole doping density p (also as a generalization of the description shown in Fig. 3.1):

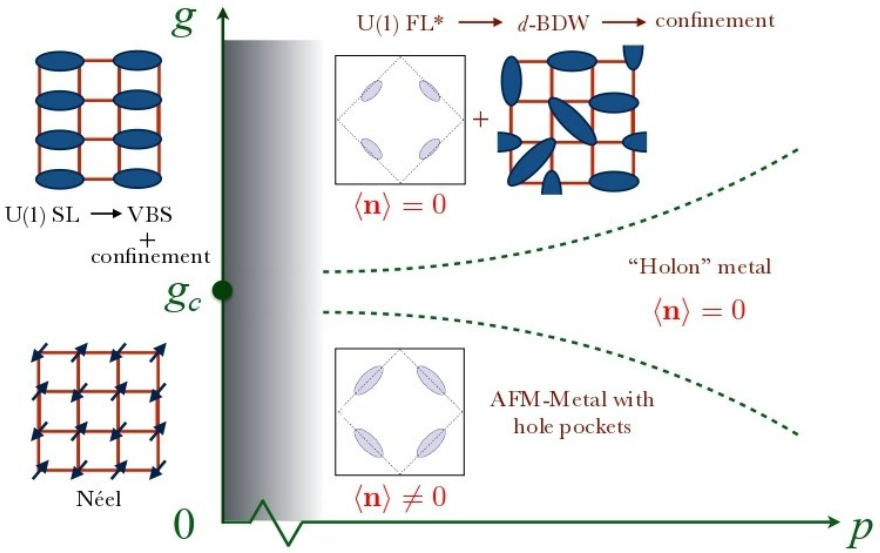

Figure 3.2. Vertical axis g represents some frustrating coupling in an insulating antiferromagnet which can drive it into a valence bond solid (VBS) across a deconfined quantum critical point at $g = g_c$ [22].

In Fig. 3.2, in the insulating phase, at doping density $p = 0$, the transition is between a Néel state and a VBS state, and we argue this transition can be described by the deconfined critical point g_c with the order parameter n_i^a, which can be [22, 33, 34, 36-38] replaced by a complex relativistic boson z_α carrying charges under an emergent $U(1)$ gauge field A_μ. Upon moving away from the insulator, we will see that, in the regime $g > g_c$, that we argue to be relevant for us, the fermions c_α can be replaced by fermions ψ_p, which do not carry spin but do carry a charge $p = \pm 1$ w.r.t. to $U(1)$ gauge field A_μ. In other words, for sufficiently small values of the coupling g_0, the model $\mathcal{L}_{sf}$ clearly has an antiferromagnetic order spin density wave (SDW) ground state with $\langle n^a \rangle \neq 0$; we are interested here in the mechanism by which this order is lost as g_0 is increased and a metallic state with no broken symmetries is obtained: in our view this transition involves intermediate non Fermi liquid phases before the large Fermi surface metal is reached at sufficiently large g, and the $O(3)$ order parameter n_i^a will be parameterized in terms of the spinon z_α. Moreover, this gauge field $U(1)$ has to be, as anticipated above, non compact: in fact the non compactness of the $U(1)$ gauge field leads to a description of the phases of the system with full monopole/hedgehog suppression within the CP^1 representation, leading to a topological conservation law and providing a rather precise characterization of a deconfined critical point. In other words the critical theory for the monopole/hedgehog suppression leads to the possibility of deconfinement of spinons, and the critical theory is expressed most naturally in terms of fractionalized degrees of freedom, clearly violating the LGW paradigm, as also anticipated in section 2.2.1 (we also refer to Appendix B.3 for the details) [74, 75, 76]. Thus in the phase diagram in Fig. 3.2 we will focus our attention to the $U(1)$ FL* region: in the resulting gauge theory z_α and ψ_p will bind to form gauge-neutral fermions of density p, which will form Fermi pockets in the Brillouin zone near, but not centered at $(\pm\pi/2\,;\pm\pi/2)$. The total area enclosed by these pockets is p, and hence the Luttinger volume of $(1 + p)$ is not obeyed, and

just a FL* phase is realized. In order to obtain this result, we transform the underlying electrons $c_{i\alpha}$ into new degrees of freedom which incorporate the change in the fermion band structure due to local spin density wave order in a more fundamental way: a new set of spinless fermions ψ_{ip} (holons), with their components $p = \pm 1$, corresponding to the two sublattices of the Néel state, polarized along the direction of the local spin density wave order. The key to do this is thus to transform the electron-spin polarization to a rotating reference frame set by the local orientation of the spin density wave order, thus allowing us to describe phases without long-range antiferromagnetic order in this way:

$$c_{i\alpha} = R^i_{\alpha p}\psi_{ip} \qquad (3.9)$$

In Eq. (3.9) we have:

- $R^i_{\alpha p}$ is a space-time dependent $SU(2)$ matrix ($R_i R_i^\dagger = R_i^\dagger R_i = \mathbb{1}$), which has $\alpha = \uparrow, \downarrow$ for the spin index, and $p = \pm 1$ for the gauge index introduced below.
- We can parameterize $R^i_{\alpha p}$ as (with $\sum_\alpha |z_{i\alpha}|^2 = 1$):

$$R^i_{\alpha p} = \begin{bmatrix} z_{i\uparrow} & -z^*_{i\downarrow} \\ z_{i\downarrow} & z^*_{i\uparrow} \end{bmatrix} \qquad (3.10)$$

From Eq. (3.9) we choose $R_{\alpha p}$ so that spin-fermion coupling is only along σ^z, and so, remembering the fluctuations of the unit vector field n_i^a in Eq. (3.8) we have:

$$n_i^a \left(R^i_{\alpha p}\right)^\dagger \sigma^a_{\alpha\beta} R^i_{\beta p'} = \sigma^z_{pp'} = p\delta_{pp'} \qquad (3.11)$$

Eq. (3.11) is equivalent to:

$$n_i^a = \frac{1}{2} Tr\left[\sigma^a R^i \sigma^z \left(R^i\right)^\dagger\right] \qquad (3.12)$$

Eq. (3.12) shows that the spin density wave order parameter n_i^a can be fully expresses in terms of the $SU(2)$ matrix R; moreover, Eqs. (3.10) and (3.12) yield the relation between the fields of the $O(3)$ NL sigma model and the $\mathbb{CP}^1$ model given by:

$$n_i^a = z^*_{i\alpha}\sigma^a_{\alpha\beta} z_{i\beta} \qquad (3.13)$$

Thus we have reformulated the spin-fermion model by replacing the electrons $c_{i\alpha}$ and the spin density wave order n_i^a by the spinless fermions (holons) ψ_{ip} and the complex bosonic spinons $z_{i\alpha}$, by the $SU(2)$ matrix R_i. We note that the representation in Eq. (3.9) introduces a $SU(2)$ gauge invariance given by (with V_i an $SU(2)$ gauge transformation acting on the right-index $p = \pm 1$ of $R_{\alpha p}$):

$$\psi_{ip} \to V_i \psi_{ip}; \qquad R_i \to R_i V_i^\dagger \qquad (3.14)$$

We can indeed introduce a $SU(2)$ gauge connection $A^a_\mu = (A^a_\tau, \boldsymbol{A}^a)$. Instead, the ordinary $SU(2)$ spin rotation acts on the left-index $\alpha = \uparrow, \downarrow$ of $R_{\alpha p}$, and rotates the direction of the physical electron and of the antiferromagnetic order (with U a global $SU(2)$ spin rotation):

$$c_{ip} \to U c_{ip}; \qquad R_i \to U R_i \qquad (3.15)$$

Thus, the fermions ψ_{ip} carry the physical $U(1)$ electromagnetical global charge, but not the $SU(2)$ spin of the electron: they are the fermionic holons of the theory: they have spin components polarized along the direction of the local spin density wave order, and finally their density is the same as that of physical electrons. The fractionalized spinons $z_{i\alpha}$ carry spin $S = 1/2$, and have neutral electromagnetical charge. We have seen in the previous chapter that a quantum-phase transition that does not involve broken symmetries is necessarily associated with a topological change in the character of the ground state wavefunction. Emergent gauge fields are thus a powerful method of describing this topological structure, and this remains applicable also to the gapless metallic phases of interest to us here. Given this important connection between emergent gauge fields and the size of the Fermi surface, we are thus led to a quantum phase transition with a change in the structure of the deconfined excitations, transforming non trivially under global gauge transformations. We can think to this change as a Higgs' transition [39, 41, 42, 73], intended as the breaking of a local gauge invariance: the presence of small Fermi surfaces, without symmetry breaking, requires the topological order and emergent gauge fields, and so also a Higgs' transition from the large Fermi surface at larger doping. Thus, considering the pseudogap phase as a $U(1)$-FL*, one can describe the evolution of this phase (and its small Fermi surface) to the conventional large Fermi surface at optimal and higher doping, by a $SU(2)$ gauge theory. Given this point of view, the transition from large to small Fermi surface can indeed be described by a Higgs' transition without any local order parameter, in which the emergent gauge structure, ruling the topological order in the ground state, changes from $SU(2)$ to $U(1)$. The Higgs field of this transition is a measure of the local antiferromagnetic correlations in a rotating reference frame. So we introduce the relativistic scalar Higgs field H_i, which measures the local spin density wave amplitude, and Eq. (3.8), which describes the coupling between this field and the ψ_{ip} fermions, can be written as a Yukawa term. Thus let us consider the more general $\boldsymbol{H} = (H_x, H_y, H_z)$, and remembering the parameterization $c_{i\alpha} = R^i_{\alpha p}\psi_{ip}$, we can write the term in the Lagrangian in Eq. (3.8) as

$$\boldsymbol{n}_i \cdot c^\dagger_{i\alpha}\boldsymbol{\sigma}_{\alpha\beta}c_{i\beta} \Rightarrow \boldsymbol{H}_i \cdot \psi^\dagger_{i\alpha}\boldsymbol{\sigma}_{\alpha\beta}\psi_{i\beta} \qquad (3.16)$$

Where we have defined the more general Higgs field $\boldsymbol{H}$ as

$$\boldsymbol{H}_i \cdot \boldsymbol{\sigma} \equiv \boldsymbol{n}_i \cdot R_i^\dagger \boldsymbol{\sigma} R_i \qquad (3.17)$$

Let us note that the Higgs field does not carry any spin, since it is invariant under global $SU(2)$ spin rotation, while it transforms under the adjoint[9] of the $SU(2)$ gauge, while the R spinons and the ψ_p holons transform as $SU(2)$ gauge fundamentals. We can also note that from Eq. (3.17) we can obtain that

$$H_i^a = \frac{1}{2} n_i^l \, Tr\left[\sigma^l R^i \sigma^a \left(R^i\right)^\dagger\right] \qquad (3.18)$$

[9] In fact, from Eqs. (3.14) and (3.18), we see that $\sigma^i H_i \rightarrow V_i \sigma^i H_i V_i^\dagger$, with V_i the $SU(2)$ gauge transformation.

$$n_i^a = \frac{1}{2} H_i^l \, Tr\left[\sigma^a R^i \sigma^l \left(R^i\right)^\dagger\right] \qquad (3.19)$$

This identifies H^a as the antiferromagnetic order in the rotating reference frame defined by Eq. (3.9), and only if

$$\boldsymbol{H} = (0, 0, 1) \qquad (3.20)$$

with the parameterization $c_{i\alpha} = R^i_{\alpha p} \psi_{ip}$, Eq. (3.19) yields again Eq. (3.13), that is $n_i^a = z^*_{i\alpha} \sigma^a_{\alpha\beta} z_{i\beta}$.

Let us summarize the work done until now, in order to better understand our final target: we are working with a $SU(2)$ gauge theory of fluctuating antiferromagnetism to describe the pseudogap phase of hole-doped cuprates: this theory describes fluctuations in the orientation of the antiferromagnetic order, while preserving a local, nonzero magnitude, and with emergent gauge fields which indicate the long-range quantum entanglement of the topologically ordered phase. This gauge theory formulation is required to keep proper track of the fermionic degrees of freedom, in the background of the fluctuating antiferromagnetic order. We have derived this theory from a lattice Hubbard model, and we are going to obtain a pseudogap phase with only small fermi surfaces (Fermi pockets), when the gauge group performs a Higgs' transition from $SU(2)$ down to the smaller $U(1)$ gauge, thus obtaining a metallic state with $U(1)$ topological order, and obtaining a theoretical connection with the results obtained in Chapter n. 2. Here we have to make a prominent observation, related to what seen in details in Appendix B.3 about the non compactness of the $U(1)$ gauge field: a key feature is given by Eq. (3.9), that is the transformation of the electrons and holes to a rotating reference frame in a state with fluctuating spin density wave order. However, this transformation is not always possibile without any obstacle, as shown in the simple example we can see in Fig. 3.3, where we consider a vortex defect in the antiferromagnetic spin density wave order, lying for simplicity in a single plane. In this case, we know that, upon parallel transport around such a vortex, the frame of reference is rotated by 2π, and a 2π rotation in the adjoint representation of $SU(2)$ maps to a double-valued spinor representation, thus the matrix R in Eq. (3.9) remaining not single-valued. Thus it is not possible to find a single-value transformation R to consistently define the fermions ψ_{ip} in the rotated reference frame around such a vortex via Eq. (3.9). We conclude that, in this easy plane spin density wave order, we can consistently transform the fermions $c_{i\alpha}$ into a rotating reference frame with uniform spin density wave order only if $\pm 2\pi$ vortices are expelled: in other words the fluctuating spin density wave order needs to have topological order with, at least, an emergent $\mathbb{Z}_2$ gauge field., while below we will discuss an unbroken $U(1)$ gauge group. This conclusion recalls what seen at pag. 24 about the necessity of the non compactness of the $U(1)$ gauge field in order to have a full monopole/hedgehog suppression [74-76] (see also Appendix B.3).

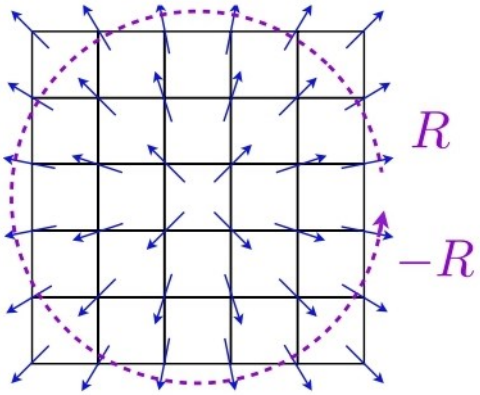

Figure 3.3. A vortex defect in the antiferromagnetic spin density wave order restricted for simplicity lying in a single plane. The staggering of the underlying spins, associated with $\eta_i = (-1)^{x_i+y_i}$, is not shown. The frame of reference, upon parallel transport around the vortex, is rotated by 2π, and thus the spinor field R changes sign [42].

Now we will present a mean-field computation of the electronic Green's function across the Brillouin zone in the $U(1)$ Higgs phase of the $SU(2)$ gauge theory, and such result can be compared with numerical computations [41] on the Hubbard model from the dynamical cluster approximation (DCA), a cluster extension of dynamical mean field theory (DMFT), and determinant quantum Monte Carlo (DQMC) calculations. Depending on the spatial configurations of the Higgs field, that is depending on the value of $\langle \boldsymbol{H}_i \rangle$, we could have different kinds of topological order, with residual group $U(1)$, $\mathbb{Z}_2$, or potentially also with broken discrete symmetries [36, 39, 41, 42]. In fact the phase with topological order is obtained simply by entering a Higgs phase with $\langle \boldsymbol{H}_i \rangle \neq 0$, while maintaning $\langle R_i \rangle = 0$: we indeed are considering states with local magnetic orientation whose orientation undergoes large quantum fluctuations, i.e. $\langle R_i \rangle = 0$, while the magnitude of the local magnetic order remains large, i.e. $\langle \boldsymbol{H}_i \rangle \neq 0$.

We will focus on the simplest case, as this scenario has the minimal number of independent parameters, only H_0, that can be adjusted to fit the numerical data and the experimental results: in fact, more complicated Higgs field configurations, with one or more additional parameters, leading to $\mathbb{Z}_2$ topological order, can indeed be treated similarly, even if the current momentum space resolution in DCA and DQMC computational results do not allow us to distinguish between the different phases. The case considered has thus the following simple features:

- No broken symmetries of the square lattice.
- $U(1)$ topological order, with the Higgs field resembling an antiferromagnetic order with

$$\langle \boldsymbol{H}_i \rangle = \eta_i H_0 \hat{\boldsymbol{e}}_z = \langle 0, 0, \eta_i H_0 \rangle^T; \quad \eta_i = (-1)^{x_i+y_i} \tag{3.21}$$

In this case, in a more general form than the simple one depicted in Fig. 3.3, eventual monopole defects are suppressed [42], and the $U(1)$ topological order is stable, as long there are Fermi surfaces of quasiparticles carrying $U(1)$ electrical charge, as fermions ψ_{ip} indeed do. In other words, the $U(1)$

topological order in this state is thus associated with the expulsion of distinct defects in the SDW order, and the consequent possible appearance of emergent deconfined $U(1)$ gauge field. This state has fractionalized gapped bosonic spinon excitations, given by the $SU(2)$ matrix R, and fermionic holon excitations, given by ψ_p, that are gapless around reconstructed Fermi surfaces. Let us now describe how the retarded electronic Green's function $G_{c,r}(\omega, \mathbf{k})$ is obtained within this $SU(2)$ gauge theory.

3.2 Electronic Green's function in the $SU(2)$ gauge theory

We modify Eqs. (3.5)-(3.8) to describe in a more general spin-fermion model the term S_n [41]:

$$S = S_c + S_n + S_{int} \qquad (3.22)$$

$$S_c = \int_0^\beta d\tau \left[\sum_i c_{i\alpha}^\dagger (\partial_\tau - \mu)\, c_{i\alpha} - \sum_{i,j} t_{ij} \left(c_{i\alpha}^\dagger c_{j\alpha} + h.c.\right)\right] \quad (3.23)$$

$$S_n = \frac{1}{4g_0} \int_0^\beta d\tau \left[\sum_i (\partial_\tau \boldsymbol{n}_i)^2 + \sum_{i,j} J_{ij} \boldsymbol{n}_i \cdot \boldsymbol{n}_j + \sum_i V(\boldsymbol{n}_i^2)\right] \qquad (3.24)$$

$$S_{int} = \int_0^\beta d\tau \left[\sum_i c_{i\alpha}^\dagger \boldsymbol{\sigma}_{\alpha\beta}\, c_{i\beta} \cdot \boldsymbol{n}_i\right] \qquad (3.25)$$

- The term S_c resumes Eq. (3.6) exactly, describing electrons hopping on the site i of the square lattice.
- The term S_n, referred to Eq. (3.7), describes the more general spin-fermion model with a continuum $O(3)$ nonlinear sigma model: g_0 controls the strength of the antiferromagnetic fluctuations associated with the orientation of the n_i^a, while we do not know the detailed form of the parameters J_{ij}, controlling the possibile interaction between $\boldsymbol{n}_i$ on different lattice sites, except for the requirements to be periodic in the Brillouin zone. The potential $V(\boldsymbol{n}_i^2)$ is the more general form of the gradient term $(\boldsymbol{\nabla}\mathbf{n})^2$ in Eq. (3.7). We also note that, respect to Eq. (3.7), Eq. (3.24) is considered in the periodic lattice and not in the continuum.
- The term S_{int} resumes Eq. (3.8), describing how electrons are coupled locally to the bosonic field $\mathbf{n} = (n_x, n_y, n_z)$, which describes as seen above spin fluctuations, with $\boldsymbol{\sigma} = (\sigma_x, \sigma_y, \sigma_z)^T$ Pauli matrices, with the this spin-fermion coupling parameter λ treated, as anticipated of order unity, absorbed in $\mathbf{n}$.

We insert the transformation in Eq. (3.9), that is $c_{i\alpha} = R_{\alpha p}^i \psi_{ip}$, into the t_{ij}-term in Eq. (3.23), obtaining (for simplicity we omit the explicit dependence by the imaginary time τ)

$$t_{ij}c_{i\alpha}^{\dagger}c_{j\alpha} = t_{ij}\psi_{i\beta}^{\dagger}(R_i^{+})_{\beta\gamma}\left(R_j\right)_{\gamma\delta}\psi_{j\delta} \qquad (3.26)$$

To make this quartic term accessible analytically, we perform the a mean-field decoupling, so defined by the mutual mean-field parameters

$$\left(U_{ij}\right)_{\alpha\beta} = \langle\left(R_i^{\dagger}R_j\right)_{\alpha\beta}\rangle \qquad (3.27)$$

$$\left(\chi_{ij}\right)_{\alpha\beta} = \langle\left(\psi_{i\alpha}^{\dagger}\psi_{j\beta}\right)\ \rangle \qquad (3.28)$$

So Eq. (3.26) becomes

$$t_{ij}c_{i\alpha}^{\dagger}c_{j\alpha} = t_{ij}\left(\psi_{i\alpha}^{\dagger}\left(U_{ij}\right)_{\alpha\beta}\psi_{j\beta} + \left(\chi_{ij}\right)_{\alpha\beta}\left(R_i^{\dagger}R_j\right)_{\alpha\beta}\right) \qquad (3.29)$$

We apply the same procedure to the ∂_τ-term in Eq. (3.23), so obtaining (with $R_i^{\dagger}R_i = \mathbb{1}$)

$$c_{i\alpha}^{\dagger}\partial_\tau c_{i\alpha} = \psi_{i\alpha}^{\dagger}R_i^{\dagger}\partial_\tau R_i\psi_{i\alpha} = \psi_{i\alpha}^{\dagger}\partial_\tau\psi_{i\alpha} + (\chi_{ii})_{\alpha\beta}\left(R_i^{\dagger}\partial_\tau R_i\right)_{\alpha\beta} \qquad (3.30)$$

In the same way, acting on the coupling action S_{int}, and introducing the Higgs field $\boldsymbol{H} = \left(H_x, H_y, H_z\right)$ as seen in Eq. (3.17), i.e. $\boldsymbol{H}_i \cdot \boldsymbol{\sigma} = R_i^{\dagger}\boldsymbol{\sigma}R_i \cdot \boldsymbol{n}_i$, we obtain

$$S_{int} = \int_0^{\beta} d\tau\left[\sum_i \psi_{i\alpha}^{\dagger}\boldsymbol{\sigma}_{\alpha\beta}\,\psi_{i\beta} \cdot \boldsymbol{H}_i\right] \qquad (3.31)$$

From Eqs. (3.29)-(3.31) we can thus obtain the holon ψ-spinon R action $S_\psi + S_R$, where the holon part is given by

$$S_\psi = \int_0^{\beta} d\tau\left[\sum_i \psi_{i\alpha}^{\dagger}(\partial_\tau - \mu)\,\psi_{i\alpha} - \sum_{i,j} t_{ij}\,\psi_{i\alpha}^{\dagger}\left(U_{ij}\right)_{\alpha\beta}\psi_{j\beta} + \sum_i \psi_{i\alpha}^{\dagger}\boldsymbol{\sigma}_{\alpha\beta}\,\psi_{i\beta} \cdot \boldsymbol{H}_i\right] \qquad (3.32)$$

The spinon action S_R has two contributions, as $S_R = S_R^c + S_R^n$, where the first term derives from the quadratic part of the electronic action S_c in Eq. (3.23), i.e. the second terms in Eqs. (3.29) and (3.30), and where $tr[\ldots]$ denotes the trace in $SU(2)$ space:

$$S_R^c = \int_0^{\beta} d\tau\ tr\left[\sum_i \chi_{ii}^T R_i^{\dagger}\partial_\tau R_i - \sum_{i,j} t_{ij}\,\chi_{ij}^T R_i^{\dagger}R_j\right] \qquad (3.33)$$

In order to obtain the term S_R^n, which contains the contributions from the spin-dynamics encoded in S_n in Eq. (3.24), we apply the transformation $c_{i\alpha} = R_{\alpha p}^{i}\psi_{ip}$ to Eq. (3.24), and we use the Higgs "condensation" by Eq. (3.21), upon noting that Eq. (3.17) now becomes

$$\mathbf{n}_i \cdot \boldsymbol{\sigma} = \boldsymbol{a} \cdot R_i\boldsymbol{\sigma}R_i^{\dagger} \qquad (3.34)$$

where we have redefined the Néel order parameter $\mathbf{n}_i \to \mathbf{n}_i = \eta_i\mathbf{n}_i/H_0$, with $\eta_i = (-1)^{x_i+y_i}$, H_0 known from Eq. (3.21), and $\boldsymbol{a}$ an arbitrary vector for which the $U(1)$ topological order expressed in Eq. (3.21) can be considered as $\langle\boldsymbol{H}_i\rangle = H_0\boldsymbol{a}\cos\left(\boldsymbol{Q} \cdot \boldsymbol{r}_i\right)$, with $\boldsymbol{Q} = (\pi, \pi)$. Thus we obtain

$$S_R^{cp} = \frac{1}{4g}\int_0^{\beta} d\tau\left[\sum_i(\partial_\tau\mathbf{n}_i)^2 + \sum_{ij}\eta_i\eta_j J_{ij}\mathbf{n}_i \cdot \mathbf{n}_j\right] \qquad (3.35)$$

where we have introduced the rescaled parameter $g = g_0/H_0^2$. Now we are able to discuss, from Eqs. (3.32), (3.33) and (3.35), the holon ψ and the spinon R Green's functions separately, as they are self-consistently coupled via Eqs. (3.27) and (3.28).

3.2.1 Holon ψ Green's function

We make the assumption that U_{ij}, as defined in Eq. (3.27), is trivial in $SU(2)$ space, and translational invariant in the gauge given by Eq. (3.21), that is

$$U_{ij} = \mathbb{1}Z_{i-j}; \quad Z_{i-j} \in \mathbb{R} \qquad (3.36)$$

In practice, we will show that the spinon theory, resulting from this assumption, will indeed reproduce it, thus giving rise to a self-consistent solution of the coupled spinon-holon problem (also remembering that all the symmetries of the square lattice now are preserved). For convenience we perform a global gauge transformation leading to $\boldsymbol{a} = (0,0,1)^T$ in Eq. (3.34) so that from Eq. (3.32), going into frequency-momentum space with $\psi_i(\tau) \to \psi_{n\boldsymbol{k}}$, we can write in quadratic form

$$S_\psi = T\sum_{\omega_n}\sum_{\boldsymbol{k}\in BZ^+}\sum_{\alpha=\pm}\Psi^\dagger_{n\boldsymbol{k}\alpha}\begin{pmatrix}-i\omega_n+\xi_{\boldsymbol{k}} & \alpha H_0\\ \alpha H_0 & -i\omega_n+\xi_{\boldsymbol{k}+\boldsymbol{Q}}\end{pmatrix}\Psi_{n\boldsymbol{k}\alpha} \qquad (3.37)$$

Where $\Psi_{n\boldsymbol{k}\alpha} = \left(\psi_{n\boldsymbol{k}\alpha}, \psi_{n\boldsymbol{k}+\boldsymbol{Q}\alpha}\right)^T$, $\boldsymbol{Q} = (\pi,\pi)$, ω_n are fermionic Matsubara frequencies, and we have defined the single-particle dispersion $\xi_{\boldsymbol{k}} = (-2t(cosk_x + cosk_y) + 4t'cosk_xcosk_y - \mu)$ (focusing on nearest-neighbor hopping t, and next-to-nearest neighbor hopping t'). Let us also note that the sum over momentum **k** in Eq. (3.37) is over only the upper half of the Brillouin zone (denoted as BZ^+), as it has been folded by the nesting vector $\boldsymbol{Q} = (\pi,\pi)$. From this action S_ψ we can obtain the holon Green's function

$$G^{\alpha\beta}_\psi(i\omega_n,\boldsymbol{k}) \equiv -T\langle\Psi_{n\boldsymbol{k}\alpha}\Psi^\dagger_{n\boldsymbol{k}\beta}\rangle = \frac{\delta_{\alpha\beta}}{(i\omega_n-\xi_{\boldsymbol{k}})(i\omega_n-\xi_{\boldsymbol{k}+\boldsymbol{Q}})-H_0^2}\begin{pmatrix}i\omega_n-\xi_{\boldsymbol{k}+\boldsymbol{Q}} & \alpha H_0\\ \alpha H_0 & i\omega_n-\xi_{\boldsymbol{k}}\end{pmatrix} \qquad (3.38)$$

We note that this Green's function is diagonal in $SU(2)$ space, as a consequence of the chosen gauge, and Eq. (3.38) also reproduces the diagonal part, i.e. with $\alpha = \beta$, of the retarded Green's function given by ($\eta \to 0^+$)

$$G^{\alpha\beta}_{\psi,r}(\omega,\boldsymbol{k}) = \frac{\delta_{\alpha\beta}}{\omega+i\eta-\xi_{\boldsymbol{k}}-\Sigma^r_\psi(\omega,\boldsymbol{k})} \qquad (3.39)$$

$$\Sigma^r_\psi(\omega,\boldsymbol{k}) = \frac{H_0^2}{\omega+i\eta-\xi_{\boldsymbol{k}+\boldsymbol{Q}}} \qquad (3.40)$$

In Eq. (3.39) we find, at zero energy, both lines of poles, defining the Fermi surface, and lines of zeros at $\{\boldsymbol{k}\,|\xi_{\boldsymbol{k}+\boldsymbol{Q}} = 0\}$, defining the Luttinger surface; in other words the Green's function $G^{\alpha\alpha}_{\psi,r}(\omega,\boldsymbol{k})$ has poles, but it also has zeros, associated with poles of the self-energy $\Sigma^r_\psi(\omega,\boldsymbol{k})$, and occurring when

$\omega = \xi_{\boldsymbol{k}+\boldsymbol{Q}}$, and, in particular at zero energy, there is a line of zeros given by $\{\boldsymbol{k}\,|\xi_{\boldsymbol{k}+\boldsymbol{Q}} = 0\}$, that is the Luttinger surface. We show in Fig. 3.4 the $\boldsymbol{k}$ dependence of the holon Green's function, displaying the spectral weight given by $A_{\boldsymbol{k}}^{Ch}(\omega) = -\frac{1}{\pi} Im G_{\psi,\boldsymbol{r}}^{\alpha\alpha}(\omega, \boldsymbol{k})$.

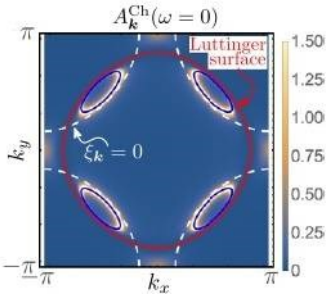

Figure 3.4. Spectral weight $A_{\boldsymbol{k}}^{ch}(\omega)$ associated with the diagonal elements of the retarded holon Green's function in Eq. (3.39) at zero energy $\omega = 0$ (color plot) together with the Fermi surface of the holon in presence (blue line) and absence (white dashed) of the Higgs condensate, as well as the Luttinger surface of the holons (red line). Parameters have values $H_0 = 0.5$, $\mu = -0.8$, $t' = -0.3$ (all in units of t, and with all further-neighbor hoppings taken to be zero) [41].

In Fig. 3.4 we can note with the blue lines the Fermi surface of the holons in the presence of the Higgs condensate, that is with $\langle \boldsymbol{H}_i \rangle \neq 0$, as chosen in Eq. (3.21), and also with the red line the Luttinger surface of the holons, as defined above. The key observation we can make is that the Higgs condensate $\langle \boldsymbol{H}_i \rangle \neq 0$ acts on the ψ_i holons just like a magnetic order does on the electrons, thus the band structure of the ψ_i is reconstructed into small Fermi surfaces, even though there is no long-range order. Clearly the ψ_i holons are not the physical electrons c_i, and neither Eq. (3.39) is the full holon Green's function, which also has momentum off-diagonal terms given by $\langle \Psi_{\boldsymbol{k}} \Psi_{\boldsymbol{k}+\boldsymbol{Q}}^{\dagger} \rangle$: thus to obtain the real electron spectral weight we have to consider also the spinon Green's function.

3.2.2 Spinon R Green's function

We first rewrite the spinon action in terms of the complex bosonic $\mathbb{CP}^1$ fields $z_{i\uparrow}$ and $z_{i\downarrow}$ just introduced and related to R_i according to Eq. (3.10), (with $\sum_\alpha |z_{i\alpha}|^2 = 1$):

$$R_i = \begin{bmatrix} z_{i\uparrow} & -z_{i\downarrow}^* \\ z_{i\downarrow} & z_{i\uparrow}^* \end{bmatrix} \qquad (3.10)$$

Now Eq. (3.34), that is $\boldsymbol{n}_i \cdot \boldsymbol{\sigma} = \boldsymbol{a} \cdot R_i \boldsymbol{\sigma} R_i^{\dagger}$, with the gauge chosen above $\boldsymbol{a} = (0,0,1)^T$, is satisfied for Eq. (3.13), that is $\boldsymbol{n}_i = z_i^{\dagger} \boldsymbol{\sigma} z_i$, $z_i = (z_{i\uparrow}, z_{i\downarrow})^T$, exactly as in the standard $\mathbb{CP}^1$ description of fluctuating antiferromagnets, that is $n_i^a = z_{i\alpha}^* \sigma_{\alpha\beta}^a z_{i\beta}$ seen in Eq. (3.13). We would like to find a way to distinguish two regimes of the spinon part of the theory:

- At weak fluctuations, with the condensation of $\mathbb{CP}^1$ bosons, thus obtaining $\langle z_i \rangle \neq 0$ and $\langle \boldsymbol{n}_i \rangle \neq 0$, with the system having long-range magnetical order as in the (close to) half-filled Hubbard model.

- When quantum fluctuations are stronger, we will have $\langle \boldsymbol{n}_i \rangle = 0$ and $\langle z_i \rangle = 0$, that is the spinons become gapped: there is no long-range magnetic order and, with all lattice symmetries preserved, the system has $U(1)$ topological order. This is indeed our candidate for the pseudogap phase of hole-doped cuprates.

Let us start by analyzing the contribution S_R^{cp} in Eq. (3.35) emanating from the collective antiferromagnetic fluctuations in S_R: using the $\mathbb{CP}^1$ fields z_i, the emergent $U(1)$ gauge field a_μ introduced above by the Higgs' transition, and taking $J_{ij} = J$ to be finite only on nearest-neighbor bonds of the square lattice, S_R^{cp} can be written as [34, 41]

$$S_z^{cp} = \frac{1}{g}\int_0^\beta d^2\mathbf{r}d\tau \left|\left(\partial_\mu - i a_\mu\right) z_\alpha\right|^2 \qquad (3.41)$$

We know that [43] we can neglect gauge-field fluctuations, not qualitatively affecting the resulting electronic Green's function, thus we can replace Eq. (3.41) by the effective lattice $\mathbb{CP}^1$ action

$$S_z^{cp} = \frac{1}{g} T \sum_{\Omega_n} \sum_{\boldsymbol{q}} z_{n\boldsymbol{q}}^\dagger \left[\Omega_n^2 + \left(E_{\boldsymbol{q}}^{cp}\right)^2\right] z_{n\boldsymbol{q}} \qquad (3.42)$$

Where $z_{n\boldsymbol{q}}$ are the frequency and momentum transform of $z_i(\tau)$, Ω_n are bosonic Matsubara frequencies. The only informations about $E_{\boldsymbol{q}}^{cp}$ are that it has to be periodic in the Brillouin zone, and to have a minimum at $\boldsymbol{q} = 0$, which follows form the fact that we are interested in phases near the antiferromagnetic phase: in fact, at sufficiently small g, the gap of the $\mathbb{CP}^1$ bosons closes, and the $\boldsymbol{q} = 0$ mode condenses leading to a spatially constant value of $\langle \boldsymbol{n}_i \rangle$, while near $\boldsymbol{q} = 0$ we expect a linear energy-momentum relation. We can also note that changing the spectrum at high energies is expected to not qualitatively affect the result of the calculation, thus, in order to meets all the general requirements seen above, we can consider the simple form

$$\left(E_{\boldsymbol{q}}^{cp}\right)^2 \sim -2J^2\left(cosq_x + cosq_y - 2\right) \qquad (3.43)$$

Let us now discuss the contribution S_R^c in Eq. (3.33) to the spinon action, that results from the hopping of electrons on the square lattice. Referring to Appendix C.1 for the detailed passages, we can write S_R^c as[10]

$$S_z^c = \int_0^\beta d\tau \left[\sum_i (-1)^{x_i+y_i} \chi_\Omega z_i^\dagger \partial_\tau z_i - \sum_{i<j} t_{ij} \chi_{i-j}^T \left(z_i^\dagger z_j + c.c\right)\right] \qquad (3.44)$$

We will treat the nonlinear constraint $\sum_\alpha |z_{i\alpha}|^2 = 1$ on quantum and thermal average at each site i, only requiring

$$\langle z_i^\dagger z_i \rangle = 1 \qquad \forall i \qquad (3.45)$$

Eq. (3.45) can be accounted for by adding to the action the term $\sum_i \lambda_i z_i^\dagger z_i$, and adjusting the λ_i Lagrange multipliers appropriately. Using a constant Lagrange multiplier $\lambda = \lambda_i$ at each site would imply that Eq. (3.45) holds only on spatial averaging over all sites; however, we note that the spinon

[10] We recall the definition of χ_Ω in Eq. (C.17) as $\chi_{ii}^{++} - \chi_{ii}^{--} = \chi_{ii}^{++} - \chi_{i+e_\mu, j+e_\mu}^{++} \equiv (-1)^{x_i+y_i}\chi_\Omega$.

action $S_z = S_z^{cp} + S_z^c$ is translation invariant, that is invariant under $z_i \to i\sigma_y z_{i+e_\mu}^*$, and this implies that $\langle z_i^\dagger z_i \rangle$ is independent of i, and thus Eq. (3.45) holds at each site for a site-independent λ. Performing a transformation to momentum and Matsubara space, we finally obtain the quadratic spinon action

$$S_z = \frac{T}{g} \sum_{\boldsymbol{\Omega}_n} \sum_{\boldsymbol{q}} \sum_{\alpha=\uparrow,\downarrow} Z_{n\boldsymbol{q}\alpha}^\dagger \begin{pmatrix} \Omega_n^2 + E_{\boldsymbol{q}}^2 & -i\Omega_n g\chi_\Omega \\ -i\Omega_n g\chi_\Omega & \Omega_n^2 + E_{\boldsymbol{q}+\boldsymbol{Q}}^2 \end{pmatrix} Z_{n\boldsymbol{q}\alpha} \qquad (3.46)$$

We have introduced $Z_{n\boldsymbol{q}\alpha} = \left(z_{n\boldsymbol{q}\alpha}, z_{n\boldsymbol{q}+\boldsymbol{Q}\alpha}\right)^T$, Ω_n are bosonic Matsubara frequencies, $q = (i\omega_n, \boldsymbol{q})$ comprises momenta and bosonic Matsubara frquencies; the term $-i\Omega_n g\chi_\Omega$, coming from the first term in Eq. (3.44) is just off-diagonal as it couples $z_{n\boldsymbol{q}\alpha}$ with $z_{n\boldsymbol{q}+\boldsymbol{Q}\alpha}$, from $\sum_i (-1)^{x_i+y_i} = e^{i(\boldsymbol{Q}\cdot(x_i,y_i))}$, remembering the nesting vector $\boldsymbol{Q} = (\pi, \pi)$**.** The spinon spectrum is

$$E_{\boldsymbol{q}}^2 = \left(E_{\boldsymbol{q}}^{cp}\right)^2 + g\left(E_{\boldsymbol{q}}^c\right)^2 + \Delta^2 \qquad (3.47)$$

In Eq. (3.47) we have introduced the spinon gap Δ and the contribution $E_{\boldsymbol{q}}^c$ to the spinon dispersion, resulting from the coupling with holons, as, using $t_{\boldsymbol{\eta}} = t_{i+\eta,i}$ for the translation symmetry, and $\chi_{\boldsymbol{\eta}}$ defined above

$$\left(E_{\boldsymbol{q}}^c\right)^2 = -2\sum_{\boldsymbol{\eta}} t_{\boldsymbol{\eta}}\chi_{\boldsymbol{\eta}}^t \left(\cos(\boldsymbol{\eta}\cdot\boldsymbol{q}) - 1\right) \qquad (3.48)$$

$$\Delta^2 = g\lambda - 2g\sum_{\boldsymbol{\eta}} t_{\boldsymbol{\eta}}\chi_{\boldsymbol{\eta}}^t \qquad (3.49)$$

In the following, to satisfy the constraint in Eq. (3.45), we will use the more meaningful parameter Δ, the spinon gap, instead of λ; in order to calculate Δ, we can obtain from Eq. (3.46) the spinon Green's function

$$G_z^{\alpha\beta}(i\Omega_n, \boldsymbol{q}) \equiv T\langle Z_{n\boldsymbol{q}\alpha} Z_{n\boldsymbol{q}\beta}^\dagger \rangle = \frac{g\delta_{\alpha\beta}}{(\Omega_n^2 + D_{q+}^2)(\Omega_n^2 + D_{q-}^2)} \begin{pmatrix} \Omega_n^2 + E_{\boldsymbol{q}+\boldsymbol{Q}}^2 & i\Omega_n g\chi_\Omega \\ i\Omega_n g\chi_\Omega & \Omega_n^2 + E_{\boldsymbol{q}}^2 \end{pmatrix} \qquad (3.50)$$

We have introduced the two branches, $s = \pm$, of the spinon dispersion

$$D_{\boldsymbol{q}s}^2 = \frac{1}{2}\left(E_{\boldsymbol{q}}^2 + E_{\boldsymbol{q}+\boldsymbol{Q}}^2 + (g\chi_\Omega)^2 + s\sqrt{\left(E_{\boldsymbol{q}}^2 - E_{\boldsymbol{q}+\boldsymbol{Q}}^2\right)^2 + 2\left(E_{\boldsymbol{q}}^2 + E_{\boldsymbol{q}+\boldsymbol{Q}}^2\right)(g\chi_\Omega)^2 + (g\chi_\Omega)^4}\right) \qquad (3.51)$$

Upon Fourier transformation, the constraint $\langle z_i^\dagger z_i \rangle = 1\ \forall i$, with N as the number of sites on the square lattice, can be rewritten as

$$\frac{T}{N}\sum_{\Omega_n,\boldsymbol{q},\alpha}\left[(G_z^{\alpha\alpha})_{11}(i\Omega_n, \boldsymbol{q}) + (G_z^{\alpha\alpha})_{12}(i\Omega_n, \boldsymbol{q})e^{i\boldsymbol{Q}\cdot\boldsymbol{r}_i}\right] = 1 \qquad (3.52)$$

We can note that the second term in Eq. (3.52) is odd in Matsubara frequency, and it is also convergent, ($\sim 1/\Omega_n^3$ as $|\Omega_n| \to \infty$), thus it vanishes upon summation over Ω_n, as indeed we could expect from translation symmetry, and this is another justification for taking a constant λ. It is thus possible to perform the remaining Matsubara sum, obtaining [41] an integral, that will be integrated numerically, over the entire Brillouin zone, given by

$$\int_{BZ} \frac{d^2\boldsymbol{q}}{(2\pi)^2} f_{\boldsymbol{q},T} = \frac{1}{g} \qquad (3.53)$$

In Eq. (3.53) we have introduced

$$f_{\boldsymbol{q},T} = \sum_{s=\pm} \frac{coth\left(\frac{D_s(\boldsymbol{q})}{2T}\right)}{D_+^2(\boldsymbol{q}) - D_-^2(\boldsymbol{q})} \frac{D_s^2(\boldsymbol{q}) - E_{\boldsymbol{q}+\boldsymbol{Q}}^2}{sD_s(\boldsymbol{q})} \qquad (3.54)$$

We will consider g, whose value is unknown, as the free parameter of this theory, thus calculating the value of g for a given value of Δ by solving Eq. (3.53) numerically, and also remembering that Δ is related to the Lagrange multiplier λ, and, hence, it is determined by all other system parameters. In order to understand in some way the dependence of Δ on g, let us consider the limit of small $g\chi_\Omega$ and $T \to 0$, where Eq. (3.53) reduces to

$$\int_{BZ} \frac{d^2\boldsymbol{q}}{(2\pi)^2} \frac{1}{E_{\boldsymbol{q}}} = \frac{1}{g} \qquad (3.55)$$

We can deduce that this integral decreases with Δ, while being finite at $\Delta = 0$: this shows that Δ becomes smaller when g is decreased, until it vanishes at some critical value $g = g_c$, where the transition to a magnetically ordered state occurs. Anyway, as we focus on the pseudogap phase, we will show results only for the regime $g > g_c$, where quantum fluctuations suppress magnetic order, no symmetries are broken, and the system has topological order.

Having derived the full spinon action in Eq. (3.50), which is diagonal in spin-space, that is $G_z^{\alpha\beta} \approx \delta_{\alpha\beta}$, now we can finally verify if the assumption $U_{ij} = \mathbb{1}Z_{i-j}$, with $Z_{i-j} \in \mathbb{R}$, made in Eq. (3.36), is a good one: recalling the definition of U_{ij} in Eq. (3.27) and using the parameterization of the R matrix in Eq. (3.10), we find $U_{ij} = diag\left(Z_{ij}, Z_{ji}\right)$, with $Z_{ij} = \langle z_i^\dagger(\tau) z_j(\tau)\rangle$. Considering again that the off-diagonal term of the spinon Green's function in Eq. (3.50) is odd in Matsubara frequency, and that $G_z(i\Omega, \boldsymbol{q}) = G_z(i\Omega, -\boldsymbol{q})$, we can write in momentum space that

$$Z_{ij} = g \int_{BZ} \frac{d^2\boldsymbol{q}}{(2\pi)^2} f_{\boldsymbol{q},T} \cos\left(\boldsymbol{q}(\boldsymbol{r}_i - \boldsymbol{r}_j)\right) \qquad (3.56)$$

From Eq. (3.56) we can verify that $Z_{ij} = Z_{ji} = Z_{i-j}$, thus obtaining the desired form $U_{ij} = \mathbb{1}Z_{i-j}$, and also, as $f_{\boldsymbol{q},T} > 0$ in Eq. (3.53), we have $Z_{i-j} < 1$. This proves that for the spinon Green's function in Eq. (3.50) there is a self-consistent mean field solution with U_{ij} satisfying Eq. (3.36).

3.2.3 Electronic Green's function

We can now calculate the electronic Green's function, given by

$$G^c_{\alpha\beta} = -\langle c_{i\alpha}(\tau) c^\dagger_{j\beta}(0)\rangle \qquad (3.57)$$

Inserting the transformation $c_{i\alpha} = R^i_{\alpha p}\psi_{ip}$, we can note that in the considered mean-field the total effective action is just the sum of the holon contribution S_ψ in Eq. (3.37) and of the spinon contribution S_z in Eq. (3.46), without any term coupling the spinons to the holons directly; thus we can write

$$G^c_{\alpha\beta}(i,j,\tau) = -\langle \left(R_i(\tau)\right)_{\alpha\alpha'} \left(R^*_j(0)\right)_{\beta\beta'} \rangle \langle \psi_{i\alpha'}(\tau)\psi^\dagger_{j\beta'}(0)\rangle \qquad (3.58)$$

We verify in Appendix C.2 that the matrix product of holon and spinon Green's functions, determining this electronic Green's function, respects both translational and spin-rotation symmetry, that is

$$G^c_{\alpha\beta}(i,j,\tau) = \delta_{\alpha\beta} G_c(i-j,\tau) \qquad (3.59)$$

In momentum-frequency space, Eq. (3.58) becomes a convolution with two different contributions as both the spinon and the holon action conserve momentum only modulo $\boldsymbol{Q} = (\pi,\pi)$.

Just remembering that Ω_n are bosonic Matsubara frequencies, $k = (i\omega_n, \boldsymbol{k})$ comprises momenta and fermionic Matsubara frequencies, while $q = (i\Omega_n, \boldsymbol{q})$ bosonic ones, we thus have the term associated with the diagonal term of the Green's function given by

$$G_c(k) = \frac{T}{2}\sum_{\Omega_n}\int_{BZ}\frac{d^2\boldsymbol{q}}{(2\pi)^2}\sum_{\alpha,\beta} G_z^{\alpha\alpha}(q)\, G_\psi^{\beta\beta}(k-q) \qquad (3.60)$$

Where G_z and G_ψ are the momentum diagonal Matsubara Green's function of the spinons and the holons, respectively, and we can even consider the diagrammatic representation of Eq. (3.60) in Fig. 3.5

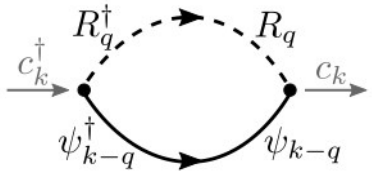

Figure 3.5. Diagrammatic representation of the diagonal term of the electronic Green's function; the solid (dashed) line refers to the Green's function of the holons (spinons) [41].

There is also the term associated with the off-diagonal terms of the Green's function, with its diagrammatic representation in Fig. 3.6: we can write it, using spin-rotation invariance of the spinon action, and noting that from Eq. (3.50) $G_z^{\alpha\alpha}(q)$ is a symmetric matrix, as

$$G_c^{off}(k) = \frac{T}{2}\sum_{\Omega_n}\int_{BZ}\frac{d^2\boldsymbol{q}}{(2\pi)^2}\sum_{\alpha,\beta}\left(G_z^{\alpha\alpha}(q)\right)\left(G_\psi^{\beta\beta}(k-q)\right)_{12} \qquad (3.61)$$

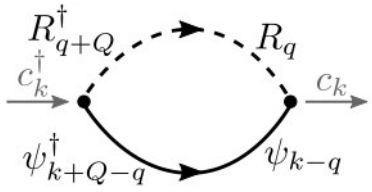

Figure 3.6. Diagrammatic representation of the off-diagonal term of the electronic Green's function; the solid (dashed) line refers to the Green's function of the holons (spinons) [41].

However, this off-diagonal contribution vanishes, as, from Eq. (3.38) we have

$$\left(G_\psi^{\alpha\alpha}\right)_{12} = -\left(G_\psi^{-\alpha-\alpha}\right)_{12} \qquad (3.62)$$

Thus the electronic Green's function G_c is solely determined by Eq. (3.60) with its diagrammatic representation in Fig. 3.5, and we can make the qualitative observation that it can be seem as a smeared version of the holon Green function G_ψ in the limit where the spinon gap Δ is the smallest energy scale. Particularly, the zeros of G_ψ (or equivalently the poles of the associated self-energy Σ_ψ as seen above) in Eq. (3.39) become only approximate zeros of G_c, as peaks of finite height. The last steps we have to do are [41]:

- Insert the explicit expressions from Eqs. (3.38) and (3.50) for the holon and the spinon Green's functions, resepctively, into Eq. (3.60).
- Evaluate the Matsubara sum analytically.
- Perform the analytical continuation $i\omega_n \to \omega + i\eta$, with $\eta \to 0^+$.

We thus finally obtain the retarded electronic Green's function $G_c^r(\omega, \boldsymbol{k})$ in form of an integral over the loop momentum $\boldsymbol{q}$, with only the momentum integration that has to be performed numerically, as

$$G_{c,r}(\omega, \boldsymbol{k}) = \int_{BZ}\frac{d^2\boldsymbol{q}}{(2\pi)^2}\, g_c^r(\boldsymbol{k}, \boldsymbol{q}, \omega) \qquad (3.63)$$

3.3 Results for the pseudogap regime

In order to do a direct and systematic comparison of the $SU(2)$ gauge theory presented here and the Hubbard model, DCA and DQMC calculations have been performed [41]: we focus on nearest (t) and next-to-nearest (t') neighbor hopping, and since we are interested in the pseudogap phase in hole-doped cuprates, we consider small hole dopings $p > 0$ in the regime of large onsite repulsion U of the initial Hubbard model, taking $U = 7t$ for concreteness, and measuring all energies in units of

t. In the $SU(2)$ gauge theory the main fitting parameter is the magnitude H_0 of the Higgs' field, as defined in our gauge in Eq. (3.21), and we choose it as to have a similar size of the antinodal pseudogap in DCA and the gauge theory. We also note that the spinon gap Δ plays the role of a Lagrange multiplier in the mean-field theory, and is hence uniquely determined by all other system parameters, see Eq. (3.49).

3.3.1. Electronic spectral weight and retarded self-energy at the antinodal point

While referring to Appendix C.3 for the details of the derivation, the $SU(2)$ gauge theory result for the spectral function at the antinodal point $\boldsymbol{k} = (\pi, 0)$ is shown in the upper image of Fig. 3.7, displaying the strong suppression of the low-energy spectral weight characterizing the pseudogap phase, while in the lower one we show the same behavior at the antinodal point in DCA results. We note that the spinon gap Δ is constrained to be of the order or smaller than the temperature, to allow for zero-frequency spectral weight in the nodal region (as seen in experiment and in numerical calculations), i.e. $\Delta < T \ll H_0$: we extract, by comparison, a value of about $H_0 \approx 0.3$. We also note in Fig. 3.7 that, while the precise positions of the minimum of the spectral functions differs in the two approaches, the asymmetry of the peaks with respect to $\omega = 0$ is qualitatively the same. Furthermore, increasing t' ($t' > -0.15$), the minimum of the antinodal spectral function moves toward positive values of ω in DCA as well.

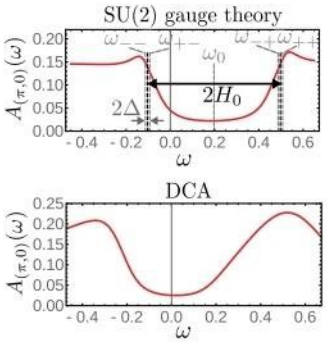

Figure 3.7. Comparison of the electronic spectral weight $A_{(\pi,0)}$ for (up) the $SU(2)$ gauge theory and (down) for the DCA in the Hubbard model. Parameters are $t' = -0.15$, $U = 7$, $p = 0.05$, and $T = 1/30$ for the DCA calculations, $t' = -0.15$, $H_0 = 0.3$, $J^2 = 1$, $\Delta = 0.01$, and $\eta = 0.04$ (for the analytical continuation $i\omega_n \to \omega + i\eta$) for the gauge theory [41].

We can also extract, from the electronic Green's function $G_{c,r}(\omega, \boldsymbol{k})$, the retarded electronic self-energy

$$\Sigma^r_{\boldsymbol{k}}(\omega) = -\left(G_{c,r}(\omega, \boldsymbol{k})\right)^{-1} + \omega - \xi_{\boldsymbol{k}} \qquad (3.64)$$

Where we have considered the bare electronic dispersion given by (with μ_0 denoting the bare electronic chemical potential, that is with $U = 0$)

$$\xi_{\boldsymbol{k}} = -\mu_0 - 2t\left(cosk_x + cosk_y\right) + 4t' cosk_x cosk_y \qquad (3.65)$$

As depicted in Fig. 3.8 there is good agreement between the gauge theory and the DCA for the real and the imaginary part of the antinodal self-energy $\Sigma^r_{(\pi,0)}(\omega)$. The imaginary part has a peak, and the real part changes sign, at positive energies for small $-t'$ (solid lines), and at negative energies for sufficiently large $-t'$ (dashed lines).

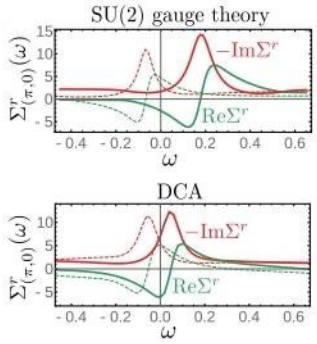

Figure 3.8. Comparison of the retarded electronic self-energy at the antinodal point for (up) the $SU(2)$ gauge theory and (down) for the DCA in the Hubbard model. The solid (dashed) lines refer to $t' = -0.15$ ($t' = -0.25$) for DCA and to $t' = -0.15$ ($t' = -0.5$) for the gauge theory. Parameters are $U = 7$, $p = 0.05$, and $T = 1/30$ for the DCA calculations, $H_0 = 0.3$, $J^2 = 1$, $\Delta = 0.01$, and $\eta = 0.04$ (for the analytical continuation $i\omega_n \to \omega + i\eta$) for the gauge theory [41].

This behavior of the antinodal self-energy, that is that the pseudogap is associated with a peak in the imaginary part of the antinodal self-energy $\Sigma^r_{(\pi,0)}(\omega)$, is also emphasized [72], and we think this condition may be studied in depth.

3.3.2. Electronic Green's function in the entire Brillouin zone

We consider again Eq. (3.63): for small values of Δ, given by Eq. (3.49), the $\boldsymbol{q} = 0$ component of the $\boldsymbol{q}$-loop integrand g_c^r is expected to yield the main contribution to the electronic Green's function $G_{c,r}$, and in Fig. 3.9 we have plotted it at $\omega = 0$ as a function of $\boldsymbol{k}$.

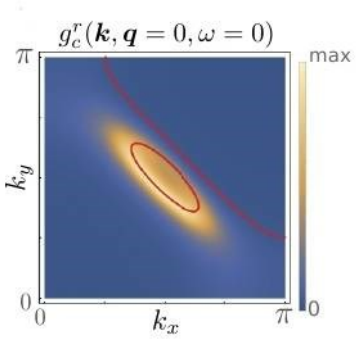

Figure 3.9. For the $\boldsymbol{q}$ integrand g_c^r in Eq. (3.63) are shown the momentum dependence of its imaginary part with color scale, and the zeros of its real part with red lines, with the same parameters U, p, T, H_0, J, Δ, as in Figs. 3.7-3.8, except for $t' = -0.25$ [41].

We can note that the momentum space structure of g_c^r, as depicted by the color plot in Fig. 3.9, closely look like that of the holons seen with the blue line in Fig. 3.4. Furthermore we show in Fig. 3.10 the momentum dependence of the resulting (after $\boldsymbol{q}$ integration) electronic Green's function $G_{c,r}$:

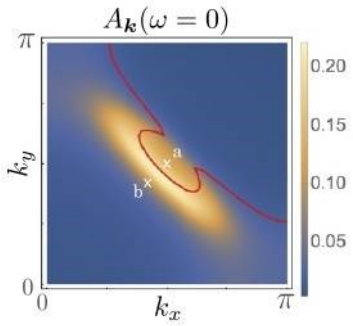

Figure 3.10. For the full electronic Green's function $G_{c,r}$ in Eq. (3.63) are shown shown the momentum dependence of its imaginary part with color scale, and the zeros of its real part with red lines, with the same parameters as in Fig. 3.9 [41].

We can see in Fig. 3.10 how the zeros associated with the Luttinger surface and the Fermi surface of the holons (remember Fig. 3.4), have merged, forming a single line of zeros of $ReG_{c,r}(0, \boldsymbol{k})$. We can also note that, even with the smoothing of the peaks of the spectral function from Fig. 3.9 to Fig. 3.10, however, for the small value of Δ in the plot, we recover the Fermi arc behavior near the nodal point $\boldsymbol{k} = (\pi/2\,, \pi/2)$ and the suppression of the low-energy spectral weight at the antinode. Furthermore, considering the red line in Fig. 3.10 as the line of zeros of $ReG_{c,r}$, we can conclude that depending on whether we consider momenta inside (point a in Fig. 3.10) or outside (point b in Fig. 3.10) the Fermi arc, the spectral weight is peaked at positive or negative energies. This is depicted in Fig. 3.11, showing the spectral weight at the nodal point, also showing the spectral weight of the DCA calculations (blue dotted line).

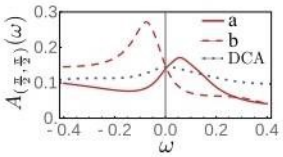

Figure 3.11. Spectral weight of the electronic Green's function $G_{c,r}$ in Eq. (3.63) at two momenta a (red solid line) and b (red dashed line) indicated in Fig. 3.9, with the spectral function of DCA (blue dotted line) averaged around the nodal point $\boldsymbol{k} = (\pi/2\,, \pi/2)$, and with the same parameters as in Fig. 3.8 [41].

The line of zeros of the $ReG_{c,r}(0, \boldsymbol{k})$ shown in Fig. 3.10, as deriving in part from the Luttinger surface of the holons, as seen above, only corresponds to approximate zeros of the Green's function. Anyway, as resulting from its proximity to an approximate zero of the Green's function, it could explain the suppression of the spectral weight at the "backside of the Fermi arc": this could be an explanation for justifying the presence of Fermi arc instead of the expected Fermi pockets, as obtained in experimental results that will be presented in Chapter n. 5.

We can finally observe in Fig. 3.12 that $ReG_{c,r}(0,\boldsymbol{k})$, the real part of the low-frequency ($\omega = 0$) Green's function, changes sign from positive at $\boldsymbol{k} = (0,0) \equiv 0$ to negative at $\boldsymbol{k} = (\pi,\pi)$, and this does not change upon small changes of the system parameters.

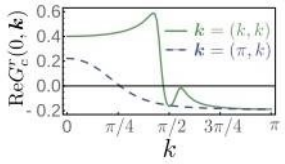

Figure 3.12. Real part of the electronic Green's function $G_{c,r}$ in Eq. (3.63), normalized to the value at $\boldsymbol{k} = 0$, and with the same parameters as in Fig. 3.8 [41].

Even in DCA calculations this sign change is present and stable under variation of t', as sketched in Fig. 3.13:

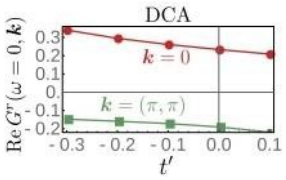

Figure 3.13. Real part of the DCA Green's function at $\boldsymbol{k} = (0,0) = 0$ and $\boldsymbol{k} = (\pi,\pi)$ as a function of t'[41].

We can say that, due to the presence of the Fermi arc as seen in Fig. 3.10, this sign change cannot be explained in the conventional band description by a hole Fermi surface, that is a Fermi pocket, in the vicinity of the nodal point. The Fermi arc needs the presence of a line of sign changes of the $ReG_{c,r}(0,\boldsymbol{k})$ without a peak in its imaginary part, that is an approximate Luttinger surface. As other theoretical approaches do, underlying the evolution of electron self-energy poles in the pseudogap state [71, 72], the $SU(2)$ gauge theory here presented yields a peak in the electron self-energy, just near the expected location of the Luttinger surface of the holons, also in agreement with DQMC, while preserving translational symmetry [41]. In the gauge theory we have presented, we could interpret this additional line of sign changes in the real part as a remnant of the Luttinger surface of the holons, and thus a possible evidence for topological order. Considering also the good agreement between DCA and the gauge theory of a metal with orientational fluctuations of antiferromagnetic order with a well-established local magnitude given by the Higgs parameter H_0, we can conclude that there is evidence for topological order in the hole doped Hubbard model of cuprates, on the square lattice over the temperature and doping ranges studied. We have considered only the simplest Higgs $U(1)$ condensation of a $SU(2)$ gauge theory, but it is clearly possibile that other flavors of topological order remain possible, requiring more precise studies to refine the theory.

3.3.3 FL of decoupled spinons and holons violating the Luttinger's theorem*

With the considerations made in the previous sections on the deconfined Higgs phase, that is the Higgs $U(1)$-FL* (condensation of a $SU(2)$ gauge theory) as a candidate for the pseudogap phase for

the hole doped cuprates, we can thus see how the modified Luttinger theorem, as discussed in Chapter n. 2, can be described. According to the mean-field treatment of the gauge theory seen above, the unitary constraint of the spinons has been treated on average, i.e. $\langle R_i^+ R_i \rangle = 1$, from $\langle z_i^\dagger z_i \rangle = 1$, and thus we can compute the expectation value of the electron density as[11]

$$\langle c_i^+ c_i \rangle = \langle z_i^\dagger z_i \rangle \langle \psi_{i\alpha}^+ \psi_{i\alpha} \rangle = \langle \psi_{i\alpha}^+ \psi_{i\alpha} \rangle \qquad (3.66)$$

Thus we can apply the standard Luttinger theorem to the holons $\psi_{i\alpha}$, that are described by the following effective Hamiltonian (we recall here Eq. (C.9) in appendix C.1), thus exhibiting well defined Fermi surfaces:

$$H_\psi = -\sum_{i,j}\left(Z_{i-j} t_{ij} + \delta_{ij}\right) \psi_{i\alpha}^\dagger \psi_{j\alpha} + \sum_i \psi_{i\alpha}^\dagger \boldsymbol{\sigma}_{\alpha\beta} \psi_{i\beta} \cdot \langle \boldsymbol{H}_i \rangle \qquad (3.67)$$

Due to the vanishing imaginary part of the zero-frequency electronic Green's function $G_{c,r}(\omega = 0, \boldsymbol{k})$ at $T \to 0$, the lines of approximate zeros of $G_{c,r}(\omega = 0, \boldsymbol{k})$, as discussed in section 3.2.3, become exact in the Brillouin zone, thus giving rise to an electronic Luttinger surface. Even with the presence of these Luttinger surfaces, we can see that the Luttinger's theorem, relating the particle density $n = (1 - p)$ to the area in $\boldsymbol{k}$ space where $Re\ G_{c,r}(\omega = 0, \boldsymbol{k}) > 0$ with

$$n = 2 \int_{BZ} \frac{d^2\boldsymbol{k}}{(2\pi)^2} \Theta\left(Re\ G_{c,r}(\omega = 0, \boldsymbol{k})\right) \qquad (3.68)$$

is violated in the Higgs phase. In fact, as depicted in Fig. 3.14, the size of the area with $Re\ G_{c,r}(\omega = 0, \boldsymbol{k}) > 0$ changes at fixed electron density n with the Higgs condensation value H_0 in eq. (3.21), keeping the area enclosed by the holon Fermi surface fixed. Eq. (3.68) clearly reminds the "hard" version of the Luttinger's theorem discussed in Chapter n. 2, see Eq. (2.5) and related considerations.

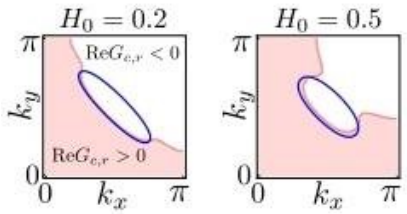

Figure 3.14. The real part of the retarded electronic Green's function $G_{c,r}$ is positive for two different values of H_0 as indicated, with fixed values $p = 0.1$, $t' = -0.3$, $J^2 = 0.3$ [41].

Thus the violation of Eq. (3.68) ("hard" Luttinger's theorem) is a manifestation of the nonperturbative nature of the Higgs phase, and thus of the necessity of a modified Luttinger theorem, as discussed in Chapter n. 2: the $SU(2)$ gauge theory discussed in this chapter indeed violates the conventional Luttinger theorem in a state with $U(1)$ topological order. This nonzero-temperature $SU(2)$ gauge theory has lines of approximate zeros of the electron Green's function G_c, that are remnants of lines

[11] The decoupling of the spinon z and the holon ψ actions, that is $G_z^{\alpha\beta}$ in Eq. (3.50) and $G_\psi^{\alpha\beta}$ in Eq. (3.38) respectively, allows to decouple spinon-holon expectation values into products.

of zeros in the mean-field Green's functions G_ψ of holons, and so we can interprete these lines of approximate zeros as "messengers" of the topological order: in fact these lines change continuosly with system parameters, without obeying the conventional Luttinger theorem, and can be considered a consequence of the underlying topological order. This conclusion can also be related to the discussion in section n. 2.4 on the validity of the Luttinger's theorem even in the presence of a Luttinger surface [71].

3.4 FL* of bounded spinons and holons satisfying the modified Luttinger's theorem

Clearly, needing higher precision, we expect that it is important to account for holon-spinon bound states in the nodal region, to give a more precise description of a FL* state as a candidate, due to the presence of topological order, for the pseudogap phase of hole doped cuprates. We can start again from the actions in Eqs. (3.5)-(3.8), considering the transformation to the rotating reference frame in Eq. (3.9), and the parametrizations seen in Eqs (3.10)-(3.13): introducing an internal dynamical gauge field A_μ associated with the $U(1)$ gauge invariance remained unbroken after the Higgs condensation, as seen in previous sections, we can obtain an Hamiltonian describing these bound states. Thus now we have again the reformulation of the spin-fermion model by the spinless fermions (holons) ψ_{ip} and the bosonic neutral charge spinons $z_{i\alpha}$. We refer to Appendix C.4 for the analytical passages, obtaining the Lagrangian [34, 37, 38]

$$\mathcal{L}_{U(1)} = \mathcal{L}_z + \mathcal{L}_\psi + \mathcal{L}_{ss} \tag{3.69}$$

$$\mathcal{L}_z = \frac{4}{g_0}[|(\partial_\tau - iA_\tau)z_\alpha|^2 + v^2|(\boldsymbol{\nabla} - i\mathbf{A})z_\alpha|^2] \tag{3.70}$$

$$\mathcal{L}_\psi = \sum_{p=\pm1}\sum_i \psi_{ip}^\dagger[\partial_\tau + ipA_\tau - \mu - \lambda p\eta_i]\psi_{ip} - \sum_{p=\pm1}\sum_{i<j} t_{ij}\left(e^{ipA_{ij}}\psi_{ip}^\dagger\psi_{jp} + e^{-ipA_{ij}}\psi_{jp}^\dagger\psi_{ip}\right) \tag{3.71}$$

$$\mathcal{L}_{ss} = \int_{\mathbf{k},\mathbf{p},\mathbf{q}}\left[\mathbf{p}\cdot\frac{\partial\varepsilon(\mathbf{k})}{\partial\mathbf{k}}\right] z_\downarrow\left(\mathbf{q}-\frac{\mathbf{p}}{2}\right) z_\uparrow\left(\mathbf{q}+\frac{\mathbf{p}}{2}\right)\psi_-^\dagger(\mathbf{k}+\mathbf{q})\psi_+(\mathbf{k}-\mathbf{q}) + \sum_i(z_{i\uparrow}\partial_\tau z_{i\downarrow} - z_{i\downarrow}\partial_\tau z_{i\uparrow})\psi_{i-}^\dagger\psi_{i+} \tag{3.72}$$

The term $\mathcal{L}_z$ in Eq. (3.70) is just the CP^1 model for the spinons $z_{i\alpha}$ in Eq. (3.7), while for $A_\mu = 0$, the term $\mathcal{L}_\psi$ in Eq. (3.71) describes the band structure in terms of the Fermi pockets; the interaction arises from the minimal coupling to the A_μ gauge field. The term $\mathcal{L}_{ss}$ in Eq. (3.72) derives from the hopping term and from the time derivative in Eq. (3.6); here $\varepsilon(\mathbf{k})$ is the single-particle dispersion of the large Fermi surface state

$$\varepsilon(\mathbf{k}) = -\sum_j t_{ij}e^{i\mathbf{k}\cdot(\mathbf{r}_j-\mathbf{r}_i)} \tag{3.73}$$

We can also note that the terms in $\mathcal{L}_{ss}$ mix fermions with different A_μ charges. We now make two important observations:

I. We remind that a key feature [34] of this analysis is that we assume that it is only the spin density wave order n_i^a which varies slowly on the lattice scale.

II. While in sections 3.3.1-3.3.2 the key parameter was H_0 from Eq. (3.21), now we have the parameter λ, which represents the potential due to the local antiferromagnetic order, introduced in Eq. (3.8). In this section thus we can consider λ as a "twin" parameter of H_0.

As anticipated, the fermions ψ_{ip} have a strong attractive interaction with the spinons $z_{i\alpha}$ [43], and so the two bind to form electron-like states carrying spin $S = 1/2$ and unit electromagnetical charge, but they are neutral under the emergent $U(1)$ gauge field: these bound states fill a Fermi sea, with a small Fermi surface of hole-like quasiparticles: we have just seen how we identify this exotic metal as a FL* phase. In practice we are in a fluctuating spin density wave state with a spin-correlation length ξ, but we are interested in phenomena at a scale larger than ξ: the confinement of the emergent $U(1)$ gauge field occurrs at a scale ξ_{conf}, and so we will restrict ourselves to the $\xi < r < \xi_{conf}$ [43, 44]. Let the bound states between the ψ_+ fermions and the z_α spinons be F_α: this bound state should have the full symmetry of the square lattice (see Appendix C.4) and so we can define a local operator $F_{i\alpha}$, which defines this bound centered at the lattice site *i*. We know also [43] there is a second bound state between the ψ_p fermions and the z_α spinons, and a consequent doubling of the fermion species, and this is the bound state between the ψ_- fermions and the z_α^* spinon, denoted by the local operator $G_{i\alpha}$. So we have

$$F_{i\alpha} \sim z_{i\alpha}\psi_{i+}; \quad G_{i\alpha} \sim \varepsilon_{\alpha\beta} z_{i\beta}^* \psi_{i-} \qquad (3.74)$$

The bare electron operator $c_{i\alpha}$ will have a nonzero overlap with both the F_α and G_α fermions, and this will be nonlocal over the scale ξ (the spin-correlation length). We can approximate this connection from $c_{i\alpha} = R_{\alpha p}^i \psi_{ip}$ as

$$c_{i\alpha} \equiv Z(F_{i\alpha} + G_{i\alpha}) \qquad (3.75)$$

where Z is some quasiparticle renormalization factor depending upon the holon-spinon bound-state wave function. When we move to length scales larger than spin-correlation length ξ (as in the ordered Néel state the sublattice location of a fermion also fixes its spin), the spin direction of the background Néel state has been averaged over: thus we can view F_α and G_α as fermions that resides preferentially, but not exclusively, on the two sublattices, and they separately have an additional degeneracy associated with carrying spin $S = 1/2$. More formally, all we really need are the properties of the F_α and G_α under the square lattice symmetry operations: for simplicity we report in Appendix C.4 the analysis which allow us to write the following effective Hamiltonian, strongly constrained by the F_α and G_α non trivial transformations under the space group of the square lattice symmetries (with $\boldsymbol{K} = (\pi, \pi)$ is the wave vector describing the antiferromagnetic Néel order):

$$H_O = \sum_{\mathbf{k}} [\xi_k^+ C_{\mathbf{k}\alpha}^+ C_{\mathbf{k}\alpha} + \xi_{k+K}^- D_{\mathbf{k}\alpha}^+ D_{\mathbf{k}\alpha} - \lambda(C_{\mathbf{k}\alpha}^+ D_{\mathbf{k}\alpha} + D_{\mathbf{k}\alpha}^+ C_{\mathbf{k}\alpha})] \qquad (3.76)$$

Where

$$C_{\mathbf{k}\alpha} = \frac{1}{\sqrt{2}}\left(F_{\mathbf{k}\alpha} + G_{\mathbf{k}\alpha}\right) \;\; ; \;\; D_{\mathbf{k}\alpha} = \frac{1}{\sqrt{2}}\left(F_{\mathbf{k}+\mathbf{K},\alpha} - G_{\mathbf{k}+\mathbf{K},\alpha}\right) \qquad (3.77)$$

$$\xi_{\boldsymbol{k}}^{+} = \varepsilon_{\boldsymbol{k}} + \tilde{\varepsilon}_{\boldsymbol{k}} \,, \quad \xi_{\boldsymbol{k}}^{-} = \varepsilon_{\boldsymbol{k}} - \tilde{\varepsilon}_{\boldsymbol{k}} \qquad (3.78a)$$

$$\varepsilon_{\boldsymbol{k}} = -2t\left(cosk_x + cosk_y\right) + 4t'cosk_x cosy - 2t''\left(cos2k_x + cos2k_y\right) - \mu \qquad (3.78b)$$

$$\tilde{\varepsilon}_{\boldsymbol{k}} = -\tilde{t}_0 - 2\tilde{t}\left(cosk_x + cosk_y\right) + 4\tilde{t}'cosk_x cosy - 2\tilde{t}''\left(cos2k_x + cos2k_y\right) \qquad (3.78c)$$

Where $t, t', t''(\tilde{t}, \tilde{t}', \tilde{t}'')$ are nearest-neighbor, next-nearest neighbor, and next-next-nearest neighbor hopping t_{ij} $(\tilde{t}_{ij})$, and $\tilde{t}_0$ is the matrix element of the on site mixing term $\left(F_i^{+}G_i \;\; + G_i^{+}F_i \;\;\right)$, allowed by symmetry. The spectrum of the original electron operator is given by

$$c_{\mathbf{k}\alpha} \approx Z(F_{\mathbf{k}\alpha} + G_{\mathbf{k}\alpha}) \approx \frac{Z}{\sqrt{2}} C_{\mathbf{k}\alpha} \quad (3.79)$$

In the Hamiltonian in Eq. (3.76) the C and D fermions are mixed through the λ term: with this mixing, gaps will open where their Fermi surfaces intersect, and the large Fermi surface becomes a Fermi pocket. When $\tilde{\varepsilon}(\mathbf{k}) = 0$, the D's Fermi surface is the same as the C's one, shifted by (π, π): in this case the pockets are perfectly symmetric under reflection with respect to the magnetic Brillouin zone boundary, and therefore are centered at $(\pi/2\,, \pi/2)$. With $\tilde{\varepsilon}(\mathbf{k}) \neq 0$, the dispersions of C and D are different, so the pockets are no longer symmetric about the magnetic Brillouin zone boundary, and are not necessarily centered at $(\pi/2\,, \pi/2)$. To show the qualitative effects of $\tilde{\varepsilon}(\mathbf{k})$ on the shape of the Fermi pockets, we draw the pockets and electron spectrum functions of some representative choice of $\tilde{\varepsilon}(\mathbf{k})$ in the following Figs. 3.15-3.16 [34, 37, 38], with phenomenological parameters $t' = 0.3t$, $t'' = -0.5t'$, $\lambda = 0.3t$, and measuring all energies in units of t. We again note that the value of the parameter λ is the same of the parameter H_0 seen in sections 3.3.1-3.3.2, steadying the observation II made above.

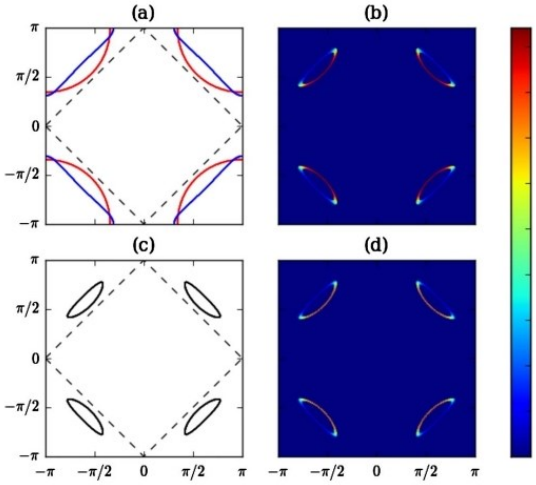

Figure 3.15. Plot of Fermi pockets of the bound state with $\tilde{\varepsilon}(\mathbf{k}) = 0.8t$. (a) Fermi surfaces of $C_{\mathbf{k}\alpha}$(red line) and $D_{\mathbf{k}\alpha}$ (blue line) with $\lambda = 0$ in Eq. (3.76). (c) Fermi pockets as in (a) with $\lambda = 0.3t$ (dashed line in (a) and (c) is the boundary of magnetic Brillouin zone in the ordered state). (b) Fermi surface with the color representing the weight of electron operator in the quasiparticle excitation. (d) as in (b) but by plotting the electron spectral weight at $\omega = 0$ as a function of momentum [34].

In Fig. 3.15 a negative $\tilde{t}_0$ shifts the hole pockets outwards, and makes their shape antisymmetric, as the inner side becomes more curved and the outer side more flat.

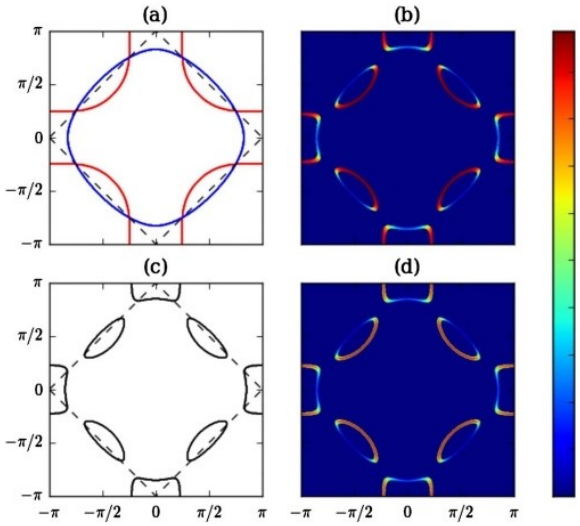

Figure 3.16. As in Fig. 3.15 but with $\tilde{\varepsilon}(\mathbf{k}) = 0.5t\left(cosk_x + cosk_y\right)$ and $\lambda = 0.3t$ [34].

In Fig 3.16 a negative $\tilde{t}$ (see Eq. (3.78c)) does not shift the position of the hole pockets significantly, but makes the shape of the hole pockets asymmetric in a similar way as in Fig. 3.15. Combining the effect of these two parameters, we can move the hole pockets inward and make their inner side more curved than the outer side with a positive $\tilde{t}_0$ and a negative $\tilde{t}$ as shown in Fig. 3.17.

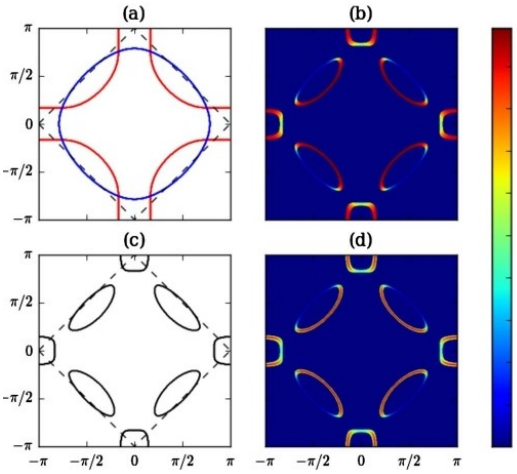

Figure 3.17. As in Fig. 3.15 but with $\tilde{\varepsilon}(\mathbf{k}) = -0.3t + 0.5t\left(cosk_x + cosk_y\right)$ and $\lambda = 0.3t$ [34].

Along the Fermi pockets the fermionic quasiparticles are a mixture of $C_{\mathbf{k}\alpha}$ and $D_{\mathbf{k}\alpha}$ fermions, while experiments can only probe electron spectrum weight; the weight of electron operator in the quasiparticle is calculated through diagonalizing Eq. (3.76) and are plotted in Figs. 3.15-3.17. In Fig. 3.18 we show a plot with larger λ ($\lambda = 0.5t$), so that the antinodal electron pocket is completely gapped.

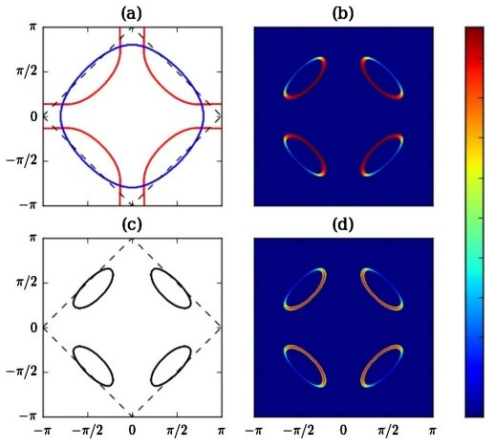

Figure 3.18. As in Fig. 3.15 but with $\tilde{\varepsilon}(\mathbf{k}) = -0.3t + 0.5t\left(cosk_x + cosk_y\right)$ and $\lambda = 0.5t$ [34].

In all these cases, the inner half of the hole pockets has higher electron quasiparticle weight, since the inner part is primarily made of $C_{\mathbf{k}\alpha}$ fermion (and the outer part is primarily made of $D_{\mathbf{k}\alpha}$ ones), and the electron operator is proportional to $C_{\mathbf{k}\alpha}$, as shown in Eq. (3.79). From the Hamiltonian in Eq. (3.76) the Green's function of the electron can be written as [22]

$$G^c(\mathbf{k},\omega) = \frac{Z^2}{\omega - \xi_{\mathbf{k}}^{+} - \lambda^2/[\omega - \xi_{\mathbf{k}+\mathbf{K}}^{-}]} \qquad (3.80)$$

The shape of the Fermi arcs seen in the experiments can be fit to this model; as seen in Figs. 3.15-3.18 the weight of the electron operator on the outer part of the pockets is tiny and may be hard to see in experiments. The spectral function corresponding to the Green's function in Eq. (3.80) is reported in Fig. 3.19a, as for comparison we report in Fig. 3.19b an experimental photoemission [77].

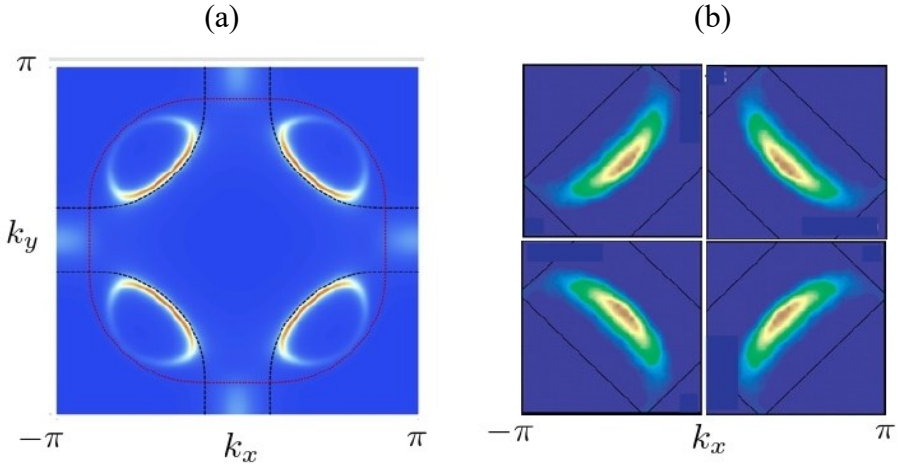

Figure 3.19. (a) The spectral function of the FL* state computed from Eq. (3.80). (b) Photoemission measurements of the pseudogap phase in [77].

Finally in Fig. 3.20 we show a comparison [37] among a conventional state with coexisting spin density wave and d-wave pairing, and to an experimental result by ARPES [63]: we can observe in Fig. 3.20a that the Fermi pocket, resulting from the traditional Hartree-Fock theory, is centered at the magnetic Brillouin zone boundary. In Fig. 3.20b we have typical results for the FL* theory seen

above, showing a Fermi pocket clearly not centered at $(\pm\pi/2, \pm\pi/2)$; furthermore, its spectral weight is not the same along the Fermi surface, and has arclike character, resembling one ARPES result shown in Fig. 3.20c. In other words, the spectral weight of the back-sides of these pockets is strongly suppressed, and we can argue that the Fermi arcs in the pseudogap regime could be modeled as pocktes whose back-sides are almost invisibles.

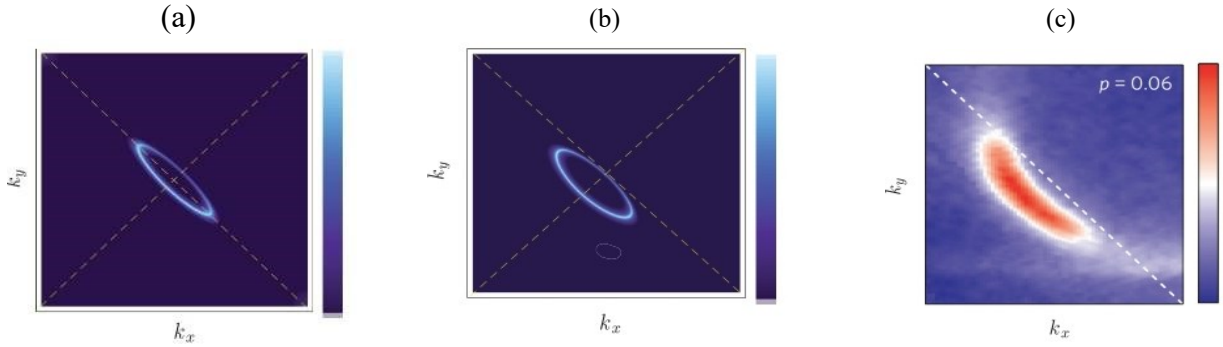

Figure 3.20. Spectral weight of the electron: (a) In the normal state by the Hartree-Fock theory with spin density wave order at wave vector $\mathbf{K} = (\pi, \pi)$. (b) In the FL* state of the gauge theory presented, from Eq. (3.80) [37]. (c) Fermi arc from a ARPES experiment [63].

We now remark the status of the conventional Luttinger theorem [34], as discussed in section 3.3.3 for the case of decoupled spinons and holons, focusing on the electronlike F_α and G_α, and dropping the $\psi_\pm$ contributions (that anyway will amount to shift in the effective doping level p). Under this assumption the total number of F_α and G_α per site is $(2-p)$, and so is the number of C_α and D_α, since the canonical transformation in Eq. (3.77) preserves particle number. As the model developed in this section is applied to the doped holes in the background of a fluctuating antiferromagnet, each such charge carrier must occupy one state within the Fermi surface. Thus, counting holelike (electronlike) Fermi surfaces as negative (positive), with the hole density p, the Fermi surfaces in Figs. 3.15-3.18 should enclose a total area of $-(2\pi)^2 2(p/4) = -(2\pi)^2(p/2)$, with the factor of 2 related to spin degeneracy [34, 44]. Recalling Eq. (2.1), we know that the Luttinger theorem controls the electron density modulo 2 per unit cell, thus the lattice effective model obeys

$$\langle F_{i\alpha}^\dagger F_{i\alpha}\rangle + \langle G_{i\alpha}^\dagger G_{i\alpha}\rangle = \langle C_{i\alpha}^\dagger C_{i\alpha}\rangle + \langle D_{i\alpha}^\dagger D_{i\alpha}\rangle = (2-p) \Rightarrow \approx p \text{ (as hole density)} \quad (3.81)$$

Moreover, from Eq. (2.4), we also know that in the conventional Fermi liquid phase the total electron density is $(1-p)$, that is the hole density given by $(1+p)$ and again, as in section 3.3.3, we can accept this difference as we are discussing a phase with U(1) topological order, that is a phase with an emergent U(1) gauge excitation. We can finally note that, even founding this difference of the hole density, this model does not yield a theory of the transition from the pseudogap state to the Fermi liquid state, and also there is no natural criterion for choosing between the electrons (holes) which form local moments and fractionalize, and those which are mobile, so leading to significant technical difficulties in obtaining the seeked small Fermi surface FL* state: thus we cannot consider this model a clear and satisfying demonstration of the modified Luttinger's theorem.

Chapter 4

Gauge approach with semionic statistics of holons and spinons

We now briefly present for comparison another well developed theory for the high-T_c superconducting cuprates [45-53, 79, 80], based on a spin-charge gauge approach and as pairing glue excitations emerging from the antiferromagnetic phase: antiferromagnetic spin vortices, so well different from the antiferromagnetic spin waves proposed in the previous chapter. We will shortly resume the main physical and mathematical steps of this theory, and in Chapter n. 6 we will make some considerations and comparisons with the theory discussed in the Chapter n. 3.

4.1. Braid and Haldane's exclusion statistics

In one and two dimensions braid statistics of particles can be characterized by the phase factor $e^{\pm i(\alpha-1)\pi}$ of the many-body wave function when we perform an oriented exchange of two particles, now called anyons [54]; $\pm$ refers to the two possible orientations, and $\alpha \in [0, 2)$, with fermions corresponding to $\alpha = 0$, bosons to $\alpha = 1$, while excitations with $\alpha = 1/2$ are called semions. The Haldane's exclusion statistics (HES) is instead a kind of generalization of the Pauli exclusion principle: if we consider a Fermi gas at $T = 0$ with fixed volume, enclosed by a Fermi surface, and with a fermion density n_0, we can say that a particle obeys HES with parameter g if the particle density n_g, with the same Fermi volume, satisfies $n_0 = n_g(1 - g)$. A particle with HES parameter $g = 1/2$ has a Fermi surface half of that of a Fermi gas with the same density, as it has, at a fixed momentum and neglecting other internal degrees of freedom, an occupation number twice that of a free fermion. In other words, particles with HES parameter g at $T = 0$ interpolates between Fermi-Dirac (FD, $g = 0$) and Bose-Einstein (BE, $g = 1$) distributions, while at finite temperature they have a much more complicated distribution than FD and BE ones, but we know that it holds a generalization of the Luttinger theorem, i.e. the interaction does not change the volume enclosed by the Fermi surface for HES. While in one-dimensional (1D) systems there is a deep connection between braid statistics and HES, in two-dimensional (2D) it does not. However in 2D we can show nonperturbativily [49] that the HES exists for incompressible[12] anyon liquid in the presence of a Hall response, that is it holds for the HES parameter g and the braid statistics parameter α

$$g = 2\pi\sigma_H\alpha \qquad (4.1)$$

Where σ_H is the Hall conductance, and if $\sigma_H = 1/2\pi$ Eq. (4.1) becomes $g = \alpha$.

[12] Incompressible means that $\partial N/\partial\mu = 0$, with N the total particle number and μ the chemical potential.

4.2. 2D *t-J* model for cuprates

Even in this model of the hole doped cuprates the Zhang-Rice singlet [7] is considered the key actor, and the model Hamiltonian is given by (summation over repeated spin and vector indices is intended, here and in the following)

$$H_{tJ} = \sum_{\langle i,j\rangle} P_G\left[-tc_{i\alpha}^{\dagger}c_{j\alpha} + J\boldsymbol{S}_i \cdot \boldsymbol{S}_j + h.c.\right]P_G \qquad (4.2)$$

where i,j denotes nearest neighbor (nn) sites of the lattice, t is the nn hopping, c the hole field operator, α is the spin index, J is the antiferromagnetic coupling, $\boldsymbol{S}_i$ is the spin on the i site ($\boldsymbol{\sigma}_{\alpha\beta}$ are the Pauli matrices) given by

$$\boldsymbol{S}_i = c_{i\alpha}^{\dagger}\frac{\boldsymbol{\sigma}_{\alpha\beta}}{2}c_{i\beta} \qquad (4.3)$$

The Gutzwiller projection P_G, clearly non linear, eliminates double occupation, and it is defined as

$$P_G \equiv \prod_i (1 - n_{i\uparrow}n_{i\downarrow}) \qquad (4.4)$$

For cuprates typical values are $t \approx 0.3 - 0.4\ eV$ and $J \approx 0.1\ eV$; in order to obtain a reasonable shape of the Fermi surface in the tight binding approximation we can add the next-to-nearest neighbor (nnn) hopping term t', $|t'| \approx 0.03 - 0.1\ eV$, strongly material-dependent. Passing to the Euclidean action of the t-J model in the path-integral representation in terms of spin $1/2$ fermionic fields $c_{i\alpha}^{*}$, $c_{i\alpha}$, and making an Hubbard-Stratonovich transformation on the quartic interaction term introducing a complex gauge field $X_{\langle ij\rangle}$, we obtain [45-47]

$$S_{tJ}[c,c^{*},X,X^{*}] = \int_0^{\beta} d\tau \left\{\sum_{\langle ij\rangle}\left[\frac{2}{J}X_{\langle ij\rangle}^{*}X_{\langle ij\rangle} + \left(-t + X_{\langle ij\rangle}\right)c_{i\alpha}^{*}c_{j\alpha} + h.c.\right] + \right.$$
$$\left. + \sum_i c_{i\alpha}^{*}(\partial_0 - \mu)c_{i\alpha} + \sum_{i,j} u_{ij}\, c_{i\alpha}^{*}c_{i\alpha}c_{j\beta}^{*}c_{j\beta}\right\} \qquad (4.5)$$

Where the two-body potential u_{ij} is, taking into account the Gutzwiller projection,

$$u_{ij} = \begin{cases} \infty & i = j \\ -\frac{J}{2} & \langle i,j\rangle \\ 0 & otherwise \end{cases} \qquad (4.6)$$

4.3. The spin-charge decomposition and the Chern-Simons gauge bosonizations in 2D

We now rewrite the hole field c_α as a product of a charge 1 spinless fermion h, the holon, and a neutral spin $1/2$ boson field $\tilde{s}_\alpha$, the spinon, that is $c_\alpha = h^* \tilde{s}_\alpha$ [47], thus getting rid of the Gutzwiller projection. In fact the holon, being spinless, implements it exactly, while imposing the constraint $\tilde{s}_\alpha^* \tilde{s}_\alpha = 1$, we obtain

$$c_i^* c_i = 1 - h_i^* h_i \qquad (4.7)$$

and thus $h_i^* h_i$ is the density of the empty sites of the model, that is the Zhang-Rice singlets. We then couple this t-J model to a $U(1)$ and an $SU(2)$ gauge fields, using the following [51-53]

Theorem. *We embed the lattice of the 2D t-J model in a 2-dimensional space, denoting by $x = (x^0, x^1, x^2)$ the coordinates of the corresponding 2+1 space-time, x^0 being the euclidean time. We couple the fermions of the t-J model to a $U(1)$ gauge field, B^μ, gauging the global charge symmetry, and to an $SU(2)$ gauge field, V^μ, gauging the global spin symmetry of the model, and we assume that the dynamics of the gauge fields is described by the Chern-Simons action $-2S_{c.s.}^{U(1)}(B) + S_{c.s.}^{SU(2)}(V)$, with*

$$S_{c.s.}^{U(1)}(B) = \frac{1}{4\pi} \int d^3x \, \varepsilon_{\mu\upsilon\rho} B^\mu \partial^\upsilon B^\rho(x) \qquad (4.8)$$

$$S_{c.s.}^{SU(2)}(V) = \frac{1}{4\pi} \int d^3x \, Tr \varepsilon_{\mu\upsilon\rho} \left[V^\mu \partial^\upsilon V^\rho + \frac{2}{3} V^\mu V^\upsilon V^\rho \right](x) \qquad (4.9)$$

where $\varepsilon_{\mu\upsilon\rho}$ is the Levi-Civita anti-symmetric tensor in 3D. Then the spin-charge, or $SU(2) \times U(1)$, gauged model so obtained is exactly equivalent to the original t-J model. In particular the spin and the charge invariant correlation functions of the fermions fields $c_{j\alpha}$ of the t-J model are exactly equal to the correlation functions of the fields $exp\left[-i \int_{\gamma_j} B\right] P\left(exp\left[i \int_{\gamma_j} V\right]\right)_{\alpha\beta} c_{j\beta}$, where c denotes now the fermion field of the gauged model, γ_j a string at constant euclidean time connecting the point j to infinity, and $P(\cdot)$ the path-ordering, which amounts to the usual time ordering $T(\cdot)$, when "time" is used to parametrize the curve along which one integrates.

It is important to observe that the role of the strings γ_j is to close the worldlines emerging, in the representation of the fields in the theorem above, when a fermion is created and annihilated, thus obtaining gauge-invariance also in the correlators, and we call the associated term a gauge string. There are no intersections between these worldlines, due to the Gutzwiller projection, so their crossings are well defined. Furthermore, referring to the decomposition $c_\alpha = h^* \tilde{s}_\alpha$ seen above, in our gauged model we can identify $exp\left[i \int_{\gamma_j} B\right] h$ as the holon and $P\left(exp\left[i \int_{\gamma_j} V\right]\right)_{\alpha\beta} \tilde{s}_{j\beta}$ as the spinon fields: in practice the electron of the t-J model is bound to a charge-vortex of flux of $-1/2$, and a spin vortex of flux of $1/2$, with the resulting identity still being a fermion. The Chern-Simons coupling automatically ensures that both "dressed" holon and spinon field operators obey semionic

braid statistics, and again we have the density of empty sites in the model, that is the Zhang-Rice singlets, given by $h_j^* h_j$. These two "dressing" vortices are necessary, in order to try to reproduce in 2D what happens in 1D: in fact we know that in going in 1D (this is done performing a dimensional reduction of the gauged model defined in the Theorem above, by restricting the spatial support of the hole fields to a line, and keeping the strings γ_j not along this line to avoid intersections with the hole worldlines, because it would make the Theorem not applicable), the holon and the spinon both should be semions, with braid statistics parameter $\alpha = 1/2$, to reproduce the correct low-frequency limit of the correlations function of the 1D t-J model, previously obtained by Bethe ansatz and conformal field theory techniques [46, 50-53]. Furthermore, in the 1D t-J model spinons form a semion gas with HES parameter $g = 1/2$, described by a Luttinger liquid theory, and adding them to the holon in the correlation functions of the physical hole, stripping away their gauge strings, the $1/2$ exclusion statistics is transferred to the holons. Thus in the 1D model we have $g = \alpha = 1/2$ statistics, so that, in agreement with the exact solution of the model, the Fermi momentum of the $U(1)$ semionic holon equals the Fermi momentum of the original spin $1/2$ fermion treated in the tight-binding approximation. Hence, since the spinon has no chemical potential and does not have a Fermi surface, while spinless holons have HES parameter $g = 1/2$, the composite hole, product of the spinon and the holon, satisfies the Luttinger theorem, and this is exactly what we are looking for in 2D with the above theorem and "dressing" charge and spin vortex. In fact, we know that in overdoped cuprates the Fermi surface seen in ARPES is close to that obtained in a tight-binding approximation of a t-t'-J model, and it also satisfies the Luttinger theorem. One option to reproduce this result in the spin-charge decomposition formalism is indeed to have a spinless holon, having Fermi surface, with HES parameter $g = 1/2$, and a spinon with no Fermi surface: in this approach, if both spinon and holon are semions, as resulting from the Theorem quoted above, it will be possible to obtain final results resembling to what happens in 1D. We have just seen in section 4.1 that in 2D we have $g = \alpha$ if the original fermionic system without Chern-Simons coupling has Hall conductivity $\sigma_H = 1/2\pi$ and is incompressible: a key step of this model is to show that these conditions can be satisfied for the holon in the 2D t-J model. We are thus looking for a semionic representation of the electron (hole) also in 2D.

4.4. Gauge symmetries of the model

In practice, correlation functions of electrons will be obtaines from the holons h and the spinons $\tilde{s}_\alpha$ via the substitutions

$$c_{j\alpha}(x) \leftrightarrow exp\left[-i \int_{\gamma_j} B\right] h_j^*(x) P \left(exp\left[i \int_{\gamma_j} V\right]\right)_{\alpha\beta} \tilde{s}_{j\beta}(x) \qquad (4.10)$$

$$c_{j\alpha}^*(x) \leftrightarrow h_j(x)\, exp\left[i \int_{\gamma_j} B\right] \tilde{s}_{j\beta}^*(x) P \left(exp\left[-i \int_{\gamma_j} V\right]\right)_{\alpha\beta} \qquad (4.11)$$

The theory has three internal symmetries:

- $U(1)$ gauge invariance, related to the electric charge of the holons, with $h_j \to h_j e^{-i\Lambda_j}$, $h_j^* \to h_j^* e^{i\Lambda_j}$, $B_\mu(x) \to B_\mu(x) + \partial_\mu \Lambda(x)$, and $\Lambda(x) \in \mathbb{R}$. This symmetry is fixed by choosing the Coulomb gauge $\partial_\mu B^\mu = 0$.
- $SU(2)$ gauge invariance, related to the spin of the spinons, with $\tilde{s}_j \to g_j \tilde{s}_j$, $\tilde{s}_j^\dagger \to \tilde{s}_j^\dagger g_j^\dagger$, $V_\mu(x) \to g^\dagger(x) V_\mu(x) g(x) + g^\dagger(x)\partial_\mu g(x)$, and $g(x) \in SU(2)$. This symmetry is fixed by choosing a condition to have an antiferromagnetic spin order as in the parent compound, that is

$$\tilde{s}_j = \sigma_x^{|j|}\begin{pmatrix}1\\0\end{pmatrix}; \qquad \tilde{s}_j^\dagger = (1 \quad 0)\sigma_x^{|j|} \tag{4.12}$$

  where $|j| = |j_x + j_y|$, i.e. the sum of the absolute value of the cartesian coordinates.We will have to integrate the field V_μ taking into account all gauge-inequivalent configurations with their gauge transformations, so we will split the integration over V in an integration over a field $\bar{V}$, satisfying the Coulomb gauge $\partial^\upsilon \bar{V}_\upsilon = 0$, with $\upsilon = 1,2$, and an integration over $\bar{V}$'s gauge transformations expressed in terms of $V_\mu = g^\dagger \bar{V}_\mu g + g^\dagger \partial_\mu g$, with $\mu = 0,1,2$ and g a $SU(2)$-valued scalar field.
- Holon/spinon (h/s) gauge invariance, related to the ambiguity in the decomposition $c_\alpha = h^* \tilde{s}_\alpha$, with $h_j \to h_j e^{i\lambda_j}$, $h_j^* \to h_j^* e^{-i\lambda_j}$, $\tilde{s}_j \to \tilde{s}_j e^{i\lambda_j}$, $\tilde{s}_j^\dagger \to \tilde{s}_j^\dagger e^{-i\lambda_j}$, $\lambda(x) \in \mathbb{R}$. This symmetry will not be fixed until the integration over the holons and spinons is required

After have integrated out the complex gauge field $X_{\langle ij\rangle}$, and considered the gauge-fixings above, we obtain an action of this gauged 2D t-J model, with $\delta = \mu + J$ proportional to the density of the hole doping [47, 51-53]

$$S[h,h^*,B,V] = \int_0^\beta d\tau \Big\{ \sum_j h_j^*[\partial_0 - iB_0(j) - \delta]h_j + iB_0(j) + i\big(1 - h_j^* h_j\big)\left(\sigma_x^{|j|} V_0(j) \sigma_x^{|j|}\right)_{11} - \sum_{\langle i,j\rangle} t h_j^* exp\left[i\int_{\langle i,j\rangle} B\right] h_i \left(\sigma_x^{|j|} P\left(exp\left[i\int_{\langle i,j\rangle} V\right]\right)\sigma_x^{|j|}\right)_{11} + \frac{J}{2}\big(1 - h_j^* h_j\big)(1 - h_i^* h_i)\left[\left|\left(\sigma_x^{|j|} P\left(exp\left[i\int_{\langle i,j\rangle} V\right]\right)\sigma_x^{|j|}\right)_{11}\right|^2 - \frac{1}{2}\right]\Big\} - 2S_{c.s.}^{U(1)}(B) + S_{c.s.}^{SU(2)}(V) \tag{4.13}$$

4.5. Gauge fixings of the model

Integrating this action over B_0, we obtain the constraint, with $\mu, \upsilon = 1,2$, $z \in \mathbb{R}^3$

$$\varepsilon_{\mu\upsilon}\partial^\mu B^\upsilon(z) = \pi\left[\sum_j \big(1 - h_j^* h_j\big)(z^0)\delta^{(2)}(\boldsymbol{z} - j)\right] \tag{4.14}$$

Imposing the Coulomb gauge $\partial_\mu B^\mu = 0$ we obtain

$$B^\mu(x) = \bar{B}^\mu + b^\mu(x) \tag{4.15}$$

$$\bar{B}^\mu = -\frac{1}{2}\sum_j \partial_\mu arg(\boldsymbol{z} - j) \tag{4.16}$$

$$b^\mu(x) = \frac{1}{2}\sum_j \partial_\mu arg(\boldsymbol{z} - j)\, h_j^* h_j(z^0) \tag{4.17}$$

The term $\bar{B}^{\mu}$ in Eq. (4.16) introduces a π-flux for every plaquette p, as it holds $exp\left[i\int_{\partial p}\bar{B}^{\mu}\right]=-1$, while in Eq. (4.17) for b^{μ} we can see the term $\partial_{\mu}arg(\boldsymbol{x}-j)$ as the vector potential of a vortex centered on an empty site j of the t-J model. These vortices are in the charge $U(1)$ group, and we will see below that their spin analogous are the antiferromagnetic vortices we are looking for the pairing. We can show that, also being a semion under braid statistics, due to the presence of vortices in Eq. (4.17), the holon field $exp\left[i\int_{\gamma_j} b\right]h_j$ also obeys an HES with parameter $g=1/2$ [49-52], where a crucial role is played by the holon-spinon gauge field, as a direct consequence of the no-double occupation constraint. Then these holons have the same Fermi surface of the fermionic spinons of the slave-boson approach in the π-flux phase [51, 52], and the same dispersion given by

$$\omega_h \sim 2t\left[\sqrt{cos^2k_x+cos^2k_y}-\delta\right] \qquad (4.18)$$

restricted to the magnetic Brillouin zone, and where we remember that δ represents the density of empty sites h^*h, which corresponds to the in-plane hole-doping of cuprates. We know [51], as also suggested by experimental results, that at high doping or temperature, i.e. the strange metal (SM) phase, in mean-field approach there is a vanishing flux per plaquette, while for sufficiently low doping and temperature, i.e. the pseudogap (PG) phase, there is an optimal flux per plaquette $\pi(1-\delta)$. Actually in this approach, going beyond the mean-field approach the δ correction to the optimal flux π per plaquette in mean-field is replaced by the phase describing charge vortices. Furthermore, the π-flux due to the Eq. (4.16) induces a Dirac structure for the holons and with Eq. (4.17) we obtain two small Fermi surfaces centered at $(\pm\pi/2\,,\pm\pi/2)$, with Fermi momenta given by $k_F\sim\delta$. We can thus conclude that these small Fermi surfaces and the Dirac structure of the holons, inducing a suppression of the spectral weight for the hole outside of the magnetic Brillouin zone, resemble the features of Fermi arcs seen in ARPES. We can denote by T^* the temperature of the crossover between these two phases, considering the PG the region $T<T^*$, and the SM the region $T>T^*$. The slave-particle generated gauge field, that is the (h/s) gauge, couples holons to spinons, and the resulting bound state, due the Dirac structure of the holons, has a hole Fermi surface modified by the spinon gap with a factor $(\delta)^{1/2}$, that has an enclosed area given by $A\sim\delta/2$, with the factor $1/2$ coming precisely from the HES parameter $g=1/2$ of the holons, as briefly outlined below [50-52]. As anticipated above, we are seeking for a field $\bar{V}$, satisfying $\partial^{\upsilon}\bar{V}_{\upsilon}=0$, from $V_{\mu}=g^{\dagger}\bar{V}_{\mu}g+g^{\dagger}\partial_{\mu}g$, with $g\in SU(2)$: thus we are searching a configuration of g, depending of the holon configuration and optimizing the holon-partition function in that g background: we call this configuration g^m, and then we will consider spinon fluctuations around g^m. In this configuration spinons are antiferromagnetically ordered along the magnetization direction of the parent compound, say along direction z, and there is a spin flip on the sites where holons are present, and also for the final site of a hopping link of holons. The spinon configuration g^m above the crossover temperature T^* also involves a phase factor deleting the contribution of $\bar{B}^{\mu}$ in the loops of hopping links of holons, thus that these hopping holons feel zero π-flux as seen above. The disappearance of this π-flux implies

that for $T > T^*$ we just recover, for the holons, the large Fermi surface of the tight-binding approximation, with an enclosed area given by $A \sim (1+\delta)/2$, with the factor $1/2$ again coming from the HES parameter $g = 1/2$ of the holons.

Having used the $SU(2)$ gauge freedom to rotate spinons to their optimal configuration g^m, we now need to integrate the $SU(2)$ field V_μ over all its configuration, thus obtaining

$$P\left[exp\left(i\int_x^y V\right)\right] = g_y^\dagger P\left[exp\left(i\int_x^y \bar{V}_\mu\right)\right] g_x \qquad (4.19)$$

where g describes the spinon fluctuations around the optimal configuration g^m, and we can write it as

$$g = \begin{pmatrix} s_1 & -s_2^* \\ s_2 & s_1^* \end{pmatrix} \qquad (4.20)$$

where we have redefined the spinons as s (instead of $\tilde{s}$ used until now), satisfying the constraint $s_{j\alpha}^* s_{j\alpha} = 1$. Assuming now that the fluctuations of g in Eq. (4.20) are small, we can neglect them, thus obtaining for the field $\bar{V}_\mu$ the following expression ($\mu = 1.2$)

$$\bar{V}^\mu(x) = -\frac{1}{2}\sum_j (-1)^{|j|} \partial_\mu arg(\boldsymbol{z} - j)\, h_j^* h_j(z^0)\sigma_z \qquad (4.21)$$

We recognize in Eq. (4.21) the factor $\sum_j (-1)^{|j|}\partial_\mu arg(\boldsymbol{z} - j)$, that is a vector potential of a vortex centered at the holon position j, with a chirality depending on the parity of $j = j_x + j_y$: these are antiferromagnetic spin vortices, recording in their vorticity the Néel structure of the lattice in the antiferromagnetic phase, and they are a peculiar manifestation of antiferromagnetic interaction, such as the antiferromagnetic spin waves discussed in Chapter n. 3. These vortices can be seen like topological excitations of the $U(1)$ subgroup of the initial $SU(2)$ spin group, unbroken in the antiferromagnetic phase, along the spin direction z of the magnetization (see σ_z in Eq. (4.21)). In other words, in 2D in the antiferromagnetic phase the spin group $SU(2)$ is broken to $U(1)$, and the quotient $SU(2)/U(1)$ is isomorphic to the 2-sphere S^2, whose points label the direction of the magnetization: in the unbroken $U(1)$ gauge group we thus have these antiferromagnetic spin vortices with opposite chirality centered in two different Néel sublattices. These vortices have a purely quantum origin, and they induce a topological effect far away from the position of the holon itself (where their classically visible field strength is supported). In this way the empty sites of the 2D t-J model, corresponding to the holon positions, are the cores of the antiferromagnetic spin vortices, seen as quantum distorsions of the antiferromagnetic spin background. These spin vortices are responsible for both short-range antiferromagnetic order and a new pairing mechanism leading to superconductivity: lowering the temperature, these vortices undergoes a Kosterlitz-Thouless transition, with the formation of a finite density of vortex/antivortex pair. As these vortices are centered at the holon positions, that is on charges, this induces a new form of charge pairing: indeed, it is again due to the antiferromagnetism, but is is really different from the spin-fluctuation pairing discussed in Chapter n. 3. While in 1D we have semionic holons with attached a spinon-derived spin

string, in 2D we have semionic holons "dressed" by antiferromagnetic spin vortices, thus in 2D vortices replace the role of kinks in 1D as topological defects.

4.6. Short range antiferromagnetism and charge pairing

In a mean-field treatment of the low-energy continuum limit of Eq. (4.13), and considering the field $\bar{V}$ in Eq. (4.21) representing the antiferromagnetic spin vortices, we can obtain the following conclusions [47, 51, 53]:

a) An interaction between vortices and spinons proportional to
$$\int d^3x\left(\bar{V}^\mu \bar{V}_\mu\right)(x)\, s_\alpha^* s_\alpha(x) \qquad (4.22)$$
b) The antiferromagnetic coupling changes from J to $J(1-2\delta)$, thus attesting the strong reduction of antiferromagnetism due to the increase of density of empty sites, corresponding to Zhang-Rice singlets discussed in Chapter n. 1.
c) An average over the positions of spin vortices yields the estimate
$$\langle \bar{V}^\mu \bar{V}_\mu \rangle \sim \delta |log\delta| \qquad (4.23)$$
and the term in Eq. (4.22) thus leads to a mass gap for the spinons as
$$m_s \sim \sqrt{\delta |log\delta|} \qquad (4.24)$$

In this way the gapless spinons s_α forming the spin waves of the $O(3)$ model describing the undoped system (see Appendix B.2) acquire a gap, while passing through the antiferromagnetic spin vortices. Thus the spinons, when the doping exceeds a critical value, convert the long-range antiferromagnetic order of the undoped model in the short-range antiferromagnetic order, produced by the antiferromagnetic spin vortices. Moreover we can show that the same term in Eq. (4.23) that describe the interaction of spinons with spin vortices generates also the charge pairing: to obtain this we have to treat in mean-field $s_\alpha^* s_\alpha(x)$, instead of $\bar{V}^\mu \bar{V}_\mu(x)$, obtaining ($\Delta$ is the 2D Laplacian)

$$J(1-2\delta)\langle s_\alpha^* s_\alpha \rangle \sum_{i,j} (-1)^{|i|+|j|} \Delta^{-1}\,(i-j) h_i^* h_i h_j^* h_j \qquad (4.25)$$

Eq. (4.25) describes a 2D lattice Coulomb gas with charges ± 1, depending on the Néel sublattice, with an attractive interaction between holons in opposite Néel sublattices, and maximal strength for nearest neighbor sites along the lattice directions with a d-wave symmetry. The coupling constant of this interaction is $J_{eff} = J(1-2\delta)\langle s_\alpha^* s_\alpha \rangle$: it decreases with doping and it is proportional to J, and not to t, as natural due to its magnetic origin (but it is reduced by the effect of the empty sites). We can thus conclude that charge pairing appears below a temperature $T_{ph} \sim J_{eff}$, and it induces also a reduction of the spectral weight of the hole, starting from the antinodal region of the Brillouin zone, exactly as seen in ARPES experiments, as anticipated in Chapter n. 1 and presented in Chapter n. 5.

4.7. Spin pairing and the pseudogap phase

The spinon gap results from the presence of the unpaired spin vortices: when charge pairing occurs at a temperature T_{ph}, the tight vortex/antivortex pairs do not contribute anymore to the spinon gap, and charge pairing thus leads to a lowering of the spinon energy proportional to the density of spinon pairs. Without going into mathematical details we can conclude that [47, 51, 53]:

a) At a temperature $T_{ps} < T_{ph}$, the slave particle gauge attraction between holon and spinon induces the formation of short-range spin-singlet spinon pairs, using the holon pairs as sources of attraction.
b) From the combined charge and spin pairing we get a gas of incoherent spin-singlet pairs.
c) At a lower temperature $T_c < T_{ps}$, with T_c the superconducting transition temperature, the hole pairs become coherent, and we have a d-wave hole condensate, which leads to superconductivity (not discussed in this paper).

Thus, due to the composite spin-charge structure of the hole of the model here discussed, we have two distinct temperatures: T_{ph} for charge-pair formation, and T_{ps} for spin-pair formation. This conclusion can be related to a particular experimental result: in fact we know that, in the presence of a temperature gradient, applying a perpendicular external magnetic field we obtain an imbalance between vortices and antivortices. This gives rise to a Nernst signal [81, 82], even if the hole pairs are not condensed yet. Therefore we can think that in the phase diagram of hole-doped cuprates T_{ps} corresponds to the onset of non-superconducting diamagnetic and vortex Nernst signal, as presented below (see Fig. 4.1). For the gas of incoherent hole pairs it has been obtained [51] an approximate evaluation of self-energy correction for the holon as

$$\Sigma(\boldsymbol{k},\omega) = \frac{|\Delta_h(\boldsymbol{k})|^2}{(i\omega+\omega_h(\boldsymbol{k}))}\left[1-\frac{m_{ph}}{\sqrt{\omega^2+\omega_h(\boldsymbol{k})^2+m_{ph}^2}}\right] \qquad (4.26)$$

where $\Delta_h(\boldsymbol{k})$ is the d-wave holon pair order parameter, $\omega_h(\boldsymbol{k})$ the holon dispersion, and the mass m_{ph} gives the scale of the inverse correlation length of the quanta of the phase of the holon field, thus separating self-consistently low energy modes with a Fermi liquid behavior from high energy modes with a d-wave superconducting behavior. The value of m_{ph} decreases with the temperature, thus lowering T we find a gradual reduction of the spectral weight on the Fermi surface at small frequency, as we move away from the diagonals of the Brillouin zone, due to the d-wave structure of $\Delta_h(\boldsymbol{k})$. Simultaneously, at large frequencies, we have the formation and increase of two peaks of intensity precursors of the excitation in the superconducting phase. This smooth interpolation between Fermi liquid and superconductivity is actually due to the interaction of the holon pairs with the gauge field. The physical hole is obtained as a holon-spinon bound state, produced by the gauge attraction, and it inherits the above holon features, but with a strongly enhanced scattering rate, due to the spinon

contribution. Loooking particularly in the pseudogap phase, we get that the suppression of the spectral weight just discussed sums up with the antinodal gap produced by the charge π-flux seen in section n. 4.5, thus leaving only small isolated segments of the Fermi surface of the hole.

4.8. Comparison with experimental results

Let us briefly review the comparison between the experimental data and the theoretical curves obtained from the model discusse in this chapter. In Fig. 4.1 we confront the phase diagram of this approach, with experimental data in hole doped cuprates [51, 53], showing the possible identifications of T_{ph} with the pseudogap temperature T^*, and of T_{ps} with the onset of Nerst signal due to vortices [81, 82].

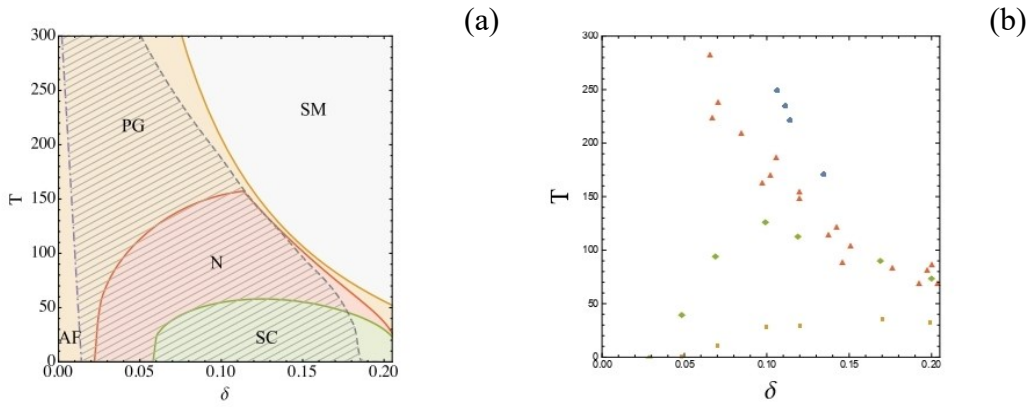

Figure 4.1. a) Theoretically derived phase diagram, with holon pairing temperature T_{ph} (yellow linw), spinon pairing temperature T_{ps} (red line), superconducting temperature T_c (green line) [51, 53, 79, 80]. b) Experimental data for T_c (yellow squares), onset of Nernst signal (green diamonds) in LSCO, low pseudogap in LSCO (red triangles), high pseudogap (blue circles) [51, 53 and references therein].

Another interesting comparison with experiments is given by the normalized in-plane resistivity when expressed as a function of the normalized temperature T^*/T (and it is also interesting that the theory produces an inflection point of the resistivity at $T^* \sim |log\delta|$) [51, 53, 80]: in Fig. 4.2 we can see a good agreement between theory and experiments, except a discrepancy at low T, perhaps due to the missing account of holon and spinon pair formation in the treatment used to determine the in-plane resistivity.

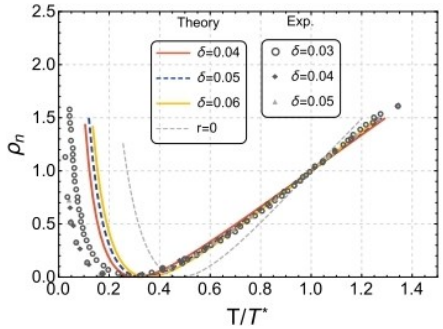

Figure 4.2. The normalized in-plane resistivity ρ_n theoretically calculated, compared with experimental results [51, 53 and references therein].

Finally we report in Fig. 4.3 how, in the pseudogap phase, the dependence on the Fermi surface angle (where $\alpha = 0$ corresponds to the nodal direction in the Brillouin zone) of the theoretically derived symmetrical spectral weight of the hole, is compared with experimental results [51, 79], showing a good qualitative agreement in terms of angle and temperature dependence.

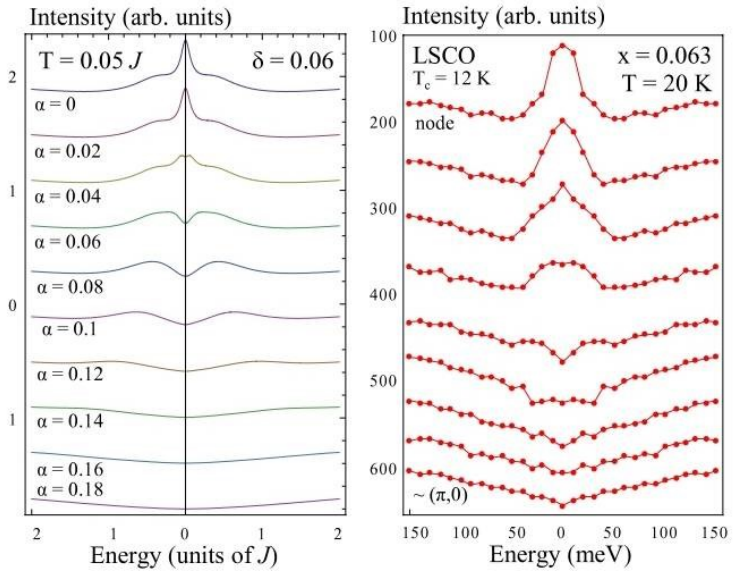

Figure 4.3. On the left there is the symmetrized spectral weight of the hole as a function of the angle α from the nodal direction in the pseudogap, while on the right there are the experimental data for Bi2212 [51, 79 and references therein].

Chapter 5

Recent experimental results on the pseudogap phase

The study of the high-temperature superconductivity in the cuprates has been driven by experiments since their discovery: numerous techniques have been brought to bear on the problem, analyzing every available aspect of the material, and the pseudogap phase has received much attention, motivated by the need to understand the "normal" state from which superconductivity emerges as temperature is decreased. Even considering only the last decade, there is an exterminated number of experimental results on the hole-doped cuprates, and, even if there are many consolidated conclusions, it is also not rare to have different interpretations. In this chapter we will present the more recent experimental results about the Fermi surface and its topology in the pseudogap regime of the phase diagram, and in relation to what we have discuss in the previous chapters. Thus we will refer to the more recent reviews [56-60] and references therein, and moreover to some singular paper particularly interesting.

5.1 Determination of pseudogap $T^*(p)$ and critical doping p^*

Remembering the discussion made in section 1.3 about the possible phase diagrams of hole-doped cuprates, in Fig. 5.1 we report a simplified one [59]. This phase diagram is reminescent of the antiferromagnetic (AF) quantum critical point (QCP): at $T = 0$, and in the absence of superconductivity, the key event on the path from the Fermi liquid (FL) to Mott insulator (AF) is the onset of the pseudogap (PG) phase, at a critical doping p^*: thus the pseudogap phase exists in all hole-doped cuprates below a temperature T^*, that decreases with doping to end at p^*, in the region $p < p^*$.

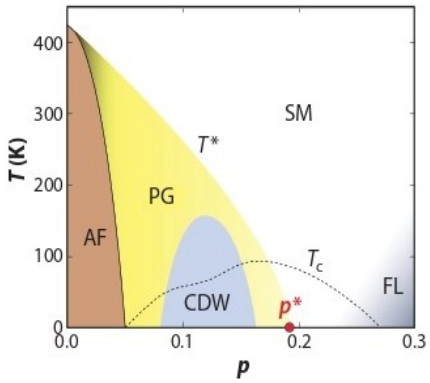

Figure 5.1. Phase diagram of hole-doped cuprates: in zero magnetic field, superconductivity exists in a dome below T_c. When superconductivity is removed by a magnetic field, various underlying ground states are revealed: doped Mott insulator with antiferromagnetic order (AF, brown); pseudogap phase (PG, yellow) below a temperature T^*, ending at a $T = 0$ critical point p^* (red point); charge-density wave phase (CDW, blue), contained inside the PG phase; a strange metal (SM, white) just above p^*, which gives way to a Fermi liquid (FL, gray) at highest doping [59].

In other words, below a temperature $T^*(p)$ a pseudogap develops, corresponding to a suppression of low-energy excitations in many experimental probes; extrapolating to $T = 0$, $T^*(p)$ defines the critical hole doping p^*, above which the pseudogap disappears. We do not go into detail about how the temperature T^* is determined, as it depends on the experimental technique employed (for example the opening of the pseudogap measured by ARPES coincides with an upturn in resistivity $\rho(T)$ at low temperatures as a function of doping p and T, thereby linking the transport anomalies directly to the pseudogap phase). We know that the pseudogap mechanism does not care about the crystal structure, while the critical doping p^* is however material-specific: in fact we have $p^* \cong 0.18$ for LSCO, $p^* \cong 0.23$ for Eu-LSCO and Nd-LSCO, $p^* \cong 0.19$ for YBCO, $p^* \cong 0.22$ for Bi2212 and $p^* \cong 0.40$ for Bi2201 [59, 61]. A series of experiments has been made, once superconductivity is removed by the application of a magnetic field [59 and references therein], and for our purposes it is important to recap these results:

- There are thermodynamic signatures of the pseudogap critical point p^*: a peak in the electronic specific heat C_{el} at low T, i.e. a huge peak at p^* of C_{el}/T in the $T = 0$ limit, and a logarithmic divergence of C_{el}/T as $T \to 0$. i.e. $C_{el}/T \sim \log(1/T)$ down to the lowest temperatures. These are the classic signatures of a QCP.

- What controls the location of p^*?. An interesting idea is that the pseudogap cannot form an electronlike Fermi surface, thus, given p_{FS} the critical doping value at which the Fermi surface changes topology from holelike to electronlike, we have the constraint $p^* \leq p_{FS}$. Numerical results on two-dimensional Hubbard model [78], also in good agreement with available experimental data, seem to confirm the idea, seen in Chapter n. 3, that the pseudogap is due to short-range antiferromagnetic correlations.

- The key transport signature of the pseudogap phase is a drop in the carrier density from $n \approx 1 + p$ at $p > p^*$, to $n \approx p$ at $p < p^*$.

- The pseudogap ground state has a Fermi surface transformed and the carrier density reduced without long-range order to break the translational symmetry: we have seen in Chapters nn. 2-3 how a possible explanation could be the presence of a state with topological order.

5.2 Fermi surfaces from ARPES

Angle-resolved photoemission spectroscopy (ARPES) experiments enable the momentum dependent single-electron spectral function at the Fermi energy to be mapped directly, thus identifying the momentum dependence of any single particle gaps in the spectral response. In fact photoemission spectroscopy measures the occupied single-particle spectral function, which describes the allowed

energies for a single-particle excitation with a given momentum. It is well known [57, 58, 60] that ARPES studies in the underdoped regime in the normal state above T_c identify the presence of the pseudogap in the antinodal directions together with disconnected Fermi arcs in the nodal directions, as depicted in Fig. 5.2a. On the other hand, ARPES studies of highly overdoped cuprates find evidence of a full Fermi surface on the normal state, with an area $A_{FS}\sim(1+p)$, as depicted in Fig. 5.2b, that well obeys the Luttinger's theorem.

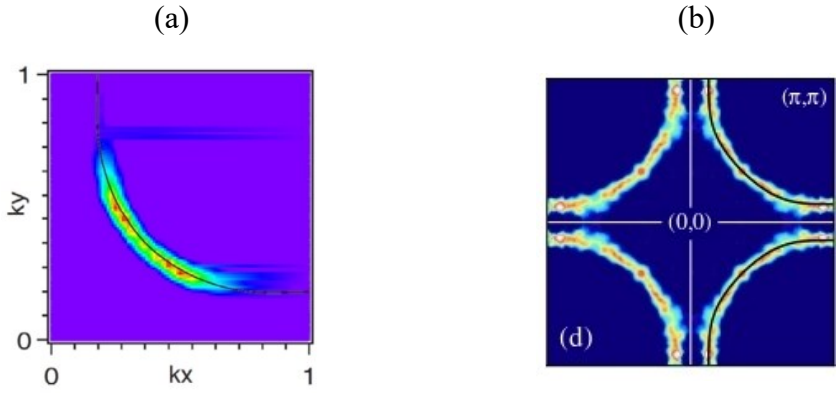

Figure 5.2. (a) ARPES measurement of the low lying excitations around the Fermi surface in the underdoped regime of the underdoped Bi2212 at $T = 140\ K$, showing the gaps observed at the end of the arcs in the $(\pi, 0)$ and $(0, \pi)$ directions [58]. (b) ARPES measurements of the overdoped Tl2201 at $T = 10\ K$ [62].

This transition from Fermi arcs at underdoping to full Fermi surface at overdoping could presumably reflects a crossover/phase transition as due to the presence of some topological order, as discussed in Chapters nn. 2-3: in this theoretical model of the pseudogap regime we have found hole pockets and not the Fermi arcs observed by ARPES. By the way the "anomalous" (as in condensed matter systems we expect closed Fermi surfaces) Fermi arcs in underdoped cuprates have been the subject of considerable investigations, with several studies interpreting them as indicating a temperature dependent arc length, others a doping dependent length [58]. However, as seen in Chapter n. 3, the hole pockets can consist of the observed Fermi arcs on one side, defined through infinities of the Green's function, and, on the back side, through zeros of the Green's function, as it switches from positive to negative values along the antiferromagnetic Brillouin zone boundary, which also coincides with the umklapp surface: the zeros of the Green's function on the backside of the hole pockets will be invisible in any ARPES experiment, conform to the generalized Luttinger sum rule [58]. Moreover it is possible to map the doping dependence of these hole pockets, providing evidence that they have an area proportional to the doping, as seen in Fig. 5.3 [58, 63]. This appears to confirm how presented in section n. 2.3, where we discuss how the FL* could explain an area of the Fermi surface proportional to the hole doping density p in the underdoped pseudogap phase for temperature $T < T^*$, and proportional to the hole doping density $(1+p)$ in the overdoped strange metal and Fermi liquid phases for temperature $T > T^*$.

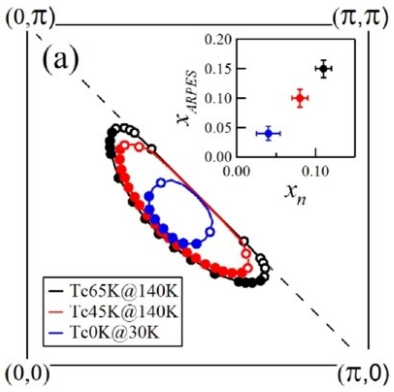

Figure 5.3. The "pseudo" hole pockets determined for three different doping levels: $p = 0.04$ at $T = 0\ K$ in blue, $p = 0.11$ at $T = 45\ K$ in red, and $p = 0.15$ at $T = 65\ K$ in black. In the inset it is shown how the area x_{ARPES} of the pockets scales with the nominal doping $p \equiv x_n$ [63].

While considering that whether the Fermi arc is indeed one side of a small nodal hole pocket is contested for deeply underdoped cuprates, we underline that recently [64] long-range antiferromagnetic order and a small hole pockets were unambiguously observed from the middle layers in the five-layer overall hole-doped cuprate $Ba_2Ca_4Cu_5O_{10}(F,O)_2$, whose crystal is free from structural distortion, and therefore free from the observation of artificial hole pockets. In Fig. 5.4 we report the ARPES intensities integrated close to the Fermi level, finding two hole pockets centered at $(\pi/2, \pi/2)$, in addition to a Fermi arc, typical for underdoped cuprates.

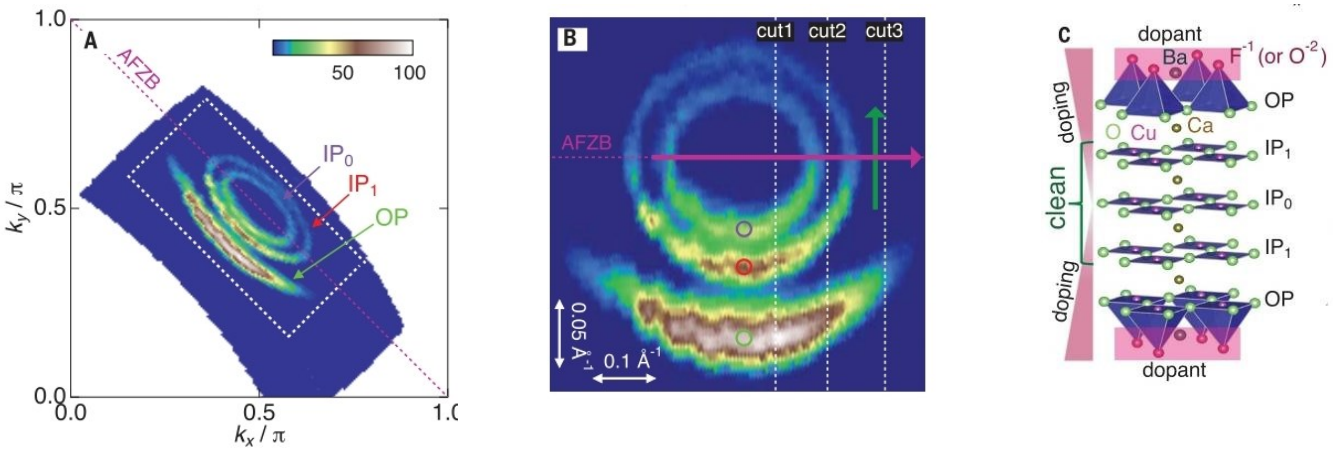

Figure 5.4. (A) Fermi surface obtained by integrating ARPES intensities within an energy window of 10 meV about the Fermi level, with the arrows pointing to Fermi surfaces dominated by the innermost plane IP_0, the second inner plane IP_1, and the outermost plane OP, which are depicted in (C). (B) Magnified image of the area enclosed by the white dashed rectangle in (A). (C) Five CuO_2 sheets in the crystal structure of $Ba_2Ca_4Cu_5O_{10}(F,O)_2$ [64].

5.3 Fermi surfaces from quantum oscillations

We know that all the physical properties of a material, that are a function of the density of states, exhibit quantum oscillations, i.e. oscillatory behavior, that is periodic in inverse applied magnetic fields: in fact, due to Landau quantization of energy levels in an interacting electron system as the applied magnetic field is increased, a discontinuos jump occurs in the density of states each time a Landau level exits the Fermi surface [56]. The frequency F of these quantum oscillations, obtained by Fast Fourier Transform, yields a measure of the Fermi surface area A_{FS} in momentum space, related to the Onsager relation[13]. We report the Fermi surface of overdoped ($p \approx 0.30, T_c \approx 10\ K$) Tl2201, as single, large and hole-like one, detected in c-axis resistance and torque measurements [35, 56, 59]. As depicted in Fig. 5.5a, the oscillatory frequence $F \approx 18100\ T$ converse to a Fermi surface area A_{FS} in excellent agreement with the k-space area (representing 65% of the first Brillouin zone) deduced from ARPES (and ADMR, as seen below), and it corresponds to a carrier density (per Cu atom) $n \approx 1.3 \approx 1 + p$, also in good agreement with the Hall number $n_H \approx 1.3$ obtained from Hall measurements at low temperatures [59]. The same behavior is found for other overdoped hole-cuprates, as YBCO and Hg1201(see also Fig. 5.10) [56, 59].

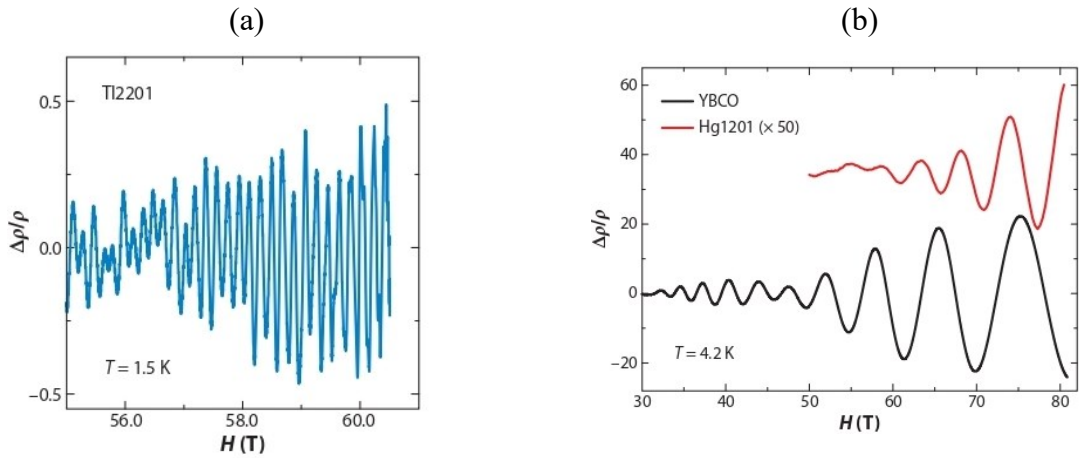

Figure 5.5. (a) Quantum oscillations of resistivity in overdoped ($p \approx 0.30, T_c \approx 10\ K$) Tl2201 [59]. (b) Quantum oscillations of resistivity in underdoped ($p \approx 0.11, T_c \approx 62\ K$) YBCO in black, and underdoped ($p \approx 0.10, T_c \approx 72\ K$) Hg1201 in red [59].

On the other hand, the underdoped one, we report in Fig. 5.5b the quantum oscillations of underdoped ($p \approx 0.11, T_c \approx 62\ K$) YBCO [35] and underdoped ($p \approx 0.10, T_c \approx 72\ K$) Hg1201 [65], both having the main oscillatory frequence $F \approx 530\ T$, that gives a Fermi surface area A_{FS} in excellent agreement with the k-space area (representing 2% of the first Brillouin zone) deduced from ARPES. In Fig. 5.6 we thus report how quantum oscillations reveal that the normal ground state of the underdoped cuprates, in contrast to the large hole-like Fermi surface calculated from the band structure and

[13] $F = \frac{\hbar}{2\pi e} A_{FS}$ is the relation connecting the frequency and the area enclosed by the Fermi surface, and $n = F/\Phi_0 = 2A_{FS}/(2\pi)^2$ is the relation giving the density carrier, where e is the charge of the electron, and $\Phi_0 = h/2e$ is the flux quantum.

measured in overdoped cuprates, comprises primally a small electron-like Fermi surface [56], and let us briefly see an explanation for this.

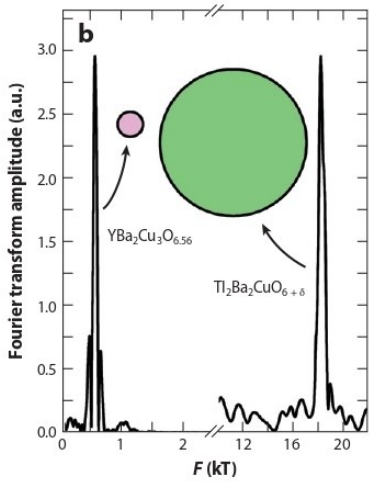

Figure 5.6. Comparison between the small Fermi surface measured in the underdoped region and the large Fermi surface measured in overdoped regime [56, 59 and references therein].

As anticipated above (see pag. 14), we will not discuss the experimental results obtaining charge (and spin) density waves (CDW and SDW), but here we must make an important consideration: many experimental results made at low temperatures and with magnetic field suppressing superconductivity [59 and references therein, 61, 66, 67] report the Hall coefficient R_H[14] (and the Seebeck coefficient S[15]) being negative in the doping interval where quantum oscillations have been observed. The combination of these observations is a strong indication of the presence of small closed electron pocket in the Fermi surface. We do not discuss about the exact mechanism of Fermi surface reconstruction by this CDW order, even because this is still debated: indeed, the relationship between CDW order and the pseudogap phase is the subject of ongoing research. However, two conclusions can be considerated well defined [59]:

- The combination of quantum oscillations and a negative Hall coefficient R_H is a strong indication for the presence of a small closed electron electron pocket in the Fermi surface, and this fact is also consistent with the magnitude and negative sign of the Seebeck coefficient S.
- The most natural interpretation for the presence of this small electron pocket is a Fermi surface reconstruction by some density wave that breaks translational symmetry: indeed careful study of the quantum oscillations in the underdoped regime [56, 59] reveals an electronic structure associated with a CDW, which appears to be characteristic of a translational symmetry broken ground state, universal to the hole doped cuprates.

[14] The Hall coefficient can be defined as $R_H = V/en_H$, where V is the volume per Cu atom in the CuO_2 plane, e is the electron charge, and the Hall number $n_H \approx n$, with n the carrier density, for a single-band metal in the $T \to 0$ limit [13].
[15] The Seebeck coefficient can be defined as $S/T = \gamma/ne$, with γ the electronic specific heat $\gamma = C_{el}/T$ [66, 67].

- For temperature $T \to 0$ the CDW phase ends at a critical doping p_{CDW} distinctly lower than p^*, thus we can consider that the CDW order is not always observed over the same range of dopings as the pseudogap phase itself.

5.4 Fermi surfaces from ADMR

After the considerations made above, a crucial question thus remains: what is the Fermi surface of the hole-doped cuprates immediately below p^*, in the absence of superconductivity or CDW order? There are two possibilities:

1. The Fermi surface is the same above and below p^*, but the quasiparticles become incoherent below p^* due to scattering or other correlation effects.
2. The Fermi surface below p^* is different from the Fermi surface above p^*: demonstration of this scenario would imply that either in the pseudogap phase the translational symmetry is broken (on some appropriate length scale), or it is a phase with a topological order, as discussed in Chapters nn. 2-3.

As a possible confirmation of the second scenario, and of the gauge theory presented in Chapter n. 3, we here report a very recent result [68]: doing angle-dependent magnetoresistance (ADMR) on Nd-LSCO (which have a critical doping $p^* \approx 0.23$ well defined by specific heat, transport and ARPES measurements [59]), one measures variations in the c-axis resistivity ρ_{zz} at dopings $p = 0.21$ (below p^*) and $p = 0.24$ (above p^*), as a function of the polar θ and the azimutal ϕ angles between the sample and an external magnetic field B. These variations are determined by the three-dimensional geometry of the Fermi surface, and the momentum dependence of the scattering rate: it is important to remark that this is the first ADMR measure made in the pseudogap phase of a hole-doped cuprate, also in the absence of CDW order. In Fig. 5.7 we plot a scheme of the experiment.

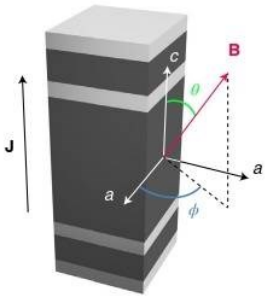

Figure 5.7. Geometry of the ADMR measurements, with the Nd-LSCO sample represented in grey with silver contacts, the black arrow identifies the direction of the electric current **J** used to measure the resistivity ρ_{zz} along the c-axis, and the angles θ and ϕ indicate the direction of magnetic field **B** with respect to the crystallographic c and a axis [68].

For doping $p = 0.24$ we see in Fig. 5.8 the data, the simulation obtained using a single-band tight-binding model, and the Fermi surface obtained from the ADMR calculations, and all these features suggest that the ADMR at $p = 0.24$ exhibits optimal agreement with a large, unrecostructed Fermi surface (obeying the Luttinger's theorem), as also observed by ARPES.

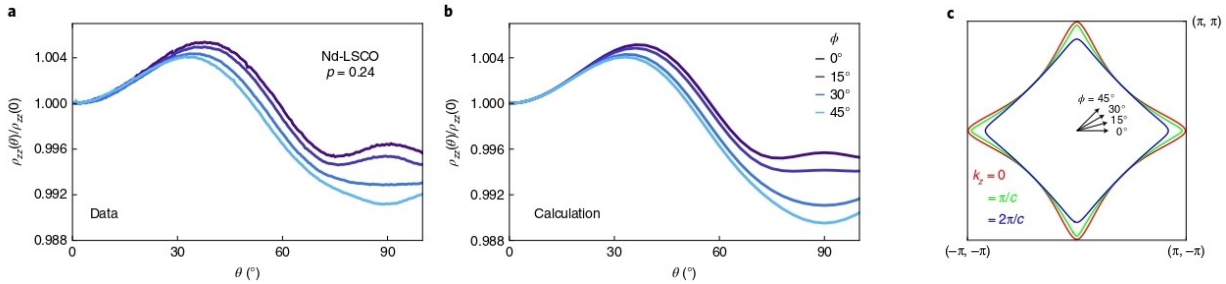

Figure 5.8. (a) The ADMR of Nd-LSCO at $p = 0.24$ as a function of θ at $T = 25\ K$ and $B = 45\ T$. (b) Simulation using tight-binding model. (c) The Fermi surface of Nd-LSCO at $p = 0.24$ obtained from the ADMR calculations, with cuts shown at $k_z = 0, \pi/c, 2\pi/c$, where c is the the height of the unit cell, and $c/2$ the distance between the CuO_2 planes. (all data are normalized by the $\theta = 0°$ value, $\rho_{zz}(0)$ [68].

For doping $p = 0.21$, well inside the pseudogap phase, we see in Fig. 5.9a the data, and we can immediately affirm, confronting with Fig. 5.8a, that the structure of the ADMR qualitatively changes on entering the pseudogap phase: in particular, at $p = 0.21$ the resisitivity peak near $\theta = 40°$ disappears. In order to understand this change in the ADMR across p^*, several different scenarios are tested:

- Change of only the quasiparticle scattering rate, simply adjusting the chemical potential.
- Isotropic scattering around the entire Fermi surface.
- Fermi arcs, with Fermi surface terminating at the antiferromagnetic zone boundary.
- Electron pocket at nodal positions in the Brillouin zone, as a result of CDW order.

One reports the inability of any of these scenarios to fit the ADMR data at $p = 0.21$ [68]: this suggests that, not only the Fermi surface must be reconstructed into a new, geometrically distinct one in the pseudogap phase, but also in a way not due to CDW order. We report in Fig. 5.9 how these data below p^* are best described by a Fermi surface composed of nodal hole pockets: clearly such pockets arise in various theoretical scenarios, inclusing the one we have discussed in Chapter n. 3 [8, 21, 22, 33, 34, 36-44, 73], where, as depicted in Fig. 5.9c, we have seen how these pockets can be generated by reconstructing the Fermi surface using antiferromagnetic order with a wavevector $\mathbf{K} = (\pi, \pi)$, even if there can be other models, like the phenomenological Yang-Rice-Zhang ansatz [69].

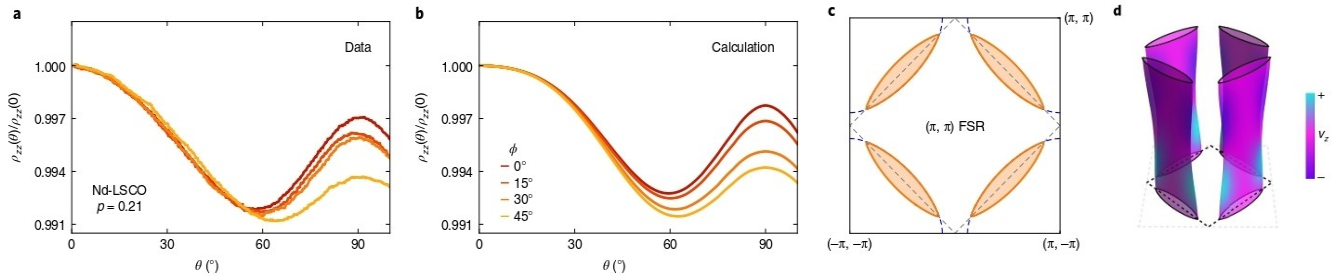

Figure 5.9. (a) The ADMR of Nd-LSCO at $p = 0.21$ as a function of θ, for $\phi = 0°, 15°, 30°, 45°$, at $T = 25\ K$ and $B = 45\ T$ (all data are normalized by the $\theta = 0°$ value, $\rho_{zz}(0)$. (b) Calculated ADMR for the Fermi surface shown in (c) with an isotropic scattering rate. (c) Fermi surface consisting of four nodal hole pockets, implemented with a model of antiferromagnetic order with the wavevector $\boldsymbol{K} = (\pi, \pi)$ and a gap of 55 K. (d) The full 3D Fermi surface at $p = 0.21$ after reconstruction [68].

We have just seen in section 5.2 how similar hole nodal hole pockets have recently been detected by both quantum oscillations and ARPES in the five-layer $Ba_2Ca_4Cu_5O_{10}(F,O)_2$ [64]. Moreover, this reconstruction is consistent with the transition form the carrier density $n = 1 + p$ at $p > p^*$ to $n = p$ at $p < p^*$, as revealed by measuring the Hall coefficient R_H: this reduction in the Hall number $n_H \approx n$ within the pseudogap phase appears universal in hole-doped cuprates [13, 59, 61, 70], as plotted in Fig 5.10.

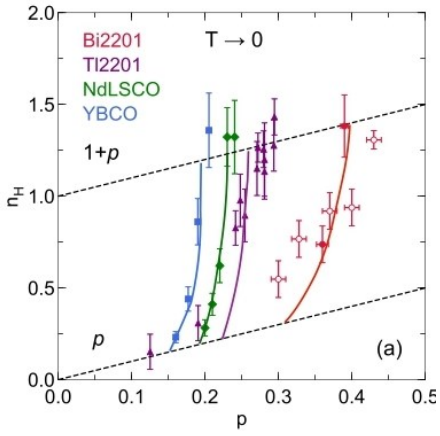

Figure 5.10. Hall number $n_H = V/eR_H$, with V the volume per Cu, as a function of doping for four different hole-doped cuprates: Bi2201 (solid red circles, $p^* = 0.4$), Nd-LSCO (green diamonds, $p^* = 0.23$), YBCO (blue squares, $p^* = 0.19$), and Tl2201 (purple triangles, p^* not currently known) [61 and references therein].

The model of Fermi surface transformation in four nodal hole pockets produces the correct Hall number n_H, both above and below p^*: this strongly suggests that this model could be universal, whereas the tendency towards CDW and SDW orders substantially varies between different cuprates, as also does the single value of p^*. This ADMR experiment appears thus to be the first experimental evidence of the Fermi surface transformation (until now missing) accompanying the T-linear resistivity near optimal T_c, and enhanced effective mass, occurring at the critical doping where the pseudogap phase appears.

Chapter 6
Conclusions

We try to make a simple discussion about what presented in this paper: for simplicity we call:

- S-model the approach presented in Chapter n. 3 from Sachdev et co-workers [8, 21, 22, 33, 34, 36-44, 73]: this model, starting from the single-band Hubbard model (see Eqs. (3.1)) for the Mott insulator of the undoped parent compound, considers a $SU(2)$ gauge theory of the angular fluctutations of the antiferromagnetic order, with the pseudogap obtained with a sort of Higgs' transition to a $U(1)$ gauge group with a topological order. The physical hole is seen as a bound state of an holon (fermionic degree of freedom with charge $+e$ and spinless) and a spinon (bosonic degree of freedom chargeless and with spin $S = 1/2$), with an emergent gauge field linked to the topological order.
- M-model the approach in Chapter n. 4 from Marchetti et co-workers [45-53, 79, 80]: this model starts from the t-J model (see Eq. (4.2)), then couples the holes to a $U(1)$ gauge field (for the global charge symmetry) and to a $SU(2)$ gauge field (for the global spin symmetry), using Chern-Simons terms to describe the dynamics of these gauge fields in the action of the model. However, all these mathematical implementations leave the correlation functions of the hole fields exactly unchanged. After, the model considers a spin-charge decomposition of the physical hole into an holon and a spinon (with the same features of the S-model), and this decomposition has a $U(1)$ gauge symmetry, clearly different from the charge gauge symmetry seen above. The final key step is to study the statistics of holon and spinon, obtaining both of them being semions in the braid statistic and obeying an exclusion statistics with parameter $g = 1/2$. Thus the model can obtain the spin antiferromagnetic vortices seen as the key feature for charge and spin pairing in the pseudogap phase, also leading to superconductivity

We will make some comments on the theoretical basis of both of the models, discussing the comparison with the experimental results, and finally we will try to look at the possible future developments of the two models.

6.1. Comments on theoretical basis of S- and M- models

Clearly from the beginning the S-model describes the pseudogap as a FL*, that is a fractionalized Fermi liquid, with electronlike quasiparticles around pocket Fermi surfaces enclosing a volume associated with hole density p. Such small pocket Fermi surface can appear even without any translational symmetry breaking by charge and spin density wave order: even if several low temperature charge and spin ordered states have been explored in the underdoped cuprates, in this paper we have not considered them, as they can be seen as low temperature instabilities of the

pseudogap phase, to be understood in a deeper and more refined treatment. The key physical feature of the transition to the pseudogap phase is considered the change in Fermi surface size, i.e. from the large Fermi surface, Fermi liquid-like, to the small pocket Fermi surface, also without symmetry breaking, and in this analysis the Luttinger's theorem is clearly considered. While this theorem is normally obeyed in the large Fermi surface phase, we have seen as the small Fermi surface phase satisfy a modified and generalized Luttinger's theorem, with a topological order given by the emergent gauge fields accompanying the fractionalized excitations. In other words, compatibility with the modified Luttinger's theorem requires the presence of additional fractionalized spinon excitations carrying charges of an emergent gauge field. The "natural" pairing glue, even leading to superconductivity, is thus provided by the *antiferromagnetic spin waves*.

The M-model instead considers as the pairing glue another kind of excitation emerging from the antiferromagnetism of the Mott insulator as the undoped parent compound: we have seen as this model leads to the presence of charge vortices centered on the holon positions (the empty sites of the 2D t-J model), converting the holons into semions, also implying the presence of *antiferromagnetic spin vortices*. These vortices, to our knowledege, do not appear in other model for the hole doped cuprates, and are also specific to the 2D structure of the cuprates, being probably the key feature of the M-model. These vortices are a consequence of the antiferromagnetic interaction, like the antiferromagnetic spin waves seen in the S-model, but they are purely of quantum origin. These vortices are a kind of topological excitation of the unbroken (in the antiferromagnetic phase) $U(1)$ subgroup of the $SU(2)$ spin group: being centered on holon positions, they have opposite chirality for positions in opposite Nèel sublattices, thus they induce charge pairing. We have seen how this model, even with a kind of mathematical complexity, discuss how superconductivity can arise through the three-step mechanism at temperatures $T_c < T_{ph} < T_{ps}$, without crossing a phase transitions at T_{ph} and T_{ps}, but with only crossover: for our analysis of the pseudogap charge pairing at T_{ph} has also the important consequence that lowering the temperature we find a gradual reduction of the spectral weight on the Fermi surface at small frequency, specially in the antinodal regions of the Brillouin zone, as also the π-flux of the charge gauge field does.

Looking particularly on the validity of the Luttinger's theorem in the pseudogap phase, we thus can say that while the S-model, as seen above, try to use a *topological point of view* with the topological order from an emergent gauge field, on the other way the M-model try to use a *statistical point of view*. In fact this model uses the fact that in 1D the hole, composite of holon and spinon, satisfies the Luttinger's theorem, due to the semionic and Haldane exclusion statistic of holon and spinon in 1D. Thus, showing that also in 2D holon and spinon are semions with Haldane statistic parameter $g = 1/2$, the Luttinger's theorem is satisfied in the pseudogap phase giving an area of the Fermi surface $A \sim \delta/2$ (where δ is proportional to the density of the hole doping). In other words while the S-model requires the modified Luttinger's theorem (see Chapter n. 2 and Appendix A) with the presence of a

topological order from the emergent gauge field, the S-Model finds an analogue emergent gauge field, that is the emergent slave particle (holon/spinon) gauge symmetry, which we know being also strictly related to the no-double occupation constraint.

6.2. Comparison with experimental results

In Chapter n. 5 we have presented the more recent experimental results, specially about the Fermi surface in the pseudogap phase, as it is obviously related to the Luttinger's theorem. Moreover, the electronic properties of a metal derive specially from the structure of its Fermi surface, as in momentum space it gives us the most energetic occupied electronic states. We have just seen in Chapter n. 3 how the S-model fits to the Fermi surface from ARPES, the well known Fermi arcs. We underline that a key point of this comparison is that the S-model gives hole pockets at the nodal positions of the Brillouin zone as Fermi surfaces in the pseudogap phase, and this can be explained by a suppression of the spectral weight at the backside as a result from its proximity to an approximate zero of the Green's function, as seen in section n. 3.3, or by the mixing of the two quasiparticles-bound states of the holon and the spinon, as seen in section n. 3.4. Anyway, referring to Figs. 3.10, 3.19, 3.20, in both cases for the S-model we obtain a good agreement amid theoretical and ARPES results. Similarly we have seen in Figs. 4.1-4.3 the good agreement between the M-model and the experimental results in the pseudogap phase for the resistivity and for the Fermi arcs seen in ARPES. Clearly neither model fits with all kinds of experiment: for example the M-model in his derived phase diagram (see Fig. 4.1) misses completely the onset of charge density wave around $\delta \approx 1/8$ (presented in Chapter n. 1), but appears well compare the Nernst signal, completely missed by the S-model [81-82]. Moreover, the series of novel experiments using intense magnetic fields to suppress the superconductivity [57-59] has revealed the reorganization of the charge density, thus showing that the pseudogap is a well distinct phase from both the superconducting and charge (and spin) ordered phases. Yet considering these kinds of experiments [59], we note that the S-model fits better to the possible quantum critical point given by the critical doping p^* at $T = 0$ (also perhaps giving rise to the strange metal phase), as discussed in section 5.1.

6.3. Developments in real time and future ?

Even with the agreement with some experimental results as seen above, we note that neither the S-model here presented [8, 21, 22, 33, 34, 36-44, 73] or similar methods cited in this paper [28, 58, 69], all obtained by the nonperturbative binding spinon and holons excitations, seem to provide a fully self-consistent method for computing the Fermi surface in both the small and large Fermi surface states, differently from the M-model, as seen in Chapter n. 4: in other words these models do not yield a theory of the transition to the Fermi liquid state. In fact, it appears that in the S-model there is no natural criterion for choosing between the electrons (holes) which form local moments and fractionalize, and those which are mobile, so leading to significant technical difficulties in obtaining the seeked small Fermi surface FL* state. This conclusion does not involve the M-model [45-53, 79,

80], as it does not involve the topological point of view, as seen above. With regard to the S-model, there are very recent works [83-86] showing that many of these difficulties can be overcome in an "ancilla qubit" approach, describing both the small and large Fermi surface states of a single band model. We only briefly summarize the key beginning steps of this approach:

- We begin with almost the same Hubbard model seen in Eqs. (3.1) with the same meaning

$$H_{HUB} = -\sum_{i<j} t_{ij}\left(c_{i\alpha}^{\dagger} c_{j\alpha} + h.c.\right) - \mu \sum_i c_{i\alpha}^{\dagger} c_{i\alpha} + U \sum_i n_{i\uparrow} n_{i\downarrow} \qquad (6.1)$$

  also making the same passages until Eq. (3.3): in the Hubbard-Stratonovich transformation we have, instead of the field $\boldsymbol{J}_i$, a new field $\boldsymbol{\Phi}_i$, the *paramagnon*, that is a bosonic collective mode representing antiferromagnetic spin fluctuations. It can be rescaled with the constraint $\boldsymbol{\Phi}_i^2 = 1$, thus its dynamic is given by a kinetic energy term of a particle with angular momentum $\boldsymbol{L}_i$ moving on a unit sphere.

- We thus obtain a Hamiltonian for electrons coupled to a paramagnon quantum rotor on each site, given by

$$H_{par} = \sum_{\boldsymbol{k}} \varepsilon_{\boldsymbol{k}}\, c_{\boldsymbol{k}\alpha}^{\dagger} c_{\boldsymbol{k}\alpha} + \frac{g}{2}\sum_i \boldsymbol{L}_i^2 + \sum_i \left(\lambda \boldsymbol{\Phi}_i + \tilde{\lambda}\boldsymbol{L}_i\right) \cdot c_{i\alpha}^{\dagger} \frac{\boldsymbol{\sigma}_{\alpha\beta}}{2} c_{i\alpha} \qquad (6.2)$$

  Where the parameters g and λ have the same meaning seen in Chapter n. 3, while $\tilde{\lambda}$ describes the coupling of the electrons with the paramagnons. We can visualize this Hamiltonian as in Fig. 6.1, with the physical electrons coupled with λ, $\tilde{\lambda}$ with the paramagnon rotor, that is a particle of mass $1/g$ moving on a unit sphere with angular momentum $\boldsymbol{L}_i$

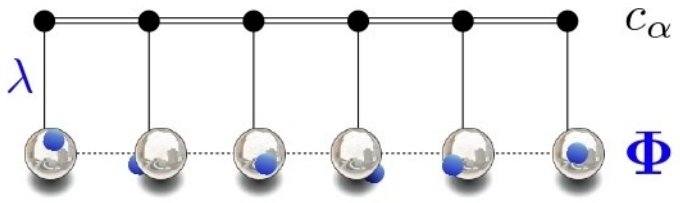

Figure 6.1. Band of physical electrons c_α in sites of a $d > 1$ lattice (although only one dimension is shown), each coupled to a paramagnon quantum rotor described by a particle of mass $1/g$ constrained to move on the unit sphere with coordinate $\boldsymbol{\Phi}$ (here it lacks the coupling $\tilde{\lambda}$) [86].

- Now we replace each paramagnon rotor by a pair of antiferromagnetic coupled spins, considering only the lowest energy $l = 0, 1$ angular momentum states of each rotor: we can represent these singlet and triplet states by a pair of $S = 1/2$ spins, $\boldsymbol{\Psi}_{1i}$, $\boldsymbol{\Psi}_{2i}$ (expressed as seen in this paper), coupled with n antiferromagnetic exchange coupling $J_\perp = g$. These spins are the so called "ancilla" qubits. As depicted in Fig. 6.2, there are also a coupling J_K between the c spin and the $\boldsymbol{\Psi}_1$ and a coupling $\tilde{J}_K$ (not displayed for simplicity) between the c spin and the $\boldsymbol{\Psi}_2$.

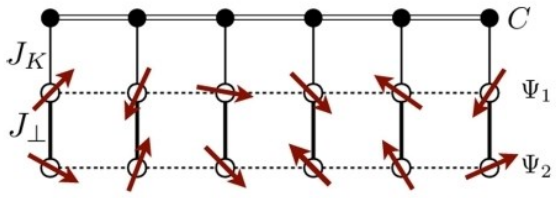

Figure 6.2. Physical layer of electrons c coupled with two layers of ancilla qubits realized by fermions $\boldsymbol{\Psi}_1$ and $\boldsymbol{\Psi}_2$, with nonrandom antiferromagnetic couplings J_K and $J_\perp$, while the dashed lines represent random exchange interactions between the $\boldsymbol{\Psi}_1$ spins and between the $\boldsymbol{\Psi}_2$ spins [85].

- In the large Fermi surface phase, that is the Fermi liquid phase of the cuprates, we assume that the coupling $J_\perp$ dominates, thus the ancilla are locked into rung singlets and can be not considered [85, 86]: thus the c electrons form a conventional Fermi liquid phase, with a Fermi surface corresponding to electron density $(1-p)$, that is hole density $(1+p)$, as displayed in Fig. 6.3

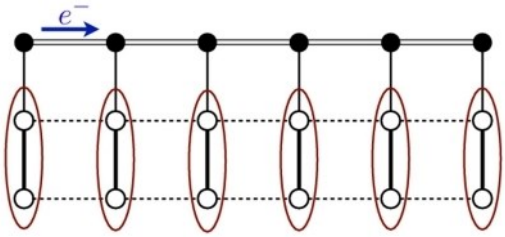

Figure 6.3. In the large Fermi surface phase, the ancilla are locked into rung singlets, the c electrons are largely decoupled and form a conventional Fermi liquid [85].

- In the small Fermi surface phase, the FL* phase, we assume that the coupling J_K dominates, and we see that [85, 86] the $\boldsymbol{\Psi}_1$ spins dissolve into the Fermi sea of the mobile c electrons (see Fig. 6.4), thus the Fermi surface corresponds to an electron density of $\big(1+(1-p)\big) = (2-p)$, which refers, remembering the validity of Luttinger's theorem $(mod 2)$, to a small Fermi surface of holes of density p, as obtained from experimental results for hole doped cuprates at low doping

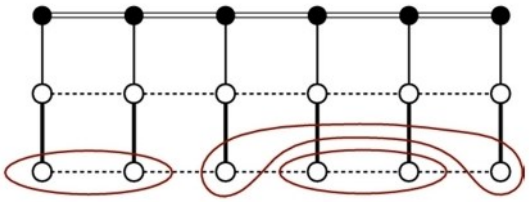

Figure 6.4. In the small Fermi surface phase, the $\boldsymbol{\Psi}_1$ ancilla spins with the c electrons form a Fermi surface with density $(2-p)$ electrons, that is density p holes [85].

In this phase the $\boldsymbol{\Psi}_2$ spins are largely decoupled from the c and $\boldsymbol{\Psi}_1$ layers, and they form a spin liquid with fractionalized spinon excitations, exactly as the bosonic spinons seen in Chapter n. 3 do, and in Ref. [85] there is a discussion on the consistency of this structure with the modified Luttinger theorem seen in Chapter n. 2.

- We report in Fig. 6.4 for this model, in the underdoped side, the spectral function $A_{cc}(\boldsymbol{k}, \omega = 0)$, obtaining a good agreement with the ARPES and ADMR results seen in Chapter n. 5: in fact we can see in Fig. 6.4 that the hole pockets have intensity largely confined to their sides closest to the Γ point, the inner sides, vanishing on the opposite sides, the outer ones.

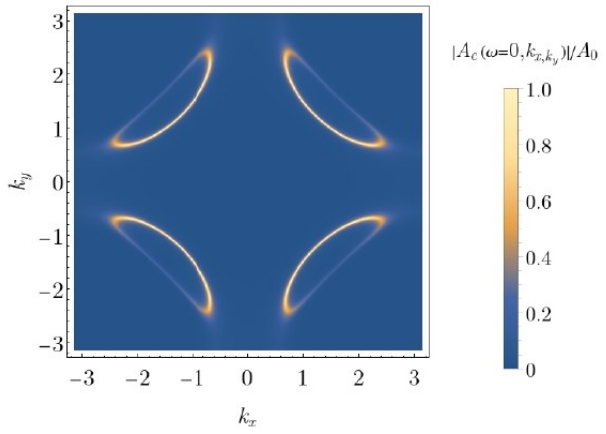

Figure 6.5. Spectral function $A_{cc}(\boldsymbol{k}, \omega = 0)$ of the c electrons for the ancilla qubits approach [86].

We can conclude saying that this recent approach, respect to the S-model discussed in Chapter n. 3, seems to make easier to implement the so-called modified Luttinger's theorem, that is, the relation between the volume enclosed by the Fermi surface and the topological order on both sides of the transition between states with distinct Fermi surfaces, and thus it will surely deserve deeper study in the future.

Appendix A

A.1. Nonperturbative demonstration of the Luttinger's theorem

Oshikawa's argument [15] starts with a periodic system of interacting fermions in its ground state, adiabatically inserting a magnetic flux along one of the directions, applying a large gauge transformation to return to the original gauge, and finally comparing the resulting state with the original one, in order to derive constraints for the system: this yields the Luttinger's theorem if the system is gapless with a Fermi surface of charged quasiparticles, and the commensurability condition if the system is gapped [14][16], thus we will focus on the gapless case, that is expected for general incommensurate particle density. We consider an interacting fermion system on a D-dimensional lattice, with periodic boundary conditions, starting from a finite system of size $L_x \times L_y \times \ldots . L_D$, where the length is defined so that the unit cell has the size $1 \times 1 \times \ldots .1$, and the number of fermions is assumed to be conserved. We start with spinless fermions of single species, and we introduce a fictitious electrical charge e for each particle, and a coupling to an externally controlled fictitious electromagnetic field. This system has a global $U(1)$ symmetry and a corresponding filling fraction υ, specifying the density per unit cell $\upsilon = p/q$, for some coprime integers p and q. We assume the system is described by a translationally invariant Hamiltonian $H(0)$ (the translational symmetry is not spontaneously broken), and it is in the ground state $|\psi(0)\rangle$, which is an eigenstate of the total momentum P_x (defined modulo 2π) with the eigenvalue P_x^0:

$$P_x|\psi(0)\rangle = P_x^0|\psi(0)\rangle \qquad \text{(A.1)}$$

The state $|\psi(0)\rangle$ is also an eigenstate of the translational operator T_x, with eigenvalue $e^{-iP_x^0}$. Since the system has periodic boundary conditions, it is topologically equivalent to a torus, as depicted in Fig. A.1.

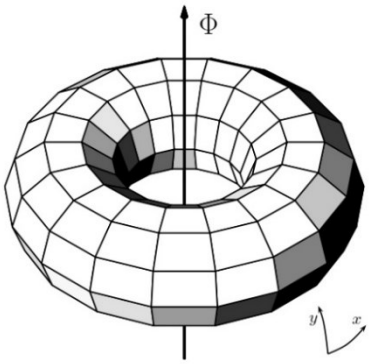

Figure A.1. A 2D periodic lattice depicted as a torus. A magnetic flux Φ inserted to induce a uniform electric field in the x-direction can be thought of as threading the handle of the torus, [29].

[16] The result obtained in Ref. [14] states that in a quantum many-particle system, defined on a periodic lattice, with an exactly conserved particle number, a finite excitation gap is possible only if the particle number per unit cell of the ground state is an integer. To have a finite gap means the commensurability condition: with the particle number per unit cell $\upsilon = p/q$, with p and q coprimes, a gapful ground state must break the translational symmetry, so that the unit cell of the ground state is enlarged by a factor of q. Thus an incommensurate filling ($q \to \infty$) gives large ground-state degeneracy if there is an excitation gap, usually implying the spectrum is actually gapless.

We consider an adiabatic increase of a fictitious magnetic flux Φ piercing through the hole of the torus in the y-direction, so that a uniform electric field is induced in the x-direction (see Fig. A.1). In general the Hamiltonian of the system $H(\Phi)$ depends on the flux Φ, reflecting the Aharonov-Bohm effect, which is yet absent when the flux reaches the unit flux quantum given by (setting $e = c = \hbar = 1$):

$$\Phi_o = \frac{hc}{e} = 2\pi \qquad \text{(A.2)}$$

Let us consider the adiabatic increase of the flux from $\Phi = 0$ to $\Phi = \Phi_0 = hc/e = 2\pi$, thus considering how the total momentum of the system is changed during this adiabatic process in two different ways, finally comparing the two results, in order to obtain a constraint for the system.

A.1.1 Trivial momentum counting

This counting depends on the filling υ, and not on the quantum phase of the system, as we analyze the momentum change in a very general system of interacting fermions. In the simplest gauge choice, the flux Φ is represented by the uniform vector potential in the x-direction by $A_x = \Phi/L_x$. After the 2π-flux threading the handle of the torus, the Hamiltonian is $H(\Phi)$ and the original ground state $|\psi(0)\rangle$ evolves into some state $|\psi(2\pi)\rangle$. While $|\psi(2\pi)\rangle$ could be different from $|\psi(0)\rangle$, it belongs to the same eigenvalue P_x^0 of P_x, as the Hamiltonian always commute with T_x, and thus with P_x[17], in the uniform gauge during the adiabatic process. Since inserting a 2π-flux returns the system to the same point in configuration space, the spectra of $H(2\pi)$ and $H(0)$ are identical, even if such Hamiltonians are different as they corresponds to different choices of the gauge for the same physics. In order to get back to the original gauge, we must perform a large gauge transformation with [14, 15, 17, 29]:

$$\boldsymbol{U_g} = exp\left[\frac{2\pi}{L_x} i \sum_{\mathbf{r}} x n_{\mathbf{r}}\right] \qquad \text{(A.3)}$$

where x is the coordinate of $\mathbf{r}$, and $n_{\mathbf{r}}$ is the particle number operator at site $\mathbf{r}$. Thus we have transformed the Hamiltonian back to the original one by

$$\boldsymbol{U_g} H(2\pi) \boldsymbol{U_g}^{-1} = H(0) \qquad \text{(A.4)}$$

After this gauge transformation the adiabatic evolution of the ground state becomes $\boldsymbol{U_g}|\psi(2\pi)\rangle$, thus $\boldsymbol{U_g}|\psi(2\pi)\rangle$ must be an eigenstate of $H(0)$. Given the unitary time evolution operator $U_T = \mathcal{T}_t exp\left[-i\int_0^T dt H(t)\right]$, with $\mathcal{T}_t$ the time-ordering operator, we thus know that the final state is

$$|\psi_{fin}\rangle = \boldsymbol{U_g} U_T |\psi(0)\rangle \qquad \text{(A.5)}$$

We act on this final state with the translation operator T_x, in order to obtain the momentum, so we have the inital and final momenta, P_x^0 and P_x, so that

[17] The x component of the total momentum, i.e. P_x, is related to T_x, as $T_x = e^{-iP_x}$: we note that P_x is only defined modulo 2π.

$$T_x|\psi_{fin}\rangle = e^{-iP_x}|\psi_{fin}\rangle; \quad T_x|\psi(0)\rangle = e^{-iP_x^0}|\psi(0)\rangle \qquad \text{(A.6)}$$

We can operate on the final state obtaining:

$$T_x|\psi_{fin}\rangle = T_x \boldsymbol{U_g} U_T|\psi(0)\rangle = \left(T_x \boldsymbol{U_g} T_x^{-1}\right)(T_x U_T T_x^{-1})T_x|\psi(0)\rangle = \left(T_x \boldsymbol{U_g} T_x^{-1}\right)U_T T_x|\psi(0)\rangle = \\ = \left(T_x \boldsymbol{U_g} T_x^{-1}\right)U_T e^{-iP_x^0}|\psi(0)\rangle \qquad \text{(A.7)}$$

Where we have used that the operator U_T commutes with the T_x, as the Hamiltonian is translationally invariant even in the uniform gauge. We can now employ the arguments used in the generalization [14, 15] of the Lieb-Schultz-Mattis (LSM)[18] theorem by using the identity

$$\boldsymbol{U_g^{-1}} T_x \boldsymbol{U_g} = T_x \, exp\left[\frac{2\pi}{L_x} i \sum_{\mathbf{r}} n_{\mathbf{r}}\right] \qquad \text{(A.8)}$$

From Eq. (A.8) we can obtain that [17]

$$T_x \boldsymbol{U_g} T_x^{-1} = exp\left[-\frac{2\pi}{L_x} i \sum_{\mathbf{r}} n_{\mathbf{r}}\right] \boldsymbol{U_g} \qquad \text{(A.9)}$$

Inserting Eq. (A.9) into Eq. (A.7), since $[H(\Phi), T_x] = 0$ throughout the flux threading process, we obtain that the state $\boldsymbol{U_g}|\psi(2\pi)\rangle$ is an eigenstate of P_x with momentum $\left(P_x^0 + 2\pi\upsilon L_y L_z \dots L_D\right) mod\ 2\pi$[19], so the momentum change is

$$\Delta P_x = 2\pi\upsilon L_y L_z \dots L_D (mod\ 2\pi) = 2\pi \frac{p}{q} L_y L_z \dots L_D (mod\ 2\pi) \qquad \text{(A.10)}$$

Clearly, an essential condition for this argument has been the conserved $U(1)$ charge, which has permitted us to couple the charge to the inserted flux. If the system is gapped and remains gapped throughout the flux threading process, the adiabaticity guarantees that $U_G|\psi(2\pi)\rangle$ is always a ground state of $H(0)$: by choosing arbitrary integers $L_y, L_z, \dots L_D$ that are coprime with q, we find q degenerate ground states with different momenta. Without a topological order, these degenerate ground states must be the result of spontaneous translational symmetry breaking: their period in the x-direction must be an integer multiple of q, and therefore the new unit cell (that is the original unit cell enlarged by a factor of q), has an integer filling fraction. If indeed there is topological order, translational symmetry need not to be spontaneously broken, since topological phases can have translationally-invariant degenerate ground states on a torus. However, in the case of 2D systems, as for the hole-doped cuprates considered in this paper, only certain topological order can coexist with $U(1)$ and translational symmetry for a given υ, as discussed in section 2.2. If the system is gapless, then $\boldsymbol{U_g}|\psi(2\pi)\rangle$ is no longer necessarily a ground state of $H(0)$; however, it is still true that momentum is shifted by Eq. (A.10), and this shift can thus be compared with the one obtained in the next subsection, from the emergent degrees of freedom. For simplicity, from now on [17] we consider the specific case of a simple 2D fermionic system, with charge e and spin $\uparrow, \downarrow$, with filling per site

[18] The LSM theorem states that a translationally invariant 1D spin systems, with an odd number of $S = 1/2$ moment per unit cell, cannot have a symmetric, gapped and non degenerate ground state: either some symmetries are spontaneously broken, either the phase is gapless, or there is non trivial topological order with emergent quasiparticle excitations having exotic exchange statistics.

[19] Here $\upsilon = N/\left(L_x L_y \dots L_D\right)$, with N the total number of the particles, is the fillig fraction, that is, the number of particle per unit cell of the lattice.

$\upsilon_\downarrow = \upsilon_\uparrow = \upsilon/2$, and imaging the 2π-flux only couples to the spin-up fermions; via the trivial momentum counting seen above the momentum variation (being in two dimensions, in Eq. (A.10) we now have only L_x, L_y) is given by

$$\Delta P_x = 2\pi\upsilon_\uparrow L_y (mod\ 2\pi) \qquad \text{(A.11)}$$

Imaging to perform the 2π-flux threading with the torus wrapped along the y-direction, this would yields the momentum change

$$\Delta P_y = 2\pi\upsilon_\uparrow L_x (mod\ 2\pi) \qquad \text{(A.12)}$$

A.1.2 Fermi liquid momentum counting

In the regular Fermi liquid phase the momentum imparted during flux threading is accounted for entirely by quasiparticles excitations generated near the Fermi surface; knowing that long-lived quasiparticles exist only near the Fermi surface, and that the Fermi liquid is adiabatically connected to the free Fermi gas, we can obtain the quasiparticle population δn_p excited during the flux threading. Clearly, for non interacting fermions, flux threading will lead to a uniform shift of the Fermi sea by $\Delta p_x = 2\pi/L_x$, from which the quasiparticle distribution can be determined. Indeed, all of these excitations are close to the Fermi surface, which is required in order to apply Fermi liquid theory, so the total momentum carried can be written as $\Delta P_x = \sum_p \delta n_p p_x$. We evaluate this expression neglecting the discrete nature of allowed momentum states in a finite volume system, threating the shift $\delta p_x = 2\pi/L_x$ as infinitesimal, and considering that $\delta n_p = \pm 1$ on a shell of thickness $\delta\mathbf{p}\cdot d\mathbf{S_p}$ (with $d\mathbf{S_p}$ an area element with a vector normal to the Fermi surface)

$$\Delta P_x = \oint_{FS} p_x \frac{\delta\mathbf{p}\cdot d\mathbf{S_p}}{\frac{2\pi 2\pi}{L_x L_y}} \qquad \text{(A.13)}$$

where $d\mathbf{S_p}$ is a vector normal to the Fermi surface and the integral is taken around the Fermi surface. Using Gauss divergence theorem[20] Eq. (A.13) can be converted into an integral over the Fermi volume:

$$\Delta P_x = \delta p_x \int_{FV} \frac{dV}{\frac{2\pi 2\pi}{L_x L_y}} = \frac{2\pi}{L_x}\frac{V_F^\uparrow}{\frac{2\pi 2\pi}{L_x L_y}} \qquad \text{(A.14)}$$

where we have used the fact that the 2π-flux only couples to the spin-up fermions, so $V_F = V_F^\uparrow = V_F^\downarrow$.

[20] For a continuosly differentiable vector field $\boldsymbol{F}$, in a volume V, compact subset of $\mathbb{R}^n$: $\iiint_V \boldsymbol{\nabla}\cdot\boldsymbol{F}dV = \oiint_{S=\partial V}\boldsymbol{F}\cdot\hat{\boldsymbol{n}}dS$, where $\hat{\boldsymbol{n}}$ is the outward pointing unit normal at each point on the boundary of the closed manifold ∂V.

A.1.3 Momentum balance

We can equate Eqs. (A.11) with (A.14), and Eq. (A.12) with the analogue of Eq. (A.14) in the y-direction, and remembering that $v_\downarrow = v_\uparrow = v/2$, we obtain

$$\begin{cases} 2\pi\frac{v}{2}L_y = \frac{2\pi}{L_x}\frac{V_F}{(2\pi)^2}L_xL_y + 2\pi m_x \\ 2\pi\frac{v}{2}L_x = \frac{2\pi}{L_y}\frac{V_F}{(2\pi)^2}L_xL_y + 2\pi m_y \end{cases} \quad \begin{cases} \frac{v}{2}L_yL_x - \frac{V_F}{(2\pi)^2}L_yL_x = L_xm_x \\ \frac{v}{2}L_xL_y - \frac{V_F}{(2\pi)^2}L_{xL_y} = L_ym_y \end{cases} \qquad \text{(A.15)}$$

So we obtain $L_xm_x = L_ym_y$: in order to obtain the strongest constraint from these equations, we consider a system with L_x and L_y mutually prime integers, then $L_xm_x = L_ym_y = pL_xL_y$, with p integer. So we can obtain the relations

$$v = \frac{V_F}{(2\pi)^2}(mod\ 1) \quad \text{(spinless fermions);} \qquad v = 2\frac{V_F}{(2\pi)^2}(mod\ 2) \quad \text{(spinful fermions)} \qquad \text{(A.16)}$$

Eqs. (A.16) represent the Luttinger's theorem, that relates the Fermi volume V_F to the filling ν, modulo an integer that represents the filled bands, with a quantization given by a trivial topological order.

A.2. Topological enrichment of the Luttinger's theorem

A.2.1 Symmetry fractionalization in 2D topological phases

A symmetric system with topological order can manifest distinct symmetry-enriched topological (SET) phases, which cannot be adiabatically connected to each other while respecting the symmetry. A distinguing signature of these phases is "symmetry fractionalization", a phenomenon that allows quasiparticles to carry fractionalized quantum numbers of the symmetry. For example, $U(1)$ fractionalization leads to quasiparticles with fractional charge, while translational symmetry fractionalization leads to a non trivial background anyonic flux in the system. Let us recap the most important definitions useful for our purposes, referring to Ref. 91 for the detailed theory:

- *Algebraic theory of anyons*. If we have a set C of superselection labels called topological or anyonic charges a, b, c ..., these conserved charges obey an associative fusion algebra given by

  $$a \times b = \sum_{c\epsilon C} N_{ab}^c\, c \qquad \text{(A.17)}$$

  where the fusion multiplicities N_{ab}^c are non-negative integers indicating the number of different ways the charge a and b can be combined to produce the charge c. If this fusion algebra is also commutative, i.e. $N_{ab}^c = N_{ba}^c$ (so that the dimension of the state space is

unaltered interchanging the positions of anyons), then it is possible to define a counterclockwise braiding exchange operator and a clockwise one as of two anyons as

$R^{ab} =$  $\left(R^{ab}\right)^{-1} =$  .

It is possible to define a related invariant quantity $\mathcal{M}_{ab}$, a monodromy scalar component that is the mutual braiding statistics between anyons a and b. If $\mathcal{M}_{ab} = e^{i\varphi(a,b)}$ is a phase, then the braiding of a and b is Abelian, that is

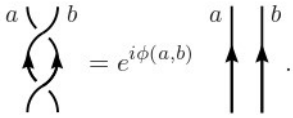

It is possible to show that, if there are phase factors, defined for all charge values, that satisfy the relation $e^{i\varphi_a}e^{i\varphi_b} = e^{i\varphi_c}$ whenever $N_{ab}^{c} \neq 0$, then it must be the case that

$$e^{i\varphi_a} = \mathcal{M}_{ae} \quad \text{(A.18)}$$

for some Abelian topological charge e.

- *Group cohomology*. Given a finite group G, let M be an Abelian group equipped with a G action $\rho: G \times G \to M$, compatible with group multiplication; for any $\boldsymbol{g}, \boldsymbol{h} \in G$ and $a, b \in M$, we have $\rho_{\boldsymbol{g}}\big(\rho_{\boldsymbol{h}}(a)\big) = \rho_{\boldsymbol{gh}}(a)$ and $\rho_{\boldsymbol{g}}(ab) = \rho_{\boldsymbol{g}}(a)\rho_{\boldsymbol{g}}(b)$. Let $\omega(\boldsymbol{g}_1, \dots, \boldsymbol{g}_n) \in M$ be a function of n group elements $\boldsymbol{g}_j \in G$ for $j = 1, \dots, n$: such a function is called a n-cochain, and we denote the set of all n-cochain as $C^n(G, M)$, and they naturally form a group under multiplication, that is $(\omega \cdot \omega')(\boldsymbol{g}_1, \dots, \boldsymbol{g}_n) = \omega(\boldsymbol{g}_1, \dots, \boldsymbol{g}_n) \cdot \omega'(\boldsymbol{g}_1, \dots, \boldsymbol{g}_n)$, where the identity is the trivial cochain $\omega(\boldsymbol{g}_1, \dots, \boldsymbol{g}_n) = 1$. We now define the coboundary map $d: C^n(G, M) \to C^{n+1}(G, M)$, acting on cochains as a kind of boundary operator, so that for any $\omega \in C^n(G, M)$ we can verify that $dd\omega = 1$, with 1 is the trivial cochain in $C^{n+2}(G, M)$. We next define $\omega \in C^n(G, M)$ to be a n-cocycle if it satisfies the condition $d\omega = 1$, and we denote the set of all n-cocycles by

$$Z_\rho^n(G, M) = ker[d: C^n(G, M) \to C^{n+1}(G, M)] = \{\omega \in C^n(G, M) | d\omega = 1\} \quad \text{(A.19)}$$

We also define $\omega \in C^n(G, M)$ to be a n-coboundary if it satisfies the condition $\omega = d\mu$ for some $(n-1)$-cochain $\mu \in C^{n-1}(G, M)$, and we denote the set of all n-coboundaries by

$$B_\rho^n(G, M) = im\big[d: C^{n-1}(G, M) \to Z_\rho^n(G, M)\big] = \{\omega \in C^n(G, M) | \exists \mu C^{n-1}(G, M): \omega = d\mu\} \quad \text{(A.20)}$$

Clearly $B_\rho^n(G,M) \subset Z_\rho^n(G,M) \subset C^n(G,M)$, as C^n, Z^n, B^n are all groups and the co-boundary maps are homomorphisms. Since d is a boundary map, we can think of the n-coboundaries as being trivial n-cocycles, and it is natural to consider the quotient group

$$H_\rho^n(G,M) = Z_\rho^n(G,M)/B_\rho^n(G,M) \qquad \text{(A.21)}$$

which is called the n-th cohomology group. In other words $H_\rho^n(G,M)$ collects the equivalence classes of n-cocycles that only differs by n-coboundaries. For our purposes it is useful to know that, for the second cohomology, we have

$$Z_\rho^2(G,M)\{\omega|\rho_{\boldsymbol{g}_1}[\omega(\boldsymbol{g}_2,\boldsymbol{g}_3)]\omega(\boldsymbol{g}_1,\boldsymbol{g}_2\boldsymbol{g}_3) = \omega(\boldsymbol{g}_1,\boldsymbol{g}_2)\omega(\boldsymbol{g}_1\boldsymbol{g}_2,\boldsymbol{g}_3)\} \qquad \text{(A.22)}$$

$$B_\rho^2(G,M)\{\omega|\omega(\boldsymbol{g}_1,\boldsymbol{g}_2) = \rho_{\boldsymbol{g}_1}[\varepsilon(\boldsymbol{g}_2)][\varepsilon(\boldsymbol{g}_1\boldsymbol{g}_2)]^{-1}\varepsilon(\boldsymbol{g}_1)\} \qquad \text{(A.23)}$$

Thus we can say that, in a 2D topologically ordered phase this symmetry fractionalization is classified by the cohomology group $H_\rho^2(G,\mathcal{A})$, where $\mathcal{A}$ is the finite group whose elements are the Abelian anyons (or topological charges) of C with group multiplication given by their corresponding fusion rules, ρ is the symmetry action which may permute anyon types, and G is the on-site or "locality preserving" symmetry group (where locality preserving action is a generalization of the notion of on-site action that may include symmetries that act non-locally, such as anti-unitary, time-reversal, translation, rotation, and other space-time symmetries) [29, 31, 32, 91]. For simplicity we will assume that the topological order is bosonic and the symmetries are unitary, also focusing on the case where the symmetry action ρ does not permute anyon types, which must be the case for the symmetries described by a continuos and connected group, such as $U(1)$. We also remember that a topological phase in 2D supports anyonic quasiparticle excitations, whose topologically distinct types are denoted by a, b, c,…(which we refer to as anyons or topological charges). We can summarize the structure of symmetry fractionalization of our symmetric 2D system in a topological phase with symmetry group G according to the following steps [29, 31, 32, 91].

A.2.1.1. Review of on-site symmetry fractionalization. Let $|\Psi_{\{a\}}\rangle$ be a state with n well-separated quasiparticles carrying topological charges $a_1, \dots a_n$ (with the shorthand $\{a\} = \{a_1, \dots, a_n\}$), which collectively fuse to the trivial (vacuum) topological charge I. We indeed assume that the overall topological charge is trivial I, so that the state $|\Psi_{\{a\}}\rangle$ can be created from the ground state by applying local operators. Moreover, let elements $\boldsymbol{g} \in G$ act linearly on the Hilbert space by the unitary on-site operators $\boldsymbol{R}_{\boldsymbol{g}} = \prod_{j=1}^n \boldsymbol{U}_{\boldsymbol{g}}^{(j)}$. Assuming that the action of the symmetry does not permute anyon types

(as it must be the case for symmetry action ρ described by a continuos and connected group, such as $U(1)$), it takes the form

$$\boldsymbol{R_g}|\Psi_{\{a\}}\rangle = \prod_{j=1}^{n} \boldsymbol{U_g^{(j)}} |\Psi_{\{a\}}\rangle \qquad \text{(A.24)}$$

where $\boldsymbol{U_g^{(j)}}$ are unitary operators whose nontrivial action is localized near the jth quasiparticle. The local operators generate a projective representation of G, with multiplication given by

$$\boldsymbol{U_g^{(j)} U_h^{(j)}}|\Psi_{\{a\}}\rangle = \eta_{a_j}(\boldsymbol{g},\boldsymbol{h})\boldsymbol{U_{gh}^{(j)}}|\Psi_{\{a\}}\rangle \qquad \text{(A.25)}$$

where $\eta_{a_j}(\boldsymbol{g},\boldsymbol{h}) \in U(1)$ is the projective phase that only depends on the topological properties localized in the neighborhood of the jth quasiparticle, which is just the topological charge a_j carried by the quasiparticle. Whenever the topological charge c is a permissible fusion channel, that is whenever $N_{ab}^{c} \neq 0$, see Eq. (A.17), of the topological charges a and b, since $\boldsymbol{R_g R_h} = \boldsymbol{R_{gh}}$, it is required that

$$\eta_a(\boldsymbol{g},\boldsymbol{h})\eta_b(\boldsymbol{g},\boldsymbol{h}) = \eta_c(\boldsymbol{g},\boldsymbol{h}) \qquad \text{(A.26)}$$

This property, as seen above in Eq. (A.18) allows us to write these projective phases η_i as

$$\eta_a(\boldsymbol{g},\boldsymbol{h}) = \mathcal{M}_{a,\mathfrak{m}(\boldsymbol{g},\boldsymbol{h})} \qquad \text{(A.27)}$$

where $\mathfrak{m}(\boldsymbol{g},\boldsymbol{h})$ is an Abelian anyon (an $\mathcal{A}$ valued function on G^2), and $\mathcal{M}_{a,b}$ is the mutual braiding statistics between anyons a and b. Since $\boldsymbol{R_g}$ is a linear representation, the projective phases must satisfy the condition

$$\prod_j \eta_{a_j}(\boldsymbol{g},\boldsymbol{h}) = 1 \qquad \text{(A.28)}$$

Apart a redundancy of the projective phases $\eta_{a_j}(\boldsymbol{g},\boldsymbol{h})$ that here we do not study [29, 31, 91], we obtain that a given equivalence class $[\mathfrak{m}] \in H^2(G,\mathcal{A})$ completely specifies the symmetry fractionalization of the system, i.e. the local projective phases $\eta_a(\boldsymbol{g},\boldsymbol{h})$ are given by Eq. (A.27) for all anyon types, thus we can call these cohomology classes the "symmetry fractionalization classes".

A.2.1.2. $U(1)$ symmetry fractionalization. The manifestation of symmetry fractionalization for the anyons may exhibit the characteristic property that anyons can carry a fractionalized quantum number of the symmetry. Here we discuss the case, of our specific interest, of a fractional charge density $\upsilon = p/q$ per unit cell (p and q coprimes), and with the on-site symmetry group $G = U(1)$ (which may be a subgroup of the full symmetry group, i.e. it can be the $U(1)$ associated with particle number conservation or $U(1) \subset SO(3)$ associated with spin rotational symmetry), thus the transformation of an object of charge Q corresponding to $e^{i\theta} \in U(1)$ is $e^{i\theta Q}$, with $\theta \in [0,2\pi)$. Topologically nontrivial quasiparticles may carry fractional charge, as long the sum of the charges of all quasiparticles in the system adds up to an integer (and clearly the state is left invariant when θ goes from 0 to 2π). In other words the fusion rules from Eq. (A.18), that is the condition imposed by the fractionalization

class, order also the fractional charge assignements. Thus we can write the action of the localized symmetry operation as

$$U_{\theta}^{(j)}\left|\Psi_{\{a\}}\right\rangle = e^{i\theta Q_{a_j}}\left|\Psi_{\{a\}}\right\rangle \qquad \text{(A.29)}$$

where Q_{a_j} is just the possibly fractional $U(1)$ charge carried by anyons with topological charge a_j. Eq. (A.22) is not gauge invariant for arbitrary θ, but only when we have wound it by 2π, giving

$$U_{2\pi}^{(j)}\left|\Psi_{\{a\}}\right\rangle = e^{i2\pi Q_{a_j}}\left|\Psi_{\{a\}}\right\rangle \Rightarrow U_{\theta}^{(j)}\,U_{2\pi-\theta}^{(j)}\left|\Psi_{\{a\}}\right\rangle = e^{i2\pi Q_{a_j}}\left|\Psi_{\{a\}}\right\rangle \qquad \text{(A.30)}$$

In this way the fractional charge Q_{a_j} is given in terms of the projective phases η_{a_j} as

$$e^{i2\pi Q_{a_j}} = \eta_{a_j}(\theta, 2\pi-\theta) \qquad \text{(A.31)}$$

Remembering Eq. (A.27), we can write

$$U_{\theta}^{(j)}\,U_{2\pi-\theta}^{(j)}\left|\Psi_{\{a\}}\right\rangle = \mathcal{M}_{a_j,\mathfrak{m}(\theta,2\pi-\theta)}\left|\Psi_{\{a\}}\right\rangle \qquad \text{(A.32)}$$

With the shorthand $v = \mathfrak{m}(\theta, 2\pi-\theta)$ we label $U(1)$ fractionalization classes by the anyon v, which is the quasiparticle created by threading a 2π $U(1)$ flux: thus, the anyon a_j has a possibly fractional charge Q_{a_j}, which is given by the relation

$$e^{i2\pi Q_{a_j}} = \mathcal{M}_{a_j,v} \qquad \text{(A.33)}$$

Thus, adiabatically threading the 2π flux results in the anyonic excitation called the "vison" v, and the mutual braiding anyonic statistics between v and an excitation carrying topological charge a_j determines the fractional $U(1)$ charge of a_j through Eq. (A.33). For simplicity in this paper we do not discuss other deeper theoretical properties, such as how anyons can carry a localized projective representation of the symmetry group G, i.e. they have an internal degeneracy (like spin), which tranforms projectively under G, and how can be considered the extrinsic symmetry defects (fluxes) [31, 32, 91].

A.2.1.3. Translational symmetry fractionalization. The analysis of symmetry fractionalization seen above can be generalized to translational symmetry: in 2D lattice translations form a $\mathbb{Z}^2$ symmetry group (i.e. the translational symmetry group $\mathbb{Z}\times\mathbb{Z}$ generated by the translational operators T_x and T_y along the x, y directions), and we note that in this case the cohomology group is $H^2(\mathbb{Z}^2, \mathcal{A}) = \mathcal{A}$. The fractionalization of this symmetry requires a modification of the on-site formalism seen above: in particular, in Eq. (A.24) the state vector $\left|\Psi_{\{a\}}\right\rangle$ on the r.h.s. must have the positions of its quasiparticles translated according to the applied translational operator with respect to $\left|\Psi_{\{a\}}\right\rangle$ on the l.h.s., and the local unitary operators $\boldsymbol{U}_{\boldsymbol{g}}^{(j)}$ should be understood to act nontrivially in a neighborhood of the translated quasiparticle positions. Now the cohomology group $H^2(\mathbb{Z}^2, \mathcal{A}) = \mathcal{A}$ can be characterized by the gauge invariant quantity $\mathfrak{b}(T_x, T_y) \equiv \mathfrak{b} \in \mathcal{A}$ in the following way: the symmetry operation $T_y^{-1}T_x^{-1}T_yT_x$ is a sequence of translations corresponding to path that encloses one unit cell

in a counterclockwise way. It is possible [29, 31] to show that this operation has the corresponding local projective phase factor of $\mathcal{M}_{a_j,\mathfrak{b}}$ for quasiparticles of topological charge a_j of the j-th quasiparticle, where this phase is just the mutual braiding statistics associated with an anyon a_j encircling an anyon $\mathfrak{b}(T_x, T_y)$ in a counterclockwise fashion. Thus, we can picture this type of symmetry fractionalization as being generated by an Abelian anyon $\mathfrak{b}(T_x, T_y)$ sitting in each unit cell, as shown in Fig. A.2:

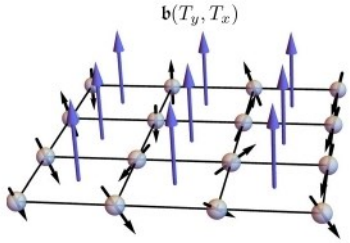

Figure A.2. Anyonic flux per unit cell $\mathfrak{b}(T_x, T_y)$ [31].

Therefore, we can label translational symmetry fractionalization classes by $\mathfrak{b} \in \mathcal{A}$: physically, the anyon $\mathfrak{b}$ can be thought of as the background anyonic flux per unit cell, from (where we label the local unitary operators corresponding to T_x and T_y as $\boldsymbol{U}_{T_x}$ and $\boldsymbol{U}_{T_y}$)

$$\left(\boldsymbol{U}_{T_y}^{(j)}\right)^{-1}\left(\boldsymbol{U}_{T_x}^{(j)}\right)^{-1}\boldsymbol{U}_{T_y}^{(j)}\boldsymbol{U}_{T_x}^{(j)}\left|\Psi_{\{a\}}\right\rangle = \mathcal{M}_{a_j,\mathfrak{b}}\left|\Psi_{\{a\}}\right\rangle \quad \text{(A.34)}$$

In other words, when an anyon a_j is transported around a unit cell, the wavefunction acquires a phase corresponding to braiding a_j around $\mathfrak{b}$.

A.2.2 Flux threading argument

We consider a system with both on-site $U(1)$ and $\mathbb{Z}^2$ translational symmetry with the geometry depicted in Fig. A.3, thus having $G = U(1) \times \mathbb{Z}^2$. If we consider a state that has 2π $U(1)$ flux through a handle of the torus, as depicted in the left image in Fig. A.3, we can summarize the most important following steps useful for our purposes [29, 31, 32]:

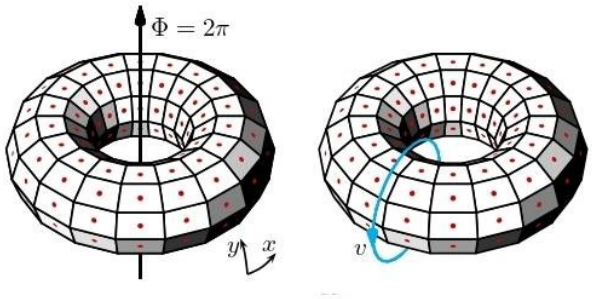

Figure A.3. Threading a 2π flux through the handle of the torus creates a ν anyon (blue), while the dots represent the anyonic flux per unit cell $\mathfrak{b}$ (red) [29].

1. The cohomology group can be factorized as

$$H^2(U(1)\times\mathbb{Z}^2,\mathcal{A}) = H^2(U(1),\mathcal{A})\times H^2(\mathbb{Z}^2,\mathcal{A}) \qquad \text{(A.35)}$$

and it means that $U(1)$ and translational symmetries can be independently specified. In other words, as seen in Appendix A.2.1, we are supposing that the system belongs to a $U(1)$ fractionalization class ν and to a translational symmetry fractionalization class $\mathfrak{b}$.

2. The initial state of the system is just the state $|\Psi_{\{a\}}\rangle$ seen in Appendix A.2.1.
3. If we consider a state that has a 2π $U(1)$ flux through the handle of the torus and transports an anyon a around the handle, so that it winds around the flux once, we know that the wavefunction will acquire a phase $e^{i2\pi Q_a}$, that, from Eq (A.33) is identical to the phase $\mathcal{M}_{a,\nu}$ that is acquired by braiding a around ν. Therefore, as illustrated in Fig. A.3, threading the flux through a handle of the torus should be gauge equivalent to creating a ν-loop that wraps around the handle (operation that can be defined through an operator $\boldsymbol{\mathcal{W}}_\nu$).
4. With the notation used in Appendix A.2.1 for the operator $\boldsymbol{U_g}$, and in Appendix A.1 for the states $|\psi(2\pi)\rangle$ and $|\psi(0)\rangle$, we can so obtain that

$$\boldsymbol{U_g}|\psi(2\pi)\rangle = \boldsymbol{\mathcal{W}}_\nu|\psi(0)\rangle \qquad \text{(A.36)}$$

From Appendix A.1.1 we also know that the state $\boldsymbol{U_g}|\psi(2\pi)\rangle$ has momentum $\left(P_x^0 + 2\pi\upsilon L_y\right) mod\ 2\pi$, see Eq. (A.10).

5. Remembering that $\mathfrak{b}$ represents the anyonic flux per unit cell (red points in Figs. A.3-A.4), we use the relation (T_x is again the translational operator along the x direction) [29]:

$$T_x^{-1}\boldsymbol{\mathcal{W}}_\nu^{-1}T_x\boldsymbol{\mathcal{W}}_\nu|\psi(0)\rangle = \left(\mathcal{M}_{\nu,\mathfrak{b}}\right)^{L_y}|\psi(0)\rangle \qquad \text{(A.37)}$$

where $\mathcal{M}_{\nu,\mathfrak{b}} = e^{i2\pi Q_{\mathfrak{b}}}$ is the mutual braiding statistics between anyons $\mathfrak{b}$ and ν. To go from the l.h.s to the r.h.s. of Eq. (A.37), we partially fused the adjacent ν anyon loops as depicted in the right image of Fig. A.4, while being careful not to pass them through the anyonic flux $\mathfrak{b}$ lines emanating from ther center of every cell of the torus. This means our system belongs to translational symmetry fractionalization class $\mathfrak{b}$.

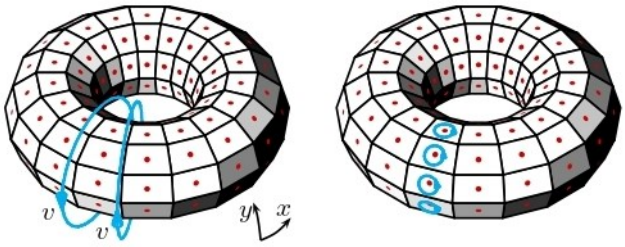

Figure A.4. The pictorial exposition of the determination of the T_x eigenvalue of $\boldsymbol{\mathcal{W}_\nu}|\psi(0)\rangle$ by the mutual braiding statistics between anyons ν and $\mathfrak{b}$, where we fuse the adjacent ν anyons being careful not to pass them through the anyonic flux b lines emanating from the center of every cell of the torus [29].

6. From Eq. (A.37), remembering Eq. (A.33), we see that the state $\boldsymbol{\mathcal{W}}_v|\psi(0)\rangle$ has momentum $\left(P_x^0 + 2\pi Q_{\mathfrak{b}} L_y\right) mod\ 2\pi$, so we can equate this momentum to the momentum $\left(P_x^0 + 2\pi\upsilon L_y\right) mod\ 2\pi$ of the state $\boldsymbol{U}_g|\psi(2\pi)\rangle$ obtained in step 4. Using Eq. (A.36), and repeating the steps in the y direction, yield our final result given by

$$\upsilon = Q_{\mathfrak{b}} \equiv \upsilon_{topo} \qquad \text{(A.38)}$$

In other words, there is an anyon $\mathfrak{b}\left(T_x, T_y\right)$ per unit cell, whose fractional $U(1)$ charge $Q_{\mathfrak{b}}$ is equal to the filling factor υ, and quasiparticles carrying this topological charge $\upsilon_{topo} \equiv Q_{\mathfrak{b}}$ are called "spinons": the filling fraction of a 2D SET phase is equal to the $U(1)$ charge of the background anyonic flux per unit cell, and we define this as υ_{topo}. Eq. (A.38), relating microscopic (υ) and emergent ($Q_{\mathfrak{b}}$) properties of the system, can be viewed as a constraint on the allowed SET order that may exist at a given filling fraction of the unit cell.

A.2.3 Fractionalized Fermi liquid

As fractionalized Fermi liquid FL* we consider a gapless system with $U(1)$ and translational SET order, whose gapless modes are well described by Fermi liquid theory, and whose symmetries are fractionalized. We assume that topological and gapless excitations coexist, but are effectively decoupled from one another: the system decouples into an SET sector and a Fermi liquid sector, and is thus in a strong quasi-topological phase. As seen above, we consider a 2D system for which the SET order belongs to $U(1)$ fractionalization class ν and translational symmetry fractionalization class $\mathfrak{b}$. We just know that, starting from a ground state $|\psi(0)\rangle$ of this fractionalized Fermi liquid, and threading a 2π flux through the handle of the torus, is gauge equivalent to applying a ν-loop that wraps around the handle to the state $|\psi'(0)\rangle$ (where $|\psi'(0)\rangle$ is $|\psi(0)\rangle$ with a Galileian boosted Fermi sea, so that it is in the same topological sector of $|\psi(0)\rangle$, but with a shifted momentum)

$$\boldsymbol{U}_g|\psi(2\pi)\rangle = \boldsymbol{\mathcal{W}}_v|\psi'(0)\rangle \qquad \text{(A.39)}$$

Here the assumption of the decoupling between the SET and the Fermi liquid sectors is crucial, since it allows us to separate the effect of flux threading on the SET sector (wrapping a ν-loop around the handle), from its effect on the Fermi liquid sector ("boosting" the Fermi sea). If the topological excitations were to interact with the Fermi liquid in a way that nontrivially coupled the SET and the Fermi liquid sectors, then the effect of flux threading may not be so cleanly separable. However, we just know that the state $\boldsymbol{U}_g|\psi(2\pi)\rangle$ has momentum $\left(P_x^0 + 2\pi\upsilon L_y\right) mod\ 2\pi$; moreover, we know that the state $\boldsymbol{\mathcal{W}}_v|\psi'(0)\rangle$ has momentum $2\pi Q_{\mathfrak{b}} L_y$ relative to the state $|\psi'(0)\rangle$, which has the momentum due to the Fermi liquid quasiparticles as seen in Eq. (A.14). Equating the momenta of the two states in Eq. (A.32) and repeating the argument in the y direction, yields:

$$\nu - Q_{\mathfrak{b}} = 2\frac{V_F}{(2\pi)^2}\,(mod\ 2) \qquad \text{(A.40)}$$

From Eqs. (A.31) and (A.33) we finally obtain

$$\nu - \nu_{topo} = 2\frac{V_F}{(2\pi)^2}(mod\ 2) \qquad \text{(A.41)}$$

Eqs. (A.34) represents a nontrivial topologically version of the Luttinger's theorem for a 2D fractionalized Fermi liquid: the background anyonic flux can appropriate some of the charges available to the emergent degrees of freedom, thus changing the Fermi volume, that is so determined by the filling fraction of the Fermi liquid sector. Moreover, this relation places constraints on the possible SET order allowed to manifest in a fractionalized Fermi liquid with an experimentally observed Fermi volume that deviates from the naïve value expected for an ordinary Fermi liquid.

Appendix B

B.1. Hubbard model on square lattice antiferromagnet – ground state

We start our discussion about a model for hole-doped cuprates remembering their parent compound [87-90]: every site i of the 2D square lattice has exactly one electron because the Coulomb repulsion between the electrons keeps their charges on the Cu lattice sites, but it is insensitive to the spins of the electron, so it would appear that each electron spin is free to rotate independently on each site. The localized electrons have a spin whose orientation remains a dynamicall degree of freedom, and virtual hopping of these electrons produces, via the Pauli exclusion principle, an antiferromagnetic interaction J between neighboring spins. This, in turns, leads to a simple Néel-ordered phase below room temperature , in which there are static magnetic moment on the Cu sites with a direction that reverses from one Cu to the next. The optimal state turns out to be the antiferromagnetic sketched in Fig. B.1,where the spins are arranged in a checkerboard pattern, so that all the spins in one sublattice are parallel to each other, and antiparallel to spins on the other sublattice (lattice spacing is set for simplicity $a = 1$)

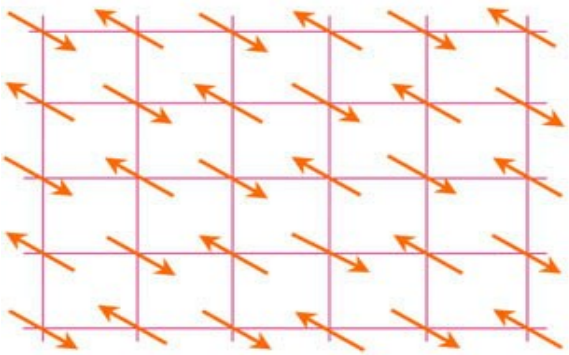

Figure B.1. The undoped insulating antiferromagnetic state [8].

Thus we can start from the one-band Hubbard model given by

$$H_{HUB} = H_t + H_U \qquad \text{(B.1a)}$$

$$H_t = -\sum_{i<j} t_{ij}\left(c_{i\alpha}^{\dagger} c_{j\alpha} + h.c.\right) - \mu \sum_i c_{i\alpha}^{\dagger} c_{i\alpha} \qquad \text{(B.1b)}$$

$$H_U = U \sum_i \left(n_{i\alpha} - \frac{1}{2}\right)\left(n_{i\beta} - \frac{1}{2}\right) \qquad \text{(B.1c)}$$

Where t_{ij} represent the hopping parameters between sites i and j, U is the on-site Coulomb repulsion, μ is the chemical potential, $c_{i\alpha}$ and $c_{i\alpha}^{\dagger}$ are usual fermionic annihilation and creation operators for electrons with spin $\alpha, \beta = \uparrow, \downarrow$ (summation over repeated indices is implied), satisfying the anticommutation relations

$$\{c_{i\alpha}, c_{j\beta}\} = 0 \; ; \left\{c_{i\alpha}^{\dagger}, c_{j\beta}^{\dagger}\right\} = 0 \; ; \left\{c_{i\alpha}, c_{j\beta}^{\dagger}\right\} = \delta_{ij}\delta_{\alpha\beta} \qquad \text{(B.2)}$$

Moreover we have the particle number operator at site i as

$$n_{i\alpha} = c_{i\alpha}^{\dagger} c_{i\alpha} \qquad \text{(B.3)}$$

and the spin operator given by ($\boldsymbol{\sigma}_{\alpha\beta}$ are the Pauli matrices)

$$\boldsymbol{S}_i = c_{i\alpha}^{\dagger} (\boldsymbol{\sigma}_{\alpha\beta}/2) c_{i\beta} \qquad \text{(B.4)}$$

We work in the imaginary-time path-integral formalism, thus having the partition function as

$$Z[\bar{C}, C] = \int D\bar{C} D\, C e^{-S_E} \qquad \text{(B.5)}$$

$$S_E = \int_0^{\beta} d\tau\, \mathcal{L}_E \qquad \text{(B.6)}$$

Where $\mathcal{L}_E$ is the imaginary-time lagrangian given by, from Eqs. (B.1)

$$\mathcal{L}_E = \sum_{i,\alpha} \bar{C}_{i\alpha} (\partial_\tau - \mu) C_{i\alpha} - \sum_{i,j} t_{ij} \left(\bar{C}_{i\alpha} C_{j\alpha} + c.c\right) + U \sum_i \left(n_{i\alpha} - \frac{1}{2}\right)\left(n_{i\beta} - \frac{1}{2}\right) \qquad \text{(B.7)}$$

Where now $\bar{C}, C$ are Grassmann fields associated to the fermionic operators $c^{\dagger}$, c. Using Eq. (B.4) we can obtain the exact operator equation (manifestly $SU(2)$ spin invariant)

$$U \sum_i \left(n_{i\alpha} - \frac{1}{2}\right)\left(n_{i\beta} - \frac{1}{2}\right) = -\frac{2}{3} U \boldsymbol{S}_i^2 + \frac{U}{4} \qquad \text{(B.8)}$$

In the r.h.s. of Eq. (B.8) the second term is a constant one, that can be dropped, and we can decouple the quartic interaction term with $\boldsymbol{S}_i^2$ via a Hubbard-Stratonovich transformation as

$$exp\left(\frac{2}{3} U \sum_i \int d\tau \boldsymbol{S}_i^2\right) = \int D\boldsymbol{J}_i \; exp\left[-\sum_i \int d\tau \left(\frac{3}{8U} \boldsymbol{J}_i^2 - \boldsymbol{J}_i \cdot \boldsymbol{S}_i\right)\right] \qquad \text{(B.9)}$$

In Eq. (B.9) we have introduced the bosonic field $\boldsymbol{J}_i$, that can be considered representing the local magnetization above the Néel-ordered phase, that is, the collective modes associated with spin fluctuations above the antiferromagnetic order. Eq. (B.7) now becomes

$$\mathcal{L}_E = \sum_{i,j,\alpha} \bar{C}_{i\alpha} \left[(\partial_\tau - \mu)\delta_{ij} - t_{ij}\right] C_{i\alpha} - \sum_{i,\alpha,\beta} \boldsymbol{J}_i \cdot \bar{C}_{i\alpha} \frac{\boldsymbol{\sigma}_{\alpha\beta}}{2} C_{i\beta} + \frac{3}{8U} \sum_i \boldsymbol{J}_i^2 \qquad \text{(B.10)}$$

We use Fourier transformation, where ω_n are Matsubara fermionic frequencies, with $\omega_n = (2n+1)\pi/\beta$, given by

$$C_{i\alpha} = \frac{1}{\sqrt{\beta}} \sum_n C_{in} e^{-i\omega_n \tau} \; ; \quad C_{in} = \frac{1}{\sqrt{\beta}} \int_0^{\beta} d\tau\, C_{i\alpha} e^{i\omega_n \tau} \qquad \text{(B.11)}$$

Integrating out the fermions we then obtain the following euclidean action, where a unit matrix in spin space is understood in the first three terms in the logarithm

$$S_{eff} = \int_0^{\beta} d\tau\, \mathcal{L}_{eff} = \int_0^{\beta} d\tau \frac{3}{8U} \sum_i \boldsymbol{J}_i^2 - \mathrm{Trln}\left[-i\omega_n - \mu - t_{ij} - \boldsymbol{J}_i \cdot \frac{\boldsymbol{\sigma}_{\alpha\beta}}{2}\right] \qquad \text{(B.12)}$$

We would like to use mean-field theory, corresponding to the saddle-point approximation with respect to the functional integration in $\boldsymbol{J}_i$, determined by $\delta S_E / \delta \boldsymbol{J}_i = 0$. For our purposes, that is the study of spin fluctuations above the Néel-ordered phase given by the antiferromagnetic order on two sublattices, we now consider $\boldsymbol{J}_i$ in this Néel-ordered phase expressed as

$$\boldsymbol{J}_i = J_0 \boldsymbol{n} e^{i\boldsymbol{Q}\cdot\boldsymbol{r}_i} \qquad \text{(B.13)}$$

Where J_0 is an amplitude, $\boldsymbol{n}$ is a unit-length vector along the direction of the antiferromagnetic order, $\boldsymbol{Q} = (\pi, \pi)$ the wave vector relative to the antiferromagnetic order, and $\boldsymbol{r}_i = (x_i, y_i)$ represents the coordinates of the i site: in fact, if we consider the four sites on a plaquette, we have

site $(0,0) \Rightarrow \boldsymbol{J}_i = \boldsymbol{J}_0 e^{i(\pi,\pi)\cdot(0,0)} = \boldsymbol{J}_0$; site $(1,0) \Rightarrow \boldsymbol{J}_i = \boldsymbol{J}_0 e^{i(\pi,\pi)\cdot(1,0)} = \boldsymbol{J}_0 e^{i\pi} = -\boldsymbol{J}_0$;
site $(0,1) \Rightarrow \boldsymbol{J}_i = \boldsymbol{J}_0 e^{i(\pi,\pi)\cdot(0,1)} = \boldsymbol{J}_0 e^{i\pi} = -\boldsymbol{J}_0$; site $(1,1) \Rightarrow \boldsymbol{J}_i = \boldsymbol{J}_0 e^{i(\pi,\pi)\cdot(1,1)} = \boldsymbol{J}_0 e^{i2\pi} = \boldsymbol{J}_0$

Thus the factor $e^{i\boldsymbol{Q}\cdot\boldsymbol{r}_i}$ in Eq. (B.13) becomes $(-1)^{x_i+y_i}$. Remembering that in $\boldsymbol{k}$-space we have

$$\varepsilon(\boldsymbol{k}) = -\sum_i t_{ij} e^{i\boldsymbol{k}\cdot(\boldsymbol{r}_i - \boldsymbol{r}_j)} \qquad \text{(B.14)}$$

For a square lattice we get

$$\varepsilon(\boldsymbol{k}) = -\varepsilon(\boldsymbol{k} + \boldsymbol{Q}) \qquad \text{(B.15)}$$

and, at half-filling, i.e. in the parent compound, the Fermi surface (FS) has the shape shown in Fig. B.2 (considering only the nearest-neighbor terms we get $\varepsilon(\boldsymbol{k}) = -2t(cosk_x + cosk_x)$).

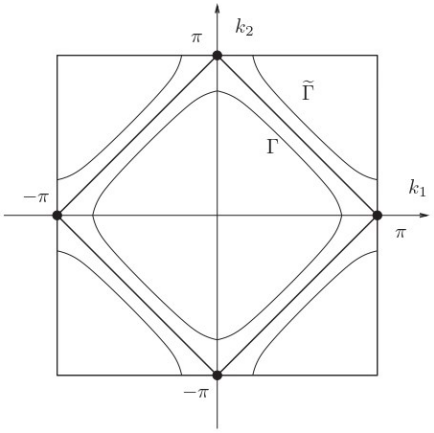

Figure B.2. The first Brillouin zone for the square lattice for a nearest-neighbor hopping band structure. The diamond shaped full curve is the Fermi surface (FS) at half-filling with Fermi energy $E_F = 0$, Γ is an FS with $E_F < 0$, hole-like, and $\tilde{\Gamma}$ is an FS with $E_F > 0$, electron-like [88].

Now we investigate the Néel-ordered phase using mean-field approximation, using the following the notations (where $\mu = 0$ corresponds to the half filled case)

$$\xi_{\boldsymbol{k}} = \varepsilon(\boldsymbol{k}) - \mu \qquad \text{(B.16)}$$

$$\boldsymbol{S}(\boldsymbol{k}) = \sum_{\boldsymbol{k}'} \bar{C}_{i\alpha}(\boldsymbol{k}') \frac{\boldsymbol{\sigma}_{\alpha\beta}}{2} C_{i\beta}(\boldsymbol{k}' + \boldsymbol{k}) \qquad \text{(B.17)}$$

We also consider the spinor notation $\Psi_\alpha(\boldsymbol{k})$ so defined

$$\Psi_\alpha(\boldsymbol{k}) = \begin{pmatrix} C_{i\alpha}(\boldsymbol{k}, \omega) \\ C_{i\alpha}(\boldsymbol{k} + \boldsymbol{Q}, \omega) \end{pmatrix} \qquad \text{(B.18)}$$

Thus, inserting Eq. (B.13) in Eq. (B.12), we obtain

$$S_{eff} = \int_0^\beta d\tau \frac{3}{8U}\sum_i J_0^2 - \sum_{\alpha,\beta,\omega_n,\boldsymbol{k}\in BZ^+} tr\ ln\begin{pmatrix} -i\omega_n + \xi_{\boldsymbol{k}} & \frac{\boldsymbol{\sigma}_{\alpha\beta}}{2}J_0 \\ \frac{\boldsymbol{\sigma}_{\alpha\beta}}{2}J_0 & -i\omega_n + \xi_{\boldsymbol{k}+\boldsymbol{Q}} \end{pmatrix} \qquad \text{(B.19a)}$$

We note that in Eq. (B.19a) the trace now is performed in momentum space and ranges over only the upper half of the Brillouin zone BZ^+, as it has been folded by the nesting vector $\boldsymbol{Q} = (\pi, \pi)$: in other words, owing to the long-range order with the wave number $\boldsymbol{Q}$, the first Brillouin zone is folded into half; as the α-summation gives a factor 2, and remembering that $trlnA = lndetA$ for non singular A

$$S_{eff} = \int_0^\beta d\tau \frac{3}{8U}\sum_i J_0^2 - 2\sum_{\omega_n,\boldsymbol{k}\in BZ^+} ln\ det\begin{pmatrix} -i\omega_n + \xi_{\boldsymbol{k}} & \frac{\boldsymbol{\sigma}_{\alpha\beta}}{2}J_0 \\ \frac{\boldsymbol{\sigma}_{\alpha\beta}}{2}J_0 & -i\omega_n + \xi_{\boldsymbol{k}+\boldsymbol{Q}} \end{pmatrix} \qquad \text{(B.19b)}$$

$$S_{eff} = \frac{3}{8U}\beta N_0 J_0^2 - 2\sum_{\omega_n,\boldsymbol{k}\in BZ^+} ln\left[-\omega_n^2 - \xi_{\boldsymbol{k}}^2 - \frac{J_0^2}{4}\right] \qquad \text{(B.19c)}$$

Where N_0 is the total number of the lattice sites. In order to find the ground state of this Néel-ordered phase we differentiate with respect to J_0, obtaining

$$\frac{\delta S_{eff}}{\delta J_0} = 0 \Rightarrow \frac{3}{4U}\beta N_0 J_0 - J_0 \sum_{\omega_n,\boldsymbol{k}\in BZ^+} \frac{1}{\omega_n^2 + \xi_{\boldsymbol{k}}^2 + \frac{J_0^2}{4}} = 0 \qquad \text{(B.20a)}$$

$$\frac{3}{4U}\beta N_0 - \sum_{\omega_n,\boldsymbol{k}\in BZ^+} \frac{1}{\omega_n^2 + E_{\boldsymbol{k}}^2} = 0 \qquad \text{(B.20b)}$$

With the band dispersion in this ordered phase thus given by

$$E_{\boldsymbol{k}} = \sqrt{\xi_{\boldsymbol{k}}^2 + \Delta^2}\ ; \quad \Delta = \frac{J_0}{2} \qquad \text{(B.21)}$$

We see that the system has acquired a gap Δ given in Eq. (B.21), of the same amplitude of the antiferromagnetic order, and from Eq. (B.20b) we get the mean-field equation of the gap, turning the Matsubara frequencies summation into the residues sum

$$\sum_{\omega_n} \frac{1}{\omega_n^2 + E_{\boldsymbol{k}}^2} = \sum_{\omega_n} h(\omega_n) = -\zeta \sum_k Res[h(-iz)g(z)]_{z=z_k} \qquad \text{(B.22)}$$

Where we sum over the isolated singularities $\{z_k\}$ of $h(-iz)$, $\zeta = -1$ for fermions (and 1 for bosons), and (f_F is the Fermi distribution function)

$$g(z) = \beta f_F(z) = \frac{\beta}{e^{\beta z}+1} \qquad \text{(B.23)}$$

Thus we obtain

$$\sum_{\omega_n} \frac{1}{\omega_n^2 + E_{\boldsymbol{k}}^2} = \frac{\beta}{2E_{\boldsymbol{k}}}[f_F(-E_{\boldsymbol{k}}) - f_F(E_{\boldsymbol{k}})] = \frac{\beta}{2E_{\boldsymbol{k}}}\sum_{\boldsymbol{k}\in BZ^+} tanh\left(\frac{\beta E_{\boldsymbol{k}}}{2}\right) \qquad \text{(B.24)}$$

And finally the mean-field equation of the gap is

$$\frac{3N_0}{4U} = \frac{1}{2E_{\boldsymbol{k}}}\sum_{\boldsymbol{k}\in BZ^+} tanh\left(\frac{\beta E_{\boldsymbol{k}}}{2}\right) \qquad \text{(B.25)}$$

Thus we can conclude that the states in the vicinity of the Fermi surface disappear, with the gap given by Eq. (B.21), and the system in the antiferromagnetic order is an insulator; antiferromagnetic ordering and period doubling seen above are essential for the emerging insulator phase. We consider this insulating antiferromagnetic ordered phase as the ground state of the parent compound of hole-doped cuprates, then studying the spin fluctuations above it, that is the spin density wave (SDW) order.

B.2. Spin fluctuations over antiferromagnetic order – NLσ model

Now, in order to create a theoretical model for the hole-doped cuprates we consider spin fluctuations over the antiferromagnetic ordered phase studied above, switching from the above description of SDW order given by Eq. (B.13) by a different perspective in which we have primarily *angular fluctuations* of the antiferromagnetic order [87-90], thus replacing Eq. (B.13) with (setting $\boldsymbol{J}_0 = 1$)

$$\boldsymbol{J}_i = \boldsymbol{n}_i e^{i\boldsymbol{Q}\cdot\boldsymbol{r}_i};\ \ \sum_i \boldsymbol{n}_i^2 = 1 \qquad \text{(B.26)}$$

We can firstly remember that for $U \gg |t_{ij}|$, as in the case of hole-doped cuprates, it is possible with a perturbative expansion in t_{ij}, to derive from the Hubbard model in Eqs. (B.1) an effective Hamiltonian, which is nothing more than the antiferromagnetic Heisenberg model given by

$$H_J = \sum_{i,j} J_{ij}\left(\boldsymbol{S}_i \cdot \boldsymbol{S}_j + \frac{1}{4}\right) \qquad \text{(B.27)}$$

Where $J_{ij} = \frac{4}{U}|t_{ij}|^2 > 0$ are the exchange couplings of the spin operators $\boldsymbol{S}_i$, $\boldsymbol{S}_j$, and this result is valid for the half-filled Hubbard model in any dimension for any lattice.

Now, for a general spin S, we consider the spin-coherent states functional integral defined by [89]

$$Z = \int_{\boldsymbol{\Omega}(\beta)=\boldsymbol{\Omega}(0)} \mathcal{D}[\boldsymbol{\Omega}] e^{-S_B[\boldsymbol{\Omega}] - \int_0^\beta d\tau H[\boldsymbol{\Omega}]} \qquad \text{(B.28)}$$

with:

a) Spin-coherent states can be defined as

$$|\boldsymbol{\Omega}\rangle = e^{-i\varphi S^z} e^{-i\vartheta S^y} e^{-i\psi S^z} |S\rangle \qquad \text{(B.29)}$$

where ψ is arbitrary and depends on the gauge choice, while ϑ and φ are the polar and azimutal angles defined by the unit length vector $\boldsymbol{\Omega} = (sin\vartheta cos\varphi, sin\vartheta sin\varphi, cos\vartheta)$; $|S^z\rangle$ represent the $2S+1$ eigenstates of S^z.

b) The Berry phase term

$$S_B[\boldsymbol{\Omega}] = \int_0^\beta d\tau \langle \boldsymbol{\Omega} | \partial_\tau \boldsymbol{\Omega} \rangle \qquad \text{(B.30a)}$$

is the sum of the single-spin contributions, and it is possible to express this term also as

$$S_B[\boldsymbol{\Omega}] = iS \int_0^\beta d\tau \int_0^1 du\ \boldsymbol{\Omega} \cdot \left(\frac{\partial \boldsymbol{\Omega}}{\partial u} \times \frac{\partial \boldsymbol{\Omega}}{\partial \tau}\right) \qquad \text{(B.30b)}$$

where u is just a dummy integration variable.

c) The last term, with $\boldsymbol{S}_i = S\boldsymbol{\Omega}_i$ (we will see below the meaning of $\boldsymbol{\Omega}_i$)

$$H[\boldsymbol{\Omega}] = \langle \boldsymbol{\Omega}|H|\boldsymbol{\Omega}\rangle \Rightarrow H[\boldsymbol{\Omega}] = -\frac{S^2}{2}\sum_{i,j} J_{ij}\, \boldsymbol{\Omega}_i \cdot \boldsymbol{\Omega}_j \qquad \text{(B.31)}$$

for the Heisenberg model seen in Eq. (B.27).

We are looking for a theoretical model for the spin fluctuations above the antiferromagnetic ordered phase discussed in the previous section: we consider the more general situation where the system exhibits short-range antiferromagnetic order, and the antiferromagnetic correlation length ξ_{AF} is then much larger than the lattice spacing a, but non necessary infinite as it would be in the presence of long-range order, that is $a < \xi_{AF} < \infty$. We expect spin-wave fluctuations about the local antiferromagnetic order to be the dominant fluctuations at length scales smaller than ξ_{AF}, and we will see that the low-energy behavior is described by a quantum non-linear sigma model (NLσM), also with a Berry phase term that could be non zero. Let us begin by introducing a parameterization of the short-range antiferromagnetic order by the unit length vector given by (in our 2D system with lattice spacing $a = 1$ for simplicity) [89]

$$\boldsymbol{\Omega}_i = (-1)^{x_i+y_i}\boldsymbol{n}_i \left(1 - \frac{a^2}{S^2}\boldsymbol{L}_i^2\right)^{1/2} + \frac{a^2}{S}\boldsymbol{L}_i \qquad \text{(B.32)}$$

The prefactor a^2/S has been associated with $\boldsymbol{L}_i$, that is the canting field which describes ferromagnetic fluctuations of the spin, so that the spatial integral of $\boldsymbol{L}_i$ over any region is precisely the total magnetization in that region. We will show a posteriori the necessity to introduce $\boldsymbol{L}_i$, as it could be tempting to write only $\boldsymbol{\Omega}_i = (-1)^{x_i+y_i}\boldsymbol{n}_i$. Both the Néel field $\boldsymbol{n}_i$ and the canting field $\boldsymbol{L}_i$ are assumed to be slowly varying on the scale of a lattice spacing (certainly true as $S \to \infty$, and we are assuming this remains valid down to $S = 1/2$); consequently we can treat $\boldsymbol{n}(x,\tau)$ and $\boldsymbol{L}(x,\tau)$ as continuum quantum fields that can be expanded in spatial gradients over separation of order a. These continuum fields satisfy the constraints

$$\boldsymbol{n}^2 = 1\,; \quad \boldsymbol{n}\cdot\boldsymbol{L} = 0 \qquad \text{(B.33)}$$

Eqs. (B.33) combined with Eq. (B.32) imply that $\boldsymbol{\Omega}_i^2 = 1$ is obeyed. Finally, as we know spins on nearby sites are expected to be predominantly antiparallel, we can consider the uniform component $\boldsymbol{L}$ small, as

$$\frac{a^2}{S^2}\boldsymbol{L}^2 \ll 1 \Rightarrow \left(1 - \frac{a^2}{S^2}\boldsymbol{L}_i^2\right)^{1/2} \approx 1 - \frac{1}{2}\frac{a^2}{S^2}\boldsymbol{L}_i^2 \qquad \text{(B.34)}$$

The field $\boldsymbol{n}(x,\tau)$ clearly plays the role of the order parameter associated with Néel ordering, thus we can look for an effective action $S[\boldsymbol{n},\boldsymbol{L}]$ in the continuum limit and to leading order in a derivative expansion, then carrying out the functional integral over $\boldsymbol{L}$, finally obtaining as the desired result the effective action $S_{eff}[\boldsymbol{n}]$. Thus we consider lattice with Hamiltonian like antiferromagnetic Heisenberg in Eq. (B.31) with $\boldsymbol{S} = S\boldsymbol{\Omega}_i$, considering for simplicity only nearest-neighbor exchange $J_{ij} = -J < 0$, and inserting the decomposition from Eq. (B.32), we obtain

$$H[\mathbf{\Omega}] = \int d^2x \left[\frac{JS^2}{2}(\nabla_x \boldsymbol{n})^2 + 4Ja^2\boldsymbol{L}^2\right] \qquad \text{(B.35)}$$

To complete the expression for the spin-coherent state path integral of in the continuum limit, we need to obtain the expression for $S_B[\mathbf{\Omega}]$ in Eq. (B.30b) in terms of $\boldsymbol{n}$ and $\boldsymbol{L}$: we insert Eq. (B.32) in Eq. (B.30b), and retain terms up to linear order in $\boldsymbol{L}$, and this yields (S_B' comes from the zeroth order in $\boldsymbol{L}$, S_B'' from the linear order in $\boldsymbol{L}$)

$$S_B[\mathbf{\Omega}] = S_B' + S_B'' \qquad \text{(B.36)}$$

$$S_B' = iS(-1)^{x_i+y_i}\int_0^\beta d\tau \int_0^1 du\, \boldsymbol{n}\cdot\left(\frac{\partial \boldsymbol{n}}{\partial u}\times\frac{\partial \boldsymbol{n}}{\partial \tau}\right) \qquad \text{(B.37)}$$

$$S_B'' = i\int d^2x \int_0^\beta d\tau \int_0^1 du\, \left[\boldsymbol{n}\cdot\left(\frac{\partial \boldsymbol{n}}{\partial u}\times\frac{\partial \boldsymbol{L}}{\partial \tau}\right) + \boldsymbol{n}\cdot\left(\frac{\partial \mathbf{L}}{\partial u}\times\frac{\partial \boldsymbol{n}}{\partial \tau}\right) + \boldsymbol{L}\cdot\left(\frac{\partial \boldsymbol{n}}{\partial u}\times\frac{\partial \boldsymbol{n}}{\partial \tau}\right)\right] \qquad \text{(B.38)}$$

We start analyzing S_B'', whose last term vanishes as the vector $\boldsymbol{L}$, $\partial\boldsymbol{n}/\partial u$ and $\partial\boldsymbol{n}/\partial\tau$ are all perpendicular to $\boldsymbol{n}$, thus lying in a plane and having a vanishing triple product, thus from Eq. (B.38) we have

$$S_B'' = i\int d^2x \int_0^\beta d\tau \int_0^1 du\, \left[\frac{\partial}{\partial\tau}\left(\boldsymbol{n}\cdot\left(\frac{\partial \mathbf{n}}{\partial u}\times\boldsymbol{L}\right)\right) + \frac{\partial}{\partial u}\left(\boldsymbol{n}\cdot\left(\boldsymbol{L}\times\frac{\partial \mathbf{n}}{\partial \tau}\right)\right)\right] \qquad \text{(B.39)}$$

Here the total derivative $\partial/\partial\tau$ yields 0, due to the periodicity of the fields in τ, while the total derivative $\partial/\partial u$ yields a surface contribution at $u = 1$, and this gives

$$S_B'' = -i\int d^2x \int_0^\beta d\tau\, \boldsymbol{L}\cdot\left(\boldsymbol{n}\times\frac{\partial \mathbf{n}}{\partial \tau}\right) \qquad \text{(B.40)}$$

In Eq. (B.40) we can also see that $\boldsymbol{L}$ and $(\boldsymbol{n}\times\partial_\tau\boldsymbol{n})$ are conjugate fields, and this shows a posteriori the necessity to introduce $\boldsymbol{L}$ in Eq. (B.32) as anticipated above. Passing to analyze S_B' we see from Eq. (B.37) that, due to the factor $(-1)^{x_i+y_i}$, it is the sum of terms that oscillate in sign on the two sublattices, thus it is tempting to assume that these oscillating terms just cancel out, yielding $S_B' = 0$ in the continuum limit. But for some purposes this assumption is not correct: without goingo into details, here we briefly summarize the most important conclusions derived for two dimensional systems:

I. $S_B' = 0$ for all smooth spacetime configurations of $\boldsymbol{n}(x,\tau)$.

II. There are important singular configurations of $\boldsymbol{n}(x,\tau)$ yielding $S_B' \neq 0$: for the specific case of a three-component vector order parameter, the only topologically stable possibility is the hedgehog singularity, that is a singularity occurring at a point in the spacetime. Thus to evaluate the partition function we have to include the phase factors arising from $e^{-S_B'}$ with such event. It has been showed that in the Néel-ordered phase these hedeghog events are completely suppressed, while when the antiferromagnetic order is lost they proliferate, leading to a spontaneous broken lattice symmetry unless S is an even integer (the ordered state associated with the broken lattice symmetry is the so-called valence bond solid (VBS)).

For our purposes, due to the assumption of $\boldsymbol{n}(x,\tau)$ being slowly varying on the scale of a lattice spacing, we can say that $S_B' = 0$. Putting Eqs. (B.35) and (B.40) in Eq. (B.28), and reminding the constraints in Eq. (B.33), we obtain

$$Z = \int \mathcal{D}\boldsymbol{n}\mathcal{D}\boldsymbol{L}\delta(\boldsymbol{n}^2-1)\delta(\boldsymbol{n}\cdot\boldsymbol{L})e^{-S_n'} \qquad \text{(B.41)}$$

$$S_n' = \int_0^\beta d\tau \int d^2x \left[\frac{JS^2}{2}(\nabla_x \boldsymbol{n})^2 + 4Ja^2\boldsymbol{L}^2 - i\boldsymbol{L}\cdot\left(\boldsymbol{n}\times\frac{\partial \mathbf{n}}{\partial\tau}\right)\right] \qquad \text{(B.42)}$$

Integrating out $\boldsymbol{L}$, after imposing the constraint $\boldsymbol{n}\cdot\boldsymbol{L}=0$, we obtain the desired final result of this section

$$Z = \int \mathcal{D}\boldsymbol{n}\mathcal{D}\boldsymbol{L}\delta(\boldsymbol{n}^2-1)e^{-S_n'} \qquad \text{(B.43)}$$

$$S_n' = \int_0^\beta d\tau \int d^2x \left[\frac{JS^2}{2}(\nabla_x \boldsymbol{n})^2 + (\partial_\tau \boldsymbol{n})^2\right] = \frac{1}{4g_o}\int_0^\beta d\tau \int d^2x\,[v^2(\nabla_x \boldsymbol{n})^2 + (\partial_\tau \boldsymbol{n})^2] \qquad \text{(B.44)}$$

Where we can consider the factor $JS^2/2 \equiv v^2/4g_o$,with v the velocity of the spin-wave modes and g_o a generic coupling measuring the degree of frustration in the insulating antiferromagnet (possibly driving into a non magnetic state as the VBS order). Thus we have showed that the low-energy behavior of the angular spin-wave fluctuations above the local antiferromagnetic order in our 2D Hubbard model can be described by a (NLσM), also with a Berry phase term that could be non zero. Let us remember that our purpose is to discuss a theory of the pseudogap phase of the hole-doped cuprates, and that the parent compound has a ground state with a Néel-ordered phase. We can recall Eqs. (B.10) and (B.44), thus yielding an explicit theory of a metal with angular fluctutations of antiferromagnetic order: being interested only in the long-wavelength fluctuations of $\boldsymbol{n}(x,\tau)$ (while retaining the full lattice dispersions for the fermions), we have thus obtained the imaginary time Lagrangian presented in Eqs. (3.5)-(3.8) of the main text, that is

$$S = \int_0^\beta d\tau \mathcal{L}_{sf} \qquad \text{with} \quad \mathcal{L}_{sf} = \mathcal{L}_f + \mathcal{L}_n + \mathcal{L}_{fn} \qquad \text{(B.45)}$$

$$\mathcal{L}_f = \sum_{i,j} c_{i\alpha}^\dagger\left[(\partial_\tau - \mu)\delta_{ij} - t_{ij}\right]c_{j\alpha} + h.c. \qquad \text{(B.46)}$$

$$\mathcal{L}_n = \frac{1}{4g_0}\int d^2\mathbf{r}\left[\left((\partial_\tau \boldsymbol{n})\right)^2 + v^2(\boldsymbol{\nabla}\boldsymbol{n})^2\right] \qquad \text{(B.47)}$$

$$\mathcal{L}_{fn} = -\lambda\sum_i (-1)^{x_i+y_i}\,\boldsymbol{n}_i\cdot c_{i\alpha}^\dagger \boldsymbol{\sigma}_{\alpha\beta}c_{i\beta} \qquad \text{(B.48)}$$

Where obviously now the fermionic fields $c_{i\alpha}^\dagger, c_{i\alpha}$ refer to the dopants, as the bare electronic fields at half filling have been integrated out, and in Eq. (B.48) it has been introduced the parameter (of order unity) λ, that is this spin-fermion coupling.

B.3. Non compactness of the $U(1)$ gauge field to suppress monopole/hedgehog

We have anticipated above how, in 2D, but even in 3D systems, smooth configurations of the Néel vector $\boldsymbol{n}$ of the model in Eqs (B.45)-(B.48) admit topological textures known as skyrmions (see Fig. B.3), and the total skyrmion number related to a configuration defines an integer topological quantum number Q [74-76]

$$Q = \frac{1}{4\pi}\int d^2\mathbf{r}\ \boldsymbol{n}\cdot\left(\partial_x\boldsymbol{n}\times\partial_y\boldsymbol{n}\right) \qquad \text{(B.49)}$$

We also have seen above how, in the Néel phase or close to it, the fluctuations of the Néel order parameter are captured by the $O(3)$ NLσM

$$S_n = \int_0^\beta d\tau\mathcal{L}_n + S_B' \qquad \text{(B.50)}$$

with $\mathcal{L}_n$ given by Eq. (B.47), and the second term is the Berry phase S_B' of all the $S = 1/2$ spins seen in Eq. (B.37), that we can write also as

$$S_B' = iS\sum_{\boldsymbol{r}}(-1)^{x_i+y_i}A_{\boldsymbol{r}} \qquad \text{(B.51)}$$

where $A_{\boldsymbol{r}}$ is the area enclosed by the path mapped by the time evolution of $\boldsymbol{n}$ on a unit sphere in spin space ($\boldsymbol{r} = (x_i, y_i)$ is the lattice coordinate promoted to a continuum spatial coordinate, as seen above). This Berry phase S_B' becomes zero for all spin time hystories with smooth equal-time configurations, as seen above, even if they contain skyrmions, and for such configurations the total skyrmion number Q is independent of time.

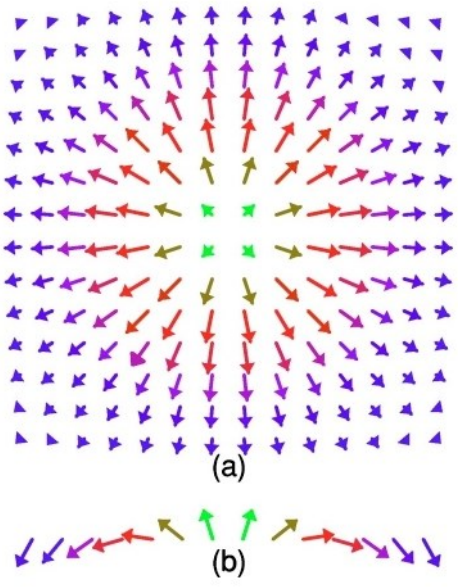

Figure B.3. A skyrmion configuration of the Néel field $\boldsymbol{n}$. a) The representation on the x, y plane. b) The representation along the x axis, with any other section of a) giving a picture similar to b), as the former is invariant under rotations about the z axis. The skyrmion above has $\boldsymbol{n}(\boldsymbol{r} = 0) = (0,0,1)$ and $\boldsymbol{n}(|\boldsymbol{r}| \to \infty) = (0,0,-1)$ [75].

As we have promoted the lattice coordinate $\mathbf{r} = (x_i, y_i)$ to a continuum spatial coordinate, the original microscopic model is defined on a lattice, thus processes where Q changes by some integer amount are allowed, and these events correspond to a monopole (or "hedgehog", which has $\boldsymbol{n}$ oriented radially outward in all spacetime directions away from its centre) singularity in spacetime of the Néel field $\boldsymbol{n}(\mathbf{r}, \tau)$, as depicted in Fig. B.4. It has been shown [74-76] that in the presence of such monopole events, the sum over $\boldsymbol{r}$ in Eq. (B.51) is non zero, and we have a total Berry phase (associated with such events) that oscillates rapidly on four sublattices of the dual lattice: this leads to destructive interference, suppressing all monopole events, unless they are quadrupled, that is, they change Q by 4. As discussed in Chapter n. 3 of the main text, the critical point can be studied by writing the Néel field $\boldsymbol{n}$ in the CP^1 parameterization

$$n_i = z_{i\alpha}^* \sigma_{\alpha\beta} z_{i\beta} \qquad \text{(B.52)}$$

where $\sigma_{\alpha\beta}$ are the Pauli matrices, and z_i is a two-component spinor of unit magnitude ($z^\dagger z = 1$), which transforms under the spin $1/2$ representation of the $SU(2)$ group of the spin rotations, thus we can consider the $z_{1,2}$ as the fractionalized spinon fields. This representation has a $U(1)$ gauge redundancy, leaving $\boldsymbol{n}$ invariant, given by ($\mu = (\mathbf{r}, \tau)$)

$$z \to e^{i\gamma_\mu} z \qquad \text{(B.53)}$$

The spinon fields are thus coupled to a $U(1)$ gauge field a_μ, and it is possible to write a Lagrangian for the critical theory for the Néel-VBS transition [74-76]. We also know that the magnetic flux of a_μ is simply related to the skyrmion density defined in Eq. (B.49), that is

$$Q = \frac{1}{2\pi} \int d^2\mathbf{r} \left(\partial_x a_y - \partial_y a_x \right) \qquad \text{(B.54)}$$

Configurations where the a_μ flux is 2π correspond to a full skyrmion (in the ordered Néel phase), thus the monopole events described above, that is where Q changes by some integer amount, are spacetime monopoles of a_μ at which 2π gauge flux can either disappear or be created: in other words, the monopoles, that change the a_μ gauge flux by $\pm 2\pi$, describe events in which the skyrmion number changes by ± 1: monopoles thus act as sources or sinks of the gauge flux. These skyrmion number changing events may be represented graphically as hedgehog configurations of the Néel vector $\boldsymbol{n}$ in spacetime, as depicted in Fig. B.4. As these monopole events are allowed, it means the a_μ gauge field is compact[21]: in fact, the compactness of the $U(1)$ gauge field means that monopole events, changing the magnetic flux by $\pm 2\pi$, are allowed configurations of the gauge field in spacetime, and thus the proliferation of these monopole events leads to confinement of the slave particle (the spinon) of the gauge theory.

[21] We remember the definition of compactness. Consider a set X and all its possible coverings; the set X is compact if, for every open covering $\{U_i | i \epsilon I\}$, there exist a finite subset J of I such that $\{U_j | j \epsilon J\}$ is also a covering of X. Furthermore, a subset X of $\mathbb{R}^n$ is compact if and only if it is closes and bounded.

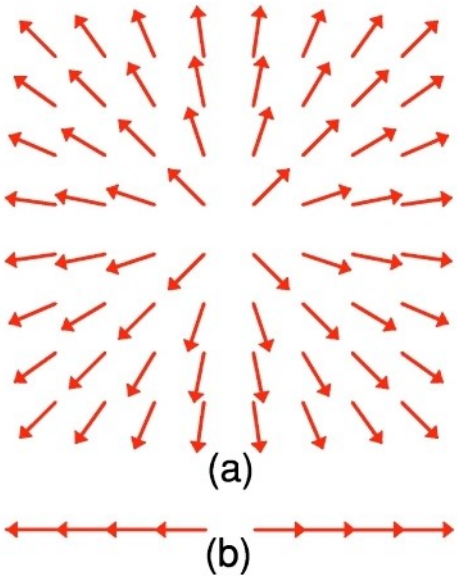

Figure B.4. A monopole event, occurring at the origin of the space-time. a) The representation on the x, y plane, with similar picture obtained along any other plane passing through the origin, as the spin configuration is radially symmetric. b) The representation along the x axis, with a similar picture obtained along any line in space-time passing through the origin. The monopole above has $\boldsymbol{n} = \boldsymbol{r}/|\boldsymbol{r}|$ [75].

But, at low energies, near the quantum critical point (QCP), it is possible to see [74-76] that the skyrmion number is strictly conserved: the emergence of this conserved topological quantum number is the most fundamental meaning of the irrelevance of the monopoles, and thus *we have the non compactness of the* $U(1)$ *gauge field* a_μ. In other words, the strict conservation of the total magnetic flux of a_μ is a topological conservation law, and may be understood as an extra emergent dual global $U(1)$ symmetry for the critical theory that is not present in the initial microscopic Hamiltonian, and this also provides a rather precise characterization of a deconfined critical point.

Summarizing, we can consider as starting point for a model of the hole doped cuprates, a hedgehog-free $O(3)$ NLσM, which involves spinons coupled to a non compact gauge field (the $NCCP^1$ model); this model consists of a doublet of spinons (bosonic fields) transforming as a spinor under spin rotations, coupled to a non compact $U(1)$ gauge field. In this representation, the hedeghogs correspond to the monopoles of the $U(1)$ gauge field, and suppressing hedgehogs leads indeed to the non compactness of the gauge field. This can also be viewed as an example of a $U(1)$ fractionalized phase with full $SU(2)$ spin rotation symmetry (albeit with complete monopoles suppression).

APPENDIX C

C.1. Symmetries of the spinon action

We start from the contribution S_R^c to the spinon action in Eq. (3.33), that we rewrite in Eq. (C.1)

$$S_R^c = \int_0^\beta d\tau \, tr\left[\sum_i \chi_{ii}^T R_i^\dagger \partial_\tau R_i - \sum_{ij} t_{ij} \chi_{ij}^T R_i^\dagger R_j\right] \qquad \text{(C.1)}$$

We insert the parameterization given by

$$R_{\alpha p}^i = \begin{bmatrix} z_{i\uparrow} & -z_{i\downarrow}^* \\ z_{i\downarrow} & z_{i\uparrow}^* \end{bmatrix} \qquad \text{(C.2)}$$

We also remember the holon action is

$$S_\psi = T\sum_{\omega_n}\sum_{\boldsymbol{k}}\sum_{\alpha=\pm} \Psi_{n\boldsymbol{k}\alpha}^\dagger \begin{pmatrix} -i\omega_n + \xi_{\boldsymbol{k}} & \alpha H_0 \\ \alpha H_0 & -i\omega_n + \xi_{\boldsymbol{k}+\boldsymbol{Q}} \end{pmatrix} \Psi_{n\boldsymbol{k}\alpha} \qquad \text{(C.3)}$$

Where $\Psi_{n\boldsymbol{k}\alpha} = \left(\psi_{n\boldsymbol{k}\alpha}, \psi_{n\boldsymbol{k}+\boldsymbol{Q}\alpha}\right)^T$, $\boldsymbol{Q} = (\pi, \pi)$, and we have defined the single-particle dispersion $\xi_{\boldsymbol{k}} = (-2t(cosk_x + cosk_y) + 4t' cosk_x cosk_y - \mu)$. Noting that $\chi_{ij}(\tau) = \chi_{ij}(0)$, S_R^c becomes

$$S_z^c = \int_0^\beta d\tau \left[\sum_i \left((\chi_{ii}^{++} - \chi_{ii}^{--}) z_i^\dagger \partial_\tau z_i + \chi_{ii}^{-+} z_{i\alpha}\varepsilon_{\alpha\beta}\partial_\tau z_{i\beta} - \chi_{ii}^{+-} z_i^* \varepsilon_{\alpha\beta}\partial_\tau z_{i\beta}^*\right) - \sum_{i<j} t_{ij}\left((\chi_{ij}^{++} + \right.\right.$$

$$\left.\left.\chi_{ji}^{--}) z_i^\dagger z_j + (\chi_{ij}^{-+} - \chi_{ji}^{-+}) z_{i\alpha}\varepsilon_{\alpha\beta} z_{j\beta} + c.c.\right)\right] \qquad \text{(C.4)}$$

Where $\varepsilon_{\alpha\beta}$ is the Levi-Civita symbol (with $\varepsilon_{\alpha\beta} = -\varepsilon_{\beta\alpha} = 1$), and we have applied the shortcut $\chi_{ij}^{\alpha\beta} \equiv \left(\chi_{ij}(0)\right)_{\alpha\beta}$. Let us remember the initial bare electronic action given by

$$S_c = \int_0^\beta d\tau \left[\sum_i c_{i\alpha}^\dagger (\partial_\tau - \mu)\, c_{i\alpha} - \sum_{ij} t_{ij}\, c_{i\alpha}^\dagger c_{j\alpha}\right] \qquad \text{(C.5)}$$

We know from the main text that we can define

$$\left(U_{ij}\right)_{\alpha\beta} = \langle \left(R_i^\dagger R_j\right)_{\alpha\beta} \rangle \qquad \text{(C.6)}$$

and that the following assumption is self-consistent with the mean-field solution

$$U_{ij} = \mathbb{1} Z_{i-j}; \quad Z_{i-j} \in \mathbb{R} \qquad \text{(C.7)}$$

Thus, being U_{ij} trivial in $SU(2)$ space, they only lead to a renormalization of the hopping amplitudes given by $t_{ij} \to Z_{i-j} t_{ij}$, inherited from the bare electrons, while the chemical potential μ in Eq. (C.5) is not renormalized, as $R_i^\dagger R_i = \mathbb{1}$, and thus is identical for electrons and holons. We also remember the action describing the coupling action S_{int} given by Eq. (3.31) that we report here

$$S_{int} = \int_0^\beta d\tau \left[\sum_i \psi_{i\alpha}^\dagger \boldsymbol{\sigma}_{\alpha\beta}\, \psi_{i\beta} \cdot \boldsymbol{H}_i\right] \qquad \text{(C.8)}$$

Combining Eq. (C.8) with the considerations make above, we obtain the holon Hamiltonian [41]

$$H_\psi = -\sum_{i,j}\left(Z_{i-j}t_{ij} + \mu\delta_{ij}\right)\psi^\dagger_{i\alpha}\psi_{j\alpha} + \sum_i \psi^\dagger_{i\alpha}\boldsymbol{\sigma}_{\alpha\beta}\,\psi_{i\beta}\cdot\langle \boldsymbol{H}_i\rangle \qquad \text{(C.9)}$$

We see that in Eq. (C.9) H_ψ is diagonal in the $SU(2)$ index α, so implying $\chi_{ij}^{\alpha\beta} = 0$ if $\alpha \neq \beta$: thus, looking at the symmetry analysis of the $\mathbb{CP}^1$ model in Appendix D of Ref. 21, in Eq. (C.4) the terms $z_{i\alpha}\varepsilon_{\alpha\beta}\partial_\tau z_{i\beta}$ and $z_{i\alpha}\varepsilon_{\alpha\beta}z_{j\beta}$ vanish. Moreover, let us define the antiunitary operator Θ given by

$$\Theta\psi_{i\alpha}\Theta^\dagger = \psi_{i\alpha} \quad \text{(C.10)}$$

H_ψ commutes with Θ, thus having an emergent time-reversal symmetry. As the operator $\left(-i\psi^\dagger_{i\alpha}\psi_{j\alpha} + i\psi^\dagger_{j\alpha}\psi_{i\alpha}\right)$ is odd under the operator Θ, we can conclude that

$$Im\chi_{ij}^{\alpha\alpha} = \frac{1}{2}\langle -i\psi^\dagger_{i\alpha}\psi_{j\alpha} + i\psi^\dagger_{j\alpha}\psi_{i\alpha}\rangle = 0 \qquad \text{(C.11)}$$

Hence we can say that

$$\chi_{ij}^{\alpha\alpha} = \chi_{ji}^{\alpha\alpha} \in \mathbb{R} \qquad \text{(C.12)}$$

Furthermore, H_ψ has other symmetries, as it is invariant under:

- Translation by one lattice site, such that

$$\chi_{ij}^{\alpha\alpha} = \chi_{i+e_\mu,j+e_\mu}^{\alpha\alpha}; \quad \mu = x,y \qquad \text{(C.13)}$$

- Translation by $\alpha \to -\alpha$ such that

$$\chi_{ij}^{\alpha\alpha} = \chi_{ij}^{-\alpha-\alpha} \qquad \text{(C.14)}$$

  From Eqs. (C.13) and (C.14) we obtain

$$\chi_{ij}^{\alpha\alpha} = \chi_{i+e_\mu,j+e_\mu}^{-\alpha-\alpha} \qquad \text{(C.15)}$$

- Translation by two lattice sites, leading to

$$\chi_{ij}^{\alpha\alpha} = \chi_{i+2e_\mu,j+2e_\mu}^{\alpha\alpha} \qquad \text{(C.16)}$$

Combining these symmetries, we find that

$$\chi_{ii}^{++} - \chi_{ii}^{--} = \chi_{ii}^{++} - \chi_{i+e_\mu,j+e_\mu}^{++} \equiv (-1)^{x_i+y_i}\chi_\Omega \qquad \text{(C.17)}$$

The resulting term in the action in Eq. (C.4) thus becomes

$$\int_0^\beta d\tau \sum_i (-1)^{x_i+y_i}\chi_\Omega z_i^\dagger \partial_\tau z_i \quad \text{(C.18)}$$

and it is translation invariant, as under translation by one lattice site along the direction $\mu = x,y$, we have $z_i \to i\sigma_y z^*_{i+e_\mu}$ [21]. Similarly, from Eqs. (C.12)-(C.16) we obtain

$$\chi_{ij}^t \equiv \chi_{ij}^{++} + \chi_{ji}^{--} = \chi_{ij}^{++} + \chi_{i+e_\mu,j+e_\mu}^{++} = \chi_{i-j}^t \qquad \text{(C.19)}$$

This means that the spinon-hopping terms in Eq. (C.4) are translation invariant, and thus we are able to obtain the compact form of S_z^c in Eq. (3.44) of the main text.

C.2. Symmetries of the electronic Green's function $G^c_{\alpha\beta}$

Let us consider [41] the real space representation of the electronic Green's function in Eq. (3.58) as

$$G^c_{\alpha\beta}(i,j,\tau) = -\langle \big(R_i(\tau)\big)_{\alpha\alpha'} \Big(R_j^*(0)\Big)_{\beta\beta'} \rangle \langle \psi_{i\alpha'}(\tau)\psi^\dagger_{j\beta'}(0)\rangle \qquad \text{(C.20)}$$

Using the parameterization given by Eq. (C.2), also noting that both the holon Green's function in Eq. (3.38) and the spinon Green's function in Eq. (3.50) are diagonal in $SU(2)$ spin space, that is $G_\psi^{\alpha\beta} \sim \delta_{\delta\beta}$ and $G_z^{\alpha\beta} \sim \delta_{\delta\beta}$, we can rewrite Eq. (C.20) as

$$G^c_{\alpha\beta}(i,j,\tau) = -\delta_{\alpha\beta}\big(\langle \psi_{i+}(\tau)\psi^\dagger_{j+}(0)\rangle\langle z_{\alpha i}(\tau)z^\dagger_{\alpha j}(0)\rangle + \langle \psi_{i-}(\tau)\psi^\dagger_{j-}(0)\rangle\langle z_{\bar\alpha j}(\tau)z^\dagger_{\bar\alpha i}(0)\rangle\big) \qquad \text{(C.21)}$$

where $\bar\alpha = \downarrow$ ($\bar\alpha = \uparrow$) for $\alpha = \uparrow$ ($\alpha = \downarrow$). Furthermore, from the spinon action in Eq. (3.46) it follows that $\langle z_{\alpha i}(\tau)z^\dagger_{\alpha j}(\tau')\rangle$ does not depend on α, and hence $G^c_{\alpha\beta}(i,j,\tau) \propto \mathbb{1}_{\alpha\beta}$, thus leading to a spin-rotation invariant fermionic Green's function. We can also note that the holon action S_ψ is invariant under $\psi_{i\alpha}(\tau) \to \psi_{i+\boldsymbol{e}_\mu,-\alpha}(\tau)$, while the spinon action S_z is invariant under $z_i \to i\sigma_y z^*_{i+e_\mu}$, thus

$$\langle \psi_{i\alpha}(\tau)\psi^\dagger_{j\alpha}(\tau')\rangle = \langle \psi_{i+\boldsymbol{e}_\mu,-\alpha}(\tau)\psi^\dagger_{j+\boldsymbol{e}_\mu,-\alpha}(\tau')\rangle \qquad \text{(C.22)}$$

$$\langle z_{i\alpha}(\tau)z^\dagger_{j\alpha}(\tau')\rangle = \langle z_{j+\boldsymbol{e}_\mu,-\alpha}(\tau')z^\dagger_{i+\boldsymbol{e}_\mu,-\alpha}(\tau)\rangle \qquad \text{(C.23)}$$

Inserting Eqs. (C.22)-(C.23) in Eq. (C.20) we find that the electronic Green's function is also translation invariant as

$$G^c_{\alpha\beta}(i,j,\tau) = G^c_{\alpha\beta}(i-j,\tau) \qquad \text{(C.24)}$$

In the gauge we use, the holon Hamiltonian in Eq. (C.9) is explicitly invariant under the remaining square lattice symmetries, that is the mirror reflection σ and the four-fold rotation C_4. In fact these symmetries transformations $g \in \{C_4, \sigma\}$ are accompanied by the gauge transformation $G_i(g) \in SU(2)$, with action

$$\psi_{i\alpha}(\tau) \to \sum_\beta \big(G_i(g)\big)_{\alpha\beta}\, \psi_{g(i)\beta} \qquad \text{(C.25)}$$

These gauge transformations can be chosen to be trivial in this gauge, that is $G_i(g) = \mathbb{1}$.
We finally point out that the presence of the full lattice and spin-rotation symmetry only holds where the spinons are gapped, that is in the limit of sufficiently strong fluctuations (large g), while in the magnetically ordered phase the condensation of the spinons spontaneously breaks spin-rotation and translational symmetry, and in this case also the electronic Green's function becomes nontrivial in

spin space and breaks translational symmetry. Anyway, as we are interested above the pseudogap regime, we do not consider this situation.

C.3. Electronic spectral function at the antinodal point

We start from the spinon Green's function in Eq. (3.50) that we rewrite here [41]

$$G_z^{\alpha\beta}(i\Omega_n,\boldsymbol{q}) \equiv T\langle Z_{n\boldsymbol{q}\alpha} Z_{n\boldsymbol{q}\beta}^{\dagger}\rangle = \frac{g\delta_{\alpha\beta}}{(\Omega_n^2+D_{\boldsymbol{q}+}^2)(\Omega_n^2+D_{\boldsymbol{q}-}^2)}\begin{pmatrix} \Omega_n^2+E_{\boldsymbol{q}+\boldsymbol{Q}}^2 & i\Omega_n g\chi_\Omega \\ i\Omega_n g\chi_\Omega & \Omega_n^2+E_{\boldsymbol{q}}^2 \end{pmatrix} \qquad \text{(C.26)}$$

We can neglect the off-diagonal term, that is $\sim g\chi_\Omega$, because this term only very weakly affects the low-energy part of the spinon spectrum, as it has been checked by numerical comparison, even at $g\chi_\Omega \sim 1$ [41]. In the limit $g\chi_\Omega \to 0$ the Green's function of the spinons simply reads as

$$G_z^{\alpha\beta} = \frac{g\delta_{\alpha\beta}}{(\Omega_n^2+E_{\boldsymbol{q}}^2)} \qquad \text{(C.27)}$$

And hence in Eq. (3.63) we have

$$g_c(\boldsymbol{k},\boldsymbol{q},i\omega_n) = 2gT\sum_{\Omega_n}\frac{1}{\Omega_n^2+E_{\boldsymbol{q}}^2}\frac{i\omega_n - i\Omega_n - \xi_{\boldsymbol{k}-\boldsymbol{q}+\boldsymbol{Q}}}{\left(i\omega_n - i\Omega_n - \rho_{\boldsymbol{k}-\boldsymbol{q}}^{+}\right)\left(i\omega_n - i\Omega_n - \rho_{\boldsymbol{k}-\boldsymbol{q}}^{-}\right)} \qquad \text{(C.28)}$$

Where we have introduced the holon dispersion given by ($s = \pm$)

$$\rho_{\boldsymbol{k}}^{s} = \frac{\xi_{\boldsymbol{k}}+\xi_{\boldsymbol{k}+\boldsymbol{Q}}}{2} + s\sqrt{\left(\frac{\xi_{\boldsymbol{k}}-\xi_{\boldsymbol{k}+\boldsymbol{Q}}}{2}\right)^2 + H_0^2} \qquad \text{(C.29)}$$

We evaluate the Matsubara sum using contour deformation and the residue theorem, and the resulting expression is analytical function in $i\omega_n$, making the analytical continuation from $g_c(\boldsymbol{k},\boldsymbol{q},i\omega_n)$ to $g_c^r(\boldsymbol{k},\boldsymbol{q},\omega)$ straightforward. The resulting $g_c^r(\boldsymbol{k},\boldsymbol{q},\omega)$ has poles at four distinct ($s,s' = \pm$)

$$\omega_{ss'}^{\boldsymbol{k},\boldsymbol{q}} = sE_{\boldsymbol{q}} + \rho_{\boldsymbol{k}-\boldsymbol{q}}^{s'} \qquad \text{(C.30)}$$

While in Eq. (3.63) a finite value of η is used in the analytical continuation to cutoff the poles for the numerical integration over $\boldsymbol{q}$, and to introduce a finite life time, here we consider the limit $\eta \to 0^+$. Thus the electronic spectral $A_{\boldsymbol{k}}(\omega) = -\frac{1}{\pi}ImG_{c,r}(\omega,\boldsymbol{k})$ can be written in the compact form

$$A_{\boldsymbol{k}}(\omega) = \sum_{ss'=\pm}\int_{BZ}\frac{d^2\boldsymbol{q}}{(2\pi)^2}Z_{ss'}^{\boldsymbol{k},\boldsymbol{q}}\delta\left(\omega - \omega_{ss'}^{\boldsymbol{k},\boldsymbol{q}}\right) \qquad \text{(C.31)}$$

Where we have the weights given by

$$Z_{ss'}^{\boldsymbol{k},\boldsymbol{q}} = gn_{ss'}^{\boldsymbol{k},\boldsymbol{q}}(T)\frac{\left|\rho_{\boldsymbol{k}-\boldsymbol{q}}^{s'} - \xi_{\boldsymbol{k}-\boldsymbol{q}+\boldsymbol{Q}}\right|}{E_{\boldsymbol{q}}\left(\rho_{\boldsymbol{k}-\boldsymbol{q}}^{+} - \rho_{\boldsymbol{k}-\boldsymbol{q}}^{-}\right)} \qquad \text{(C.32)}$$

$$n_{ss'}^{\boldsymbol{k},\boldsymbol{q}} = n_B\left(E_{\boldsymbol{q}}\right) + n_F\left(-s\rho_{\boldsymbol{k}-\boldsymbol{q}}^{s'}\right) \qquad \text{(C.33)}$$

With n_B (n_F) in Eq. (C.33) denoting the Bose (Fermi) distribution function.
From these expressions we can see that the spectral weight $A_{\boldsymbol{k}}(\omega)$ vanishes at zero frequency $\omega = 0$ in the entire Brillouin zone in the limit $T \ll \Delta$, with Δ the spinon gap: in fact the delta function in Eq. (C.31) leads to $sE_{\boldsymbol{q}} = -\rho^{s'}_{\boldsymbol{k}-\boldsymbol{q}}$ at zero frequency, and this allows to simplify in Eq. (C.33) the thermal factors as $n^{\boldsymbol{k},\boldsymbol{q}}_{ss'} \to n_B(E_{\boldsymbol{q}}) + n_F(E_{\boldsymbol{q}})$. Consequently $A_{\boldsymbol{k}}(\omega = 0)$ vanishes exponentially for $T \ll \Delta$. This is not unexpected, as any zero energy electronic excitation must necessarily involve the thermal excitation of a spinon, with a minimal energetic cost of Δ. Because we are focusing on the pseudogap metal state, we focus on the parameter regime $\Delta < T$, and this allows to have finite spectral weights at zero energy in the nodal part of the Brillouin zone, as seen in numerical studies of the Hubbard model and in experiments. Furthermore, we can qualitatively understand the antinodal spectral function in Fig. 3.7: in fact, at and near the antinodal point $\boldsymbol{k} = (\pi, 0)$, we have $\rho^-_{\boldsymbol{k}} < 0$ and $\rho^+_{\boldsymbol{k}} > 0$. While near the nodal point $\boldsymbol{k} = (\pi/2, \pi/2)$ it holds $\rho^-_{\boldsymbol{k}} > 0$, which also contributes to the spectral weight at the antinode, due to the integration over the loop momentum $\boldsymbol{q}$ in Eq. (C.31), its contribution requires large $\boldsymbol{q}$, of order of $(\pi/2, \pi/2)$, where the spinon energy $E_{\boldsymbol{q}}$ is large. Therefore this contribution is suppressed. Furthermore, in the limit $T \ll H_0$, where $T \ll |\rho^s_{\boldsymbol{k}}|$ for $\boldsymbol{k}$ near the anti-node, the thermal factor seen above become

$$n_{++} \sim n_{--} \sim 1 + n_B(E_{\boldsymbol{q}}); \qquad n_{+-} \sim n_{-+} \sim n_B(E_{\boldsymbol{q}}) \qquad \text{(C.34)}$$

We see that the contribution of $\omega^{\boldsymbol{k}=(\pi,0),\boldsymbol{q}}_{ss'}$ with $s \neq s'$ to the low frequency ($|\omega| \ll H_0$) spectral function is suppressed, due to the thermal factors, as $\omega^{\boldsymbol{k}=(\pi,0),\boldsymbol{q}}_{ss'}$ requires $E_{\boldsymbol{q}}$ of order H_0, We also note that the magnitude $\left|\omega^{\boldsymbol{k}=(\pi,0),\boldsymbol{q}}_{ss'}\right|$ of the frequency of the other two poles, with $s = s'$, is a growing function of $E_{\boldsymbol{q}}$. We thus expect a suppression of the anti-nodal spectral weight in the range of frequencies ω given by $\omega_{--}, \omega_{+-} < \omega < \omega_{-+}, \omega_{++}$, where $\omega_{ss'} = \omega^{\boldsymbol{k}=(\pi,0),\boldsymbol{q}}_{ss'}$. This agrees well with Fig. 3.7, and we also refer to the following Fig. C.1, where the four frequencies $\omega_{--}, \omega_{+-}, \omega_{-+}, \omega_{++}$ are shown as dots, together with the corresponding anti-nodal spectra function for many different values of the system parameters. Using the explicit form of $E_{\boldsymbol{q}}$ and $\rho^s_{\boldsymbol{k}}$ entering $\omega^{\boldsymbol{k},\boldsymbol{q}}_{ss'}$, we thus can estimate a gap of size $2H_0$ centered around $\omega_0 = \xi_{(\pi,0)}$, and the same Mott-insulating behavior at the antinodal point is also found in the DCA result.

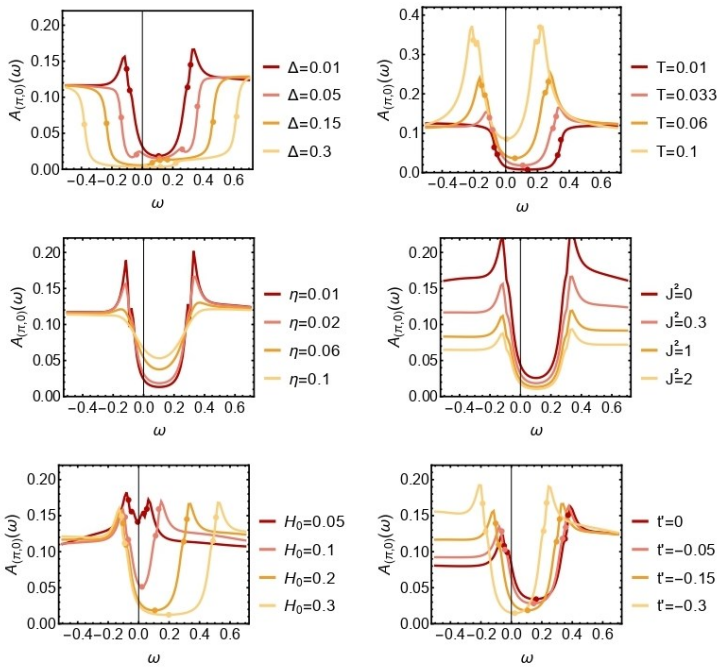

Figure C.1. Dependence of the anti-nodal spectral function $A_{(\pi,0)}(\omega)$ on various parameters of the system. If non specified otherwise, we use $t' = -0.15, p = 0.05, T = 1/30, H_0 = 0.2, J^2 = 0.3, \Delta = 0.01, \eta = 0.02$. The horizontal axis reports the frequencies $\omega_{ss'} = \omega_{ss'}^{\boldsymbol{k}=(\pi,0),\boldsymbol{q}}$ in Eq. (C.30), with color and vertical positions indicating the curve the respective point corresponds to [41]

C.4. Electronic Green's function for the FL*

The term in Eq. (3.70) is just the CP^1 model for the spinons $z_{i\alpha}$ as [34, 36-38]

$$\mathcal{L}_z = \frac{4}{g_0}[|(\partial_\tau - iA_\tau)z_\alpha|^2 + v^2|(\boldsymbol{\nabla} - i\mathbf{A})z_\alpha|^2] \qquad \text{(C.35)}$$

The fermion hopping in term $\mathcal{L}_\psi$ in Eq. (3.71) can ben written as:

$$\mathcal{L}_\psi = -\sum_{i<j} t_{ij}\big[\big(z_{i\alpha}^* z_{j\alpha}\big)\big(\psi_{i+}^\dagger \psi_{j+} + \psi_{j-}^\dagger \psi_{i-}\big) + \big(z_{j\alpha}^* z_{i\alpha}\big)\big(\psi_{i-}^\dagger \psi_{j-} + \psi_{j+}^\dagger \psi_{i+}\big) + \\ +\big(\varepsilon_{\alpha\beta} z_{j\alpha}^* z_{i\beta}^*\big)\big(\psi_{i+}^\dagger \psi_{j-} - \psi_{j+}^\dagger \psi_{i-}\big) + \big(\varepsilon_{\alpha\beta} z_{i\alpha} z_{j\beta}\big)\big(\psi_{i-}^\dagger \psi_{j+} - \psi_{j-}^\dagger \psi_{i+}\big)\big] \qquad \text{(C.36)}$$

From the derivation of the CP^1 model we know that

$$z_{i\alpha}^* z_{j\alpha} \approx e^{iA_{ij}} \qquad \text{(C.37)}$$

We can thus incorporate Eq. (C.37) into the two first terms in Eq. (C.36) yeldings terms which are gauge invariant of the following Lagrangian:

$$\mathcal{L}_\psi = \sum_{p=\pm 1}\sum_i \psi_{ip}^\dagger[\partial_\tau + ipA_\tau - \mu - \lambda p(-1)^{x_i+y_i}]\psi_{ip} \\ -\sum_{p=\pm 1}\sum_{i<j} t_{ij}\big(e^{ipA_{ij}}\psi_{ip}^\dagger \psi_{jp} + e^{-ipA_{ij}}\psi_{jp}^\dagger \psi_{ip}\big) \qquad \text{(C.38)}$$

For $A_\mu = 0$, $\mathcal{L}_\psi$ describes the band structure in terms of the Fermi pockets; the interaction arises from the minimal coupling to the A_μ gauge field. Finally we have to consider the last two terms in Eq.

(C.36): combining these terms with the analogous terms arising from the time derivative of the c_α, we obtain to leading order in the derivative of the z_α:

$$\mathcal{L}_{ss} = \int_{\mathbf{k},\mathbf{p},\mathbf{q}} \left[\mathbf{p}\cdot\frac{\partial\varepsilon(\mathbf{k})}{\partial\mathbf{k}}\right] z_\downarrow\left(\mathbf{q}-\frac{\mathbf{p}}{2}\right) z_\uparrow\left(\mathbf{q}+\frac{\mathbf{p}}{2}\right)\psi_-^\dagger(\mathbf{k}+\mathbf{q})\psi_+(\mathbf{k}-\mathbf{q}) + c.c +$$
$$+\sum_i (z_{i\uparrow}\partial_\tau z_{i\downarrow} - z_{i\downarrow}\partial_\tau z_{i\uparrow})\psi_{i-}^\dagger\,\psi_{i+} + c.c \qquad \text{(C.39)}$$

Where $\varepsilon(\mathbf{k})$ is the single-particle dispersion of the large Fermi surface state

$$\varepsilon(\mathbf{k}) = -\sum_j t_{ij} e^{i\mathbf{k}\cdot(\mathbf{r}_j-\mathbf{r}_i)} \qquad \text{(C.40)}$$

We remember the definitions of the bound states of the ψ_p fermions and the z_α spinons, i.e. F_α and G_α in Eq. (3.74) as

$$F_{i\alpha}\sim z_{i\alpha}\psi_{i+} \quad ; \quad G_{i\alpha}\sim\varepsilon_{\alpha\beta}z_{i\beta}^*\psi_{i-} \qquad \text{(C.41)}$$

The base of our analysis, in order to write an effective Hamiltonian, is given by properties under the square lattice symmetry operations, which we report in Table C.1. We can underline that any Hamiltonian which is invariant under the symmetry transformations in Table C.1, is acceptable, but we use simple physical requirements to restrict the large class of possibilities, as:

- For the diagonal terms which do not mix the F_α and G_α, we assume for simplicity that they just inherit terms for ψ_+ and ψ_- in $\mathcal{L}_\psi$ in Eq. (C.38).
- The mixing between the F_α and G_α is provided by the term $\mathcal{L}_{ss}$ in Eq. (C.39); physically this can be understood as the mixing corresponds to hopping between two sublattices, as F_α and G_α reside preferentially, but not exclusively, on different sublattices (and they separately have an additional degeneracy associated with carrying spin $S = 1/2$). These terms are more simply considered in their real space form, and are the last two terms in Eq. (C.36).

The bare electron operator $c_{i\alpha}$ will have a nonzero overlap with both the F_α and G_α fermions, and this will be nonlocal over the scale ξ (the spin-correlation length). We can approximate this connection from $c_{i\alpha} = R^i_{\alpha p}\psi_{ip}$ as

$$c_{i\alpha} \equiv Z(F_{i\alpha} + G_{i\alpha}) \qquad \text{(C.42)}$$

where Z is some quasiparticle renormalization factor depending upon the holon-spinon bound-state wave function.

	T_x	$R^{\text{dual}}_{\pi/2}$	I^{dual}_x	$\mathcal{T}$
z_α	$\epsilon_{\alpha\beta}z^{\beta *}$	$\epsilon_{\alpha\beta}z^{\beta *}$	$\epsilon_{\alpha\beta}z^{\beta *}$	$\epsilon_{\alpha\beta}z^{\beta *}$
ψ_+	$-\psi_-$	$-\psi_-$	$-\psi_-$	$\psi_+^\dagger$
ψ_-	ψ_+	ψ_+	ψ_+	$\psi_-^\dagger$
A_τ	$-A_\tau$	$-A_\tau$	$-A_\tau$	A_τ
A_x	$-A_x$	$-A_y$	A_x	$-A_x$
A_y	$-A_y$	A_x	$-A_y$	$-A_y$
n^a	$-n^a$	$-n^a$	$-n^a$	$-n^a$
F_α	G_α	G_α	G_α	$\epsilon^{\alpha\beta}F_\beta^\dagger$
G_α	F_α	F_α	F_α	$\epsilon^{\alpha\beta}G_\beta^\dagger$

Table C.1. Transformations of the lattice fields under square lattice symmetry operations. T_x is the translation by one lattice spacing along the x direction, $R^{\pi/2}_{dual}$ is the rotation about a dual lattice site on the plaquette center $(x \to y, y \to -x)$, I^x_{dual} is the reflection about the dual lattice y axis $(x \to -x, y \to y)$, T is time recersal, defined as a symmetry of the imaginary time path integral [34].

Combining these considerations, we can write the following effective Hamiltonian:

$$H_{eff} = H_0 + H_{int} \qquad \text{(C.43a)}$$

$$H_0 = -t_{ij}\left(F^+_{i\alpha}F_{i\alpha} + G^+_{i\alpha}G_{i\alpha}\right) - \lambda\sum_i(-1)^{x_i+y_i}\left(F^+_{i\alpha}F_{i\alpha} - G^+_{i\alpha}G_{i\alpha}\right) + \\ - \sum_{ij}\tilde{t}_{ij}\left(F^+_{i\alpha}G_{j\alpha} + G^+_{i\alpha}F_{j\alpha}\right) \qquad \text{(C.43b)}$$

In Eqs. (C.43) we have:

- The hopping terms t_{ij} are taken to be similar to the bare electron dispersion characterizing the Fermi surface in the overdoperd region.
- λ represents the potential, at distances shorter than the spin-correlation length ξ, due to the local antiferromagnetic order, introduced in Eq. (3.8), and we will treat it as a spin-fermion coupling of order unity.
- The last term in Eq. (C.43) comes from the term $\mathcal{L}_{ss}$ in Eq. (C.39). The hopping terms $\tilde{t}_{ij}$ couple the two species of electronlike quasiparticles F_α and G_α to each other: it is this term which is responsible for shifting the center of the pocket Fermi surface in the normal state away from the magnetic Brillouin zone boundary: in the absence of these terms, but with $\lambda \neq 0$, we obtain holelike pockets centered at $(\pi/2, \pi/2)$. However, when the $\tilde{t}_{ij}$ are finite, the pockets can be shifted away from this special point.
- H_{int} is the invariant interaction Hamiltonian: there could be many interaction channels, which induce superconductivity of the F_α and G_α particles, such as negative contact interaction, interaction with order parameters, and the gauge field fluctuation: here we do not specify particular interaction and we assume that pairings are indiced.

The Hamiltonian H_0 of bound states in Eq. (C.43) can be diagonalized in momentum space, firstly we can rewrite it in momentum space:

$$H_0 = \sum_{\mathbf{k}}\left[\varepsilon(\mathbf{k})\left(F^+_{\mathbf{k}\alpha}F_{\mathbf{k}\alpha} + G^+_{\mathbf{k}\alpha}G_{\mathbf{k}\alpha}\right)\right] + \sum_{\mathbf{k}}\left[\tilde{\varepsilon}(\mathbf{k})\left(F^+_{\mathbf{k}\alpha}G_{\mathbf{k}\alpha} - G^+_{\mathbf{k}\alpha}F_{\mathbf{k}\alpha}\right) - \lambda\left(F^+_{\mathbf{k}\alpha}F_{\mathbf{k}+\mathbf{K},\alpha} - G^+_{\mathbf{k}\alpha}G_{\mathbf{k}+\mathbf{K},\alpha}\right)\right] \qquad \text{(C.44)}$$

Where $\mathbf{K} = (\pi, \pi)$ is the wave vector of the antiferromagnetic Néel order. In Eq. (C.44) we parameterize $\varepsilon(\mathbf{k})$ and $\tilde{\varepsilon}(\mathbf{k})$ as:

$$\varepsilon(\mathbf{k}) = -2t\left(cosk_x + cosk_y\right) + 4t'cosk_x cosy - 2t''\left(cos2k_x + cos2k_y\right) - \mu \qquad \text{(C.45)}$$

$$\tilde{\varepsilon}(\mathbf{k}) = -\tilde{t}_0 - 2\tilde{t}\left(cosk_x + cosk_y\right) + 4\tilde{t}'cosk_x cosy - 2\tilde{t}''\left(cos2k_x + cos2k_y\right) \qquad \text{(C.46)}$$

Where $t, t', t''(\tilde{t}, \tilde{t}', \tilde{t}'')$ are nearest-neighbor, next-nearest neighbor, and next-next-nearest neighbor hopping t_{ij} $(\tilde{t}_{ij})$, and $\tilde{t}_0$ is the matrix element of the on site mixing term $\left(F_i^+ G_i \ + G_i^+ F_i \ \right)$, allowed by symmetry (here we only include terms up to third nearest-neighbor hopping, which is capable to capture the shape of the Fermi surface, but higher order terms can be included in a similar fashion). We diagonalize Eq. (C.44), changing basis to:

$$C_{i\alpha} = \frac{1}{\sqrt{2}}\left(F_{i\alpha} + G_{i\alpha}\right) \ ; \ \ D_{i\alpha} = \frac{1}{\sqrt{2}}(-1)^{x_i+y_i}\left(F_{i\alpha} - G_{i\alpha}\right) \qquad \text{(C.47)}$$

$$C_{\mathbf{k}\alpha} = \frac{1}{\sqrt{2}}\left(F_{\mathbf{k}\alpha} + G_{\mathbf{k}\alpha}\right) \ ; \ \ D_{\mathbf{k}\alpha} = \frac{1}{\sqrt{2}}\left(F_{\mathbf{k}+\mathbf{K},\alpha} - G_{\mathbf{k}+\mathbf{K},\alpha}\right) \qquad \text{(C.48)}$$

The C and D fermions have the same space-group transformations properties as the physical electron, and in the new basis the Hamiltonian becomes

$$H_0 = \sum_{\mathbf{k}}\{[\varepsilon(\mathbf{k}) + \tilde{\varepsilon}(\mathbf{k}) - \mu]C_{\mathbf{k}\alpha}^+ C_{\mathbf{k}\alpha} + [\varepsilon(\mathbf{k}+\mathbf{K}) - \tilde{\varepsilon}(\mathbf{k}+\mathbf{K}) - \mu]D_{\mathbf{k}\alpha}^+ D_{\mathbf{k}\alpha} + -\lambda\left(C_{\mathbf{k}\alpha}^+ D_{\mathbf{k}\alpha} + D_{\mathbf{k}\alpha}^+ C_{\mathbf{k}\alpha}\right)\} \qquad \text{(C.49)}$$

The spectrum of the original electron operator c_α can be obtained by diagonalizing the Hamiltonian in Eq. (C.49), and $c_{\mathbf{k}\alpha}$ is related to $C_{\mathbf{k}\alpha}$ and $D_{\mathbf{k}\alpha}$, from Eqs. (C.41), (C.42) and (C.47) by:

$$c_{\mathbf{k}\alpha} \approx Z\left(F_{\mathbf{k}\alpha} + G_{\mathbf{k}\alpha}\right) \approx \frac{Z}{\sqrt{2}} C_{\mathbf{k}\alpha} \qquad \text{(C.50)}$$

In Eq. (C.50) in general Z should be nonlocal over a scale of the spin-correlation length ξ, but now for simplicity we consider Z as momentum independent. Note also that Eq. (C.50) and the symmetry transformations in Table C.1 ensure that $c_{\mathbf{k}\alpha}$ is invariant under all operations of the square lattice symmetry (the possible nonlocal terms in Eq. (C.50) can be deduced by the requirements of symmetry).

Bibliography

[1] J. G. Bednorz, K. A. Muller, Possible high T_c superconductivity in the $BaLaCuO$ system, Zeitschrift für Physik B Condensed Matter **64**, 189 (1986).

[2] S. Uchida, High-temperature superconductivity: the road to higher critical temperature, 1st ed. Springer Series in Material Sciences 213, Springer Japan (2015).

[3] P. W. Anderson, The resonating valence bond state in La_2CuO_4 and superconductivity, Science **235**, 1196-1198 (1987).

[4] N. Barišic, M. K. Chan, Y. Li, X. Zhao, M. Dressel, A. Smontara, M. Greven, Universal sheet resistance and revised phase diagram of the cuprate high-temperature superconductors, Proc. Nat. Acad. Sci. Usa 110, 12235-12240 (2013).

[5] B. Keimer, S. A. Kivelson, M. R. Norman, S. Uchida, J. Zaanen, From quantum matter to high-temperature superconductivity in copper oxides, Nature 518, 179-186 (2015).

[6] M. Hashimoto. I. M. Vishik, R. -H He, T. P. Deveraux, Z. -X. Shen, Energy gaps in high-transition-temperature cuprate superconductors, Nat. Phys. 10, 483-495 (2014).

[7] F. C. Zhang, T. M. Rice, Effective Hamiltonian for the superconducting Cu oxides, Phys. Rev. B **37**, 3759 (1989).

[8] S. Sachdev, Emergent gauge fields and the high-temperature superconductors, Phil. Trans. R. Soc. A 374, 20150248 (2015).

[9] P. A. Lee, N. Nagaosa, X. -G. Wen, Doping a Mott insulator: Physics of high-temperature superconductivity, Rev. Mod. Phys. **78**, 17-85 (2006).

[10] S. I. Mirzaei, D. Stricker, J. N. Hancock, C. Berthod, A. Georges, E. Van Helmen, M. K. Chan, X. Zhao, Y. Li, M. Greven, N. Barišic, D. Van der Marel, Spectroscopic evidence for Fermi liquid-like energy and temperature dependence of the relaxation rate in the pseudogap phase of the cuprates, Proc. Nat. Acad. Sci. Usa 110, 5774-5778 (2013).

[11] M. K. Chan, M. J. Veit, C. J. Dorow, Y. Ge, Y. Li, W. Tabis, Y. Tang, X. Zhao, N. Barišic, M. Greven, In-plane magnetoresistance obeys Kohler's rule in the pseudogap phase of cuprate superconductors, Phys. Rev. Lett. 113, 177005 (2014).

[12] J. M. Luttinger, Fermi surface and some simple equilibrium properties of a system of interacting fermions, Phys. Rev. **119**, 1153-1163 (1960).

[13] S. Badoux, W. Tabis, F. Laliberté, G. Grissonnanche, B. Vignolle, J. Béard, D. A. Bonn, W. N. Hardy, R. Liang, N. Doiron-Leyraud, L. Taillefer & C. Proust, Change of carrier density at the pseudogap critical point of a cuprate superconductor, Nature 531, 210 (2016).

[14] M. Oshikawa, Commensurability, excitation gap, and topology in quantum many-particle systems on a periodic lattice, Phys. Rev. Lett. 84, 1535 (1999).

[15] M. Oshikawa, Topological approach to Luttinger's theorem and the Fermi surface of a Kondo lattice, Phys. Rev. Lett. 84, 3370 (2000).

[16] T. Senthil, M. Vojta, S, Sachdev, Weak magnetism and non-Fermi liquids near heavy-fermion critical points, Phys. Rev. B, 69, 035111 (2004).

[17] A. Paramekanti, A. Vishwanath, Extending Luttinger's theorem to $\mathbb{Z}_2$ fractionalized phase of matter, Phys. Rev. B 70, 245118 (2004).

[18] T. Senthil, S. Sachdev, M. Vojta, Fractionalized Fermi liquids, Phys. Rev. Lett. 90, 216403 (2003).

[19] I. M. Vishik. M. Hashimoto, R. -H. He, W. -S. Lee, F. Schmitt, D. Lu, R. G. Moore, C. Zhang, W. Meevasana, T. Sasagawa, S. Uchida, K. Fujita, S. Ishida, M. Ishikado, Y. Yoshida, H. Eisaki, Z. Hussain, T. P. Devereaux, Z. -X. Shen, Phase competition in trisected superconducting dome, Proc. Nat. Acad. Sci. Usa **109**, 18332-18337 (2012).

[20] G. R. Stewart, Unconventional superconductivity, Adv. Phys. **66**, 75 (2017).

[21] S. Chatterjee, S. Sachdev, M. S. Scheurer, Intertwining topological order and broken symmetry in a theory of fluctuating spin-density waves, Phys. Rev. Lett. 119, 227002 (2017).

[22] D. Chowdhury. S. Sachdev, The enigma of the pseudogap phase of the cuprate superconductors. In *Quantum criticality in condensed matter: Phenomena, materials and ideas in theory and experiments. 50th Karpacz Winter School of Theoretical Physycs, Karpacz, Poland, 2-9 March 2014* (ed. J Jędrzejewski), pp. 1-43. Singapore: World Scientific (2015).

[23] M. R. Norman, D. Pines, C. Kallin, The pseudogap: friend or foe of high T_c?, Adv. Phys. **54**, 715-733, (2005).

[24] M. R. Norman, Cuprates – An overview, J. Supercond. Nov. Magn. **25**, 2131-2134 (2012).

[25] J. -L. Luo, The electronic state phase diagram of copper oxide high-temperature superconductors. In *Advances in theoretical and experimental research of high temperature cuprate superconductivity*. Ru-Shan Han, Peking University, China, pp. 1-26, World Scientific (2020).

[26] S. Hüfner, M. A. Hossain, A. Damascelli, G.A. Sawatzky, Two gaps make a high-temperature superconductor, Rep. Progr. Phys. **71**, 062501 (2008).

[27] M. Hashimoto, E. A. Nowadnick, R. H. He, I. M. Vishik, B. Moritz, Y. He, K. Tanaka, R. G. Moore, D. Lu, Y. Yoshida, M. Ishikado, T. Sasagawa, K. Fujita, S. Ishida, S. Uchida, H. Eisaki, Z. Hussain, T. P. Deveraux, Z. -X Shen, Direct spectroscopic evidence for phase competion between the pseudogap and superconductivity in $Bi_2Sr_2CaCu_2O_{8+\delta}$, Nat. Mater. **14**, 37-42 (2015).

[28] J. -W Wei, S. Kawasaki, G. -Q. Zheng, Z. -Y. Weng, X. -G. Wen, Luttinger-volume violating Fermi liquid in the pseudogap phase of the cuprate superconductors, Phys. Rev. B 85, 134519 (2012).

[29] P. Bonderson, M. Cheng, K. Patel, E. Plamadeala, Topological enrichment of Luttinger's theorem, arXiv:1601.07902v1 [cond-mat.str-el] (2018).

[30] M. B. Hastings, Lieb-Schultz-Mattis in higher dimensions, Phys. Rev. B **69**, 104431 (2004).

[31] M. Cheng, M. Zaletel, M. Barkeshli, A. Vishwanath, P. Bonderson, Translational symmetry and microscopic constraints on symmetry-enriched topological phases: a view from the surface, Phys. Rev. X **6**, 041068 (2016).

[32] D. V. Else, R. Thorngren, T. Senthil, Non-Fermi liquid as ersatz Fermi liquids: general constraints on compressible metals, Phys. Rev. X **11**, 021005 (2021).

[33] S. Sachdev, M. A. Metlitski, M. Punk, Antiferromagnetism in metals: from the cuprate superconductors to the heavy fermion materials, J. Phys.: Condens. Matter 24, 294205 (2012).

[34] Y. Qi, S. Sachdev, Effective theory of Fermi pockets in fluctuating antiferromagnets, Phys. Rev. B 81, 115129 (2010).

[35] B. Vignolle, D. Vignolles, M. -H. Julien, C. Proust, From quantum oscillations to charge order in high-T_c copper oxides in high magnetic fields, Comp. Rend. Physique 14, 39-52 (2013).

[36] S. Sachdev, M. A. Metlitski, Y. Qi, C. Xu, Fluctuating spin density wave in metals, Phys. Rev. B 80, 155129 (2009).

[37] E. G. Moon, S. Sachdev, Underdoped cuprates as fractionalized Fermi liquids: Transition to superconductivity, Phys. Rev. B **83**, 224508 (2011).

[38] D. Chowdhury. S. Sachdev, Density-wave instabilities of fractionalized Fermi liquids, Phys. Rev. B 90, 245136 (2014).

[39] D. Chowdhury. S. Sachdev, Higgs criticality in a two-dimensional metal, Phys. Rev. B 91, 115123 (2015).

[40] S. Sachdev, D. Chowdhury, The novel metallic states of the cuprates, Progr. Theor. Exp. Phys, 2016, 12C102 (2016).

[41] M. S. Scheurer, S. Chatterjee, W. Wu, M. Ferrero, A. Georges, S. Sachdev, Topological order in the pseudogap metal, Proc. Nat. Acad. Sci. Usa 115, 3665-3672 (2018).

[42] S. Sachdev, Topological order, emergent gauge fields, and Fermi surface reconstruction, Rep. Progr. Phys 82, 1-29 (2018).

[43] R. K. Kaul, A. Kolezhuk, M. Levin, S. Sachdev, T. Senthil, Hole dynamics in an antiferromagnet across a deconfined quantum critical point, Phys. Rev. B 75, 235122 (2007).

[44] R. K. Kaul, Y. B. Kim. S. Sachdev, T. Senthil, Algebric charge liquids, Nat. Phys. 4, 28 (2008).

[45] J. Fröhlich, P. A. Marchetti, Slave fermions, slave bosons, and semions form bosonization of the two-dimensional t-J model, Phys. Rev. B **46**, 6535 (1992).

[46] P. A. Marchetti, Z. B. Su, L. Yu, Dimensional rediction of $U(1) \times SU(2)$ Chern-Simons bosonization: application to the t-J model, Nucl. Phys. B **482**, 731 (1996).

[47] P. A. Marchetti, Z. B. Su, L. Yu, $U(1) \times SU(2)$ Chern-Simons gauge theory of underdoped cuprate superconductros, Phys. Rev. B **58**, 5808 (1998).

[48] P. A. Marchetti, L. de Leo, G. Orso, Z. B. Su, L. Yu, Spin-charge gauge approach to the pseudogap of high-T_c cuprates: theory versus experiments, Phys. Rev. B **69**, 024527 (2004).

[49] F. Ye, P. A. Marchetti, Z. B. Su, L. Yu, Hall effect, edge states, and Haldane exclusion statistics in two-dimensional space, Phys. Rev. B **92**, 235151 (2015).

[50] F. Ye, P. A. Marchetti, Z. B. Su, L. Yu, Fractional exclusion and braid statistics on one dimension: a study via dimensional reduction of Chern-Simons theory, J. Phys. A: Math. Theor. **50**, 395401 (2017).

[51] P. A. Marchetti, The attraction between antiferromagnetic quantum vortices as origin of superconductivity in cuprates. In *Topological phase transitions and new developments,* World Scientific, Singapore (2018).

[52] P. A. Marchetti, F. Ye, Z. B. Su, L. Yu, Charge carriers with fractional exclusion statistics in cuprates, Phys. Rev. B **100**, 035103 (2019).

[53] P. A. Marchetti, Fractional statistics of charge carriers in the one- and two-dimensional t-J model: a hint for the cuprates?, Condens. Matt. **5**, 12 (2020).

[54] F. Wilczek, *Fractional statistics and anyon superconductivity*, World Scientific, Singapore, (1990).

[55] F. D. M. Haldane, "Fractional statistics" in arbitrary dimensions: a generalization of the Pauli principle, Phys. Rev. Lett. **67**, 937 (1991).

[56] S. E. Sebastian, C. Proust, Quantum oscillations in hole-doped cuprates, Annu. Rev. Condens. Matter Phys. **6**, 411 (2015).

[57] I. M. Vishik, Photoemission perspective on pseudogap superconducting fluctuations, and charge order in cuprates: a review of recent progress, Rep. Progr. Phys **81**, 062501 (2018).

[58] N. J. Robinson, P. D. Johnson, T. M. Rice, A. M. Tsvelik, Anomalies in the pseudogap phase of the cuprates: competing ground stated and the role of umklapp scattering, Rep. Progr. Phys **82**, 126501 (2019).

[59] C. Proust, L. Taillefer, The remarkable underlying ground states of cuprate superconductors, Annu. Rev. Condens. Matter Phys. **10**, 409 (2019).

[60] J. A. Sobota, Y. He, Z. X. Shen, Angle-resolved photoemission studies of quantum materiale, Rev. Mod. Phys. **93**, 025006 (2021).

[61] M. Lizaire, A. Legros, A. Gourgot, S. Benhabib, S. Badoux, F. Laliberté, M. -E. Boulanger, A. Ataei, G. Grissonanche, D. LeBoeuf, S. Licciardello, S. Wiedmann, S. Ono, H. Raffy, S. Kawasaki, G. -Q. Zheng, N. Doiron-Leyraud, C. Proust, L. Taillefer, Transport signatures of the pseudogap critical point in the cuprate superconductor $Bi_2Sr_{2-x}La_xCuO_{6+\delta}$, Phys. Rev. B **104**, 014515 (2021).

[62] M. Platé, J. D. F. Mottershead, I. S. Elfimov, D. C. Peets, R. Liang, D. A. Bonn, W. N. Hardy, S. Chiuzbaian, M. Falub, M. Shi, L. Patthey, A. Damascelli, Fermi surface and quasiparticle excitations of overdoped $Tl_2Ba_2CuO_{6+\delta}$, Phys. Rev. Lett. **95**, 077001 (2005).

[63] H. -B. Yang, J. D. Rameau, Z. -H. Pan, G. D. Gu, P. D. Johnson, H. Claus, D. G. Hinks. T. E. Kidd, Reconstructed Fermi surface of underdoped $Bi_2Sr_2CaCu_2O_{8+\delta}$ cuprate superconductors, Phys. Rev. Lett. 107, 047003 (2011).

[64] S. Kunisada, S. Isono, Y. Kohama, S. Sakai, C. Bareille, S. Sakuragi, R. Noguchi, K. Kurokawa, K. Kuroda, Y. Ishida, S. Adachi, R. Sekine, T. K. Kim, C. Cacho, S. Shin, T. Tohyama, K. Tokiwa, T. Kondo, Observation of small Fermi pockets protected by clean CuO_2 sheets of a high-T_c superconductor, Science **369**, 833 (2020).

[65] N. Barišic, S. Badoux, M. K. Chan, C. Dorow, W. Tabis, B. Vignolle, G. Yu, J. Beard, X. Zhao, C. Proust, M. Greven, Universal quantum oscillations in the underdoped cuprate superconductors, Nat. Phys. **9**, 761 (2013).

[66] C. Collignon, A. Ataei, A. Gourgout, S. Badoux, M. Lizaire, A. Legros, S. Licciardello, S. Wiedmann, J. -Q. Yan, J. -S. Zhou, Q. Ma, B.D. Gaulin, N. Doiron-Leyraud, L. Taillefer, Thermopower across the phase diagram of the cuprate $La_{1.6}Nd_{0.4}Sr_xCuO_4$: signatures of the pseudogap and charge density waves, Phys. Rev. B **103**, 155102 (2021).

[67] A. Gourgout, G. Grissonnanche, F. Laliberté, A. Ataei, L. Chen, S. Verret, J. -S. Zhou, J. Mravlje, A. Georges, N. Doiron-Leyraud, L. Taillefer, Seebeck coefficient in a cuprate superconductor: particle-hole asymmetry in the strange metal phase and Fermi surface transformation in the pseudogap phase, Phys. Rev. X **12**, 011037 (2022).

[68] Y. Fang, G. Grissonnanche, A. Legros, S. Verret, F. Laliberté, C. Collignon, A. Ataei, M. Dion, J. Zhou, D. Graf, M.J. Lawler, P.A. Goddard, L. Taillefer, B.J. Ramshaw, Fermi surface transformation at the pseudogap critical point of a cuprate superconductor, Nat. Phys. **18**, 558 (2022).

[69] T. M. Rice, K. -Y. Yang, F. C. Zhang, A phenomenological theory of the anomalous pseudogap phase in underdoped cuprates, Rep. Progr. Phys **75**, 016502 (2012).

[70] C. Collignon, S. Badoux, S. A. A. Afshar, B. Michon, F. Laliberté, O. Cyr-Choiniére, J. -S. Zhou, S. Licciardello, S. Wiedmann, N. Doiron-Leyraud, L. Taillefer, Fermi-surface transformation across the pseudogap critical point of the cuprate superconductor $La_{1.6-x}Nd_{0.4}Sr_xCuO_4$, Phys. Rev. B 95, 224517 (2017).

[71] J. T. Heath, K. S. Bedell, Necessary and sufficient conditions for the validity of Luttinger's theorem, New J. Phys. **22**, 063011 (2020).

[72] S. Sakai, M. Civelli, M. Imada, Direct connection between Mott insulators and d-wave high-temperature superconductors revealed by continuos evolution of self-energy poles, Phys. Rev. B **98**, 195109 (2018).

[73] S. Sachdev, H. D. Scammell, M. S. Scheurer, G. Tarnopolsky, Gauge theory for the cuprates near optimal doping, Phys. Rev. B **99**, 054516 (2019).

[74] T. Senthil, A. Vishwanath, L. Balents, S. Sachdev, M. P. A. Fisher, Deconfined quantum critical points, Science **303**, 1490 (2004).

[75] T. Senthil, L. Balents, S. Sachdev, A. Vishwanath, M. P. A. Fisher, Quantum criticality beyond the Landau-Ginsburg-Wilson paradigm, Phys. Rev. B **70**, 144407 (2004).

[76] O. I. Motrunich, A. Vishwanath, Emergent photons and transitions in the $O(3)$ sigma model with hedegehog suppression, Phys. Rev. B **70**, 075104 (2004).

[77] K. M. Shen, F. Ronning, D. H. Lu, F. Baumberger, N. J. C. Ingle, W. Meevasana, Y. Kohsaka, M. Azuma, M. Takano, M. Takagi, Z. -X. Shen, Nodal quasiparticles in antinodal charge ordering in $Ca_{2-x}Na_xCuO_2Cl_2$, Science **307**, 901 (2005).

[78] W. Wu, M. S. Schurer, S. Chatterjee, S. Sachdev, A. Georges, M. Ferrero, Pseudogap and Fermi surface topology in the two-dimensional Hubbard model, Phys. Rev. X **8**, 021048 (2018).

[79] P. A. Marchetti, M. Gambaccini, Gauge approach to the pseudogap phenomenology of the spectral weight in high T_c cuprates, J. Phys: Condens. Matter **24**, 475601 (2012).

[80] P. A. Marchetti, G. Bighin, Universality in cuprates: a gauge approach, J. Low Temp. Phys **185**, 87 (2016).

[81] Y. Wang, L. Li, N. P. Ong, Nerst effect in high-T_c superconductors, Phys. Rev. B **73**, 024510 (2006).

[82] L. Li, Y. Wang, S. Komiya, S. Ono, Y. Ando, G. D. Gu, N. P. Ong, Diamagnetism and Cooper pairing above T_c in cuprates, Phys. Rev. B **81**, 054510 (2010).

[83] Y. -H. Zhang, S. Sachdev, From the pseudogap metal to the Fermi liquid using ancilla qubits, Phys. Rev. Research **2**, 023172 (2020).

[84] Y. -H. Zhang, S. Sachdev, Deconfined criticality and ghost Fermi surfaces at the onset of antiferromagnetism in a metal, Phys. Rev. B **102**, 155124 (2020).

[85] A. Nikolaenko, M. Tikhanovskaya, S. Sachdev, Y. -H. Zhang, Small to large Fermi surface transition in a single-band model using randomly copuled ancillas, Phys. Rev. B **103**, 235138 (2021).

[86] E. Mascot, A. Nikolaenko, M. Tikhanovskaya, Y. -H. Zhang, D. K. Morr, S. Sachdev, Electronic spectra with paramagnon fractionalization in the single band Hubbard model, arXiv: 2111.13703v2 2 Apr 2022.

[87] N. Nagaosa, *Quantum Field Theory in Strongly Correlated Electronic Systems*, Springer-Verlag Berlin (1999).

[88] E. Fradkin, *Field Theories of Condensed Matter Physics*, Cambridge University Press (2013).

[89] S. Sachdev, *Quantum Phase Transitions*, Cambridge University Press (2011).

[90] N. Dupuis, *Notes on the many-body problem* https://www.lptmc.jussieu.fr/users/dupuis?start=4.

[91] M. Barkeshli, P. Bonderson, M. Cheng, Z. Wang, Symmetry fractionalization, defects and gauging of topological phases, arXiv: 1410:4540v4 15 Oct 2019

Also important textbooks considered for this thesis:

A. Altland, B. Simons, *Condensed Matter Field Theory*, Cambridge University Press (2013).

M. El-Batanouny, *Quantum Condensed Matter Physics*, Cambridge University Press (2020).